

## Durham E-Theses

---

### *Post-stack inversion of seismic reflection data from the belvoir coalfield*

Tian Gang

#### How to cite:

---

Gang, Tian (1995) Post-stack inversion of seismic reflection data from the belvoir coalfield. Doctoral thesis, Durham University.

#### Use policy

---

The full-text may be used and/or reproduced, and given to third parties in any format or medium, without prior permission or charge, for personal research or study, educational, or not-for-profit purposes provided that:

- a full bibliographic reference is made to the original source
- a <https://etheses.durham.ac.uk/id/eprint/5219/> is made to the metadata record in Durham E-Theses
- the full-text is not changed in any way

The full-text must not be sold in any format or medium without the formal permission of the copyright holders.

Please consult the [full Durham E-Theses policy](#) for further details.

The copyright of this thesis rests with the author.  
No quotation from it should be published without  
his prior written consent and information derived  
from it should be acknowledged.

**Post-stack inversion of seismic reflection data  
from the Belvoir Coalfield**

by

**TIAN Gang**

**A thesis submitted in partial fulfilment of the requirements  
for the degree of Doctor of Philosophy**

**Department of Geological Sciences**

**University of Durham  
1995**



**08 DEC 1995**

## ACKNOWLEDGEMENTS

I am grateful to my supervisor, Dr Neil Goulty, for his supervision, including his helpful guidance and consistent encouragement throughout my research work, his constructive criticism and patient corrections of my manuscript during my thesis writing. I especially enjoyed many discussions which we had during the past three years which usually sparked many new ideas.

I would like to thank Professor E Ebsworth, Vice-Chancellor of University of Durham, Professor R C Searle, former head of the Department of Geological Sciences, Professor M E Tucker, head of the Department of Geological Sciences, and Mr. Peter Grundy, deputy principal of the Graduate Society, for their help which enabled me to stay in Durham with the support of a University of Durham studentship. Thanks go also to my home University, Changchun University of Earth Sciences in People's Republic of China, for their permission to complete my PhD research project.

I acknowledge the support of the British Council in administering my first year scholarship; and the ORS award which provided funding for my second and third years. Thanks also to British Coal for providing the seismic dataset and well log information.

I have to thank my wife, Wei Li, and our son, Junfeng Tian, for their support and for helping me to overcome the inevitable homesickness.

I wish to thank all those in the department who have helped make this work possible, in particular Dave Stevenson, Peter Rowbotham, Salim Al-Rawahy and Biwen Xu for all their help with computing and plotting.

## ABSTRACT

Post-stack inversion of reflection data in seismic exploration can be used to obtain detailed information about lithology variations in the zone of interest. Generalized Linear Inversion (GLI) has previously been applied as a useful tool to achieve this. The purpose of my investigation is to apply GLI to data from the Coal Measures. It is known that in the Coal Measures the most strongly reflecting horizons are the coal seams, which are the exploration targets. In the seismic bandwidth they are thin beds, which causes particular problems associated with vertical resolution for the inversion.

The method is applied to a seismic line from the Belvoir Coalfield supplied by British Coal. In order to get better relative amplitudes and to keep the same bandwidth down the whole section, the data were carefully reprocessed using the ProMAX software. Wireline log data from two boreholes intersected by the seismic line were edited to generate acoustic impedance logs as functions of time. Software was developed to implement GLI, and tested on synthetic data before applying it to the reprocessed data.

The initial guesses for earth and wavelet models at the boreholes were obtained after systematic studies to determine the best strategy. The construction of the initial guess for the boundary locations elsewhere on the section is very critical for the success of the search for the global minimum. A combination of structural interpretation and the inversion results obtained from the previous trace was found to do the best job. I have tried to invert separately for the boundary locations, acoustic impedances and the wavelet, with the wavelet parameterized in the frequency domain. I found that, provided that the wavelet extracted at a borehole is a good estimate with low error energy, the most successful strategy is just to invert for the boundary locations, keeping the acoustic impedances and the extracted wavelet fixed. If the extracted wavelet is not a good estimate, then parameterizing the wavelet in the frequency domain and optimizing those parameters at the borehole is a useful approach.

None of the implemented inversion strategies produced a perfect result. Discrepancies were due to the difficulty in obtaining true relative amplitude values on the processed section. The inversion results and systematic studies on the field dataset indicate that the assumptions of the convolutional model are not satisfied by the processed section.

## CONTENTS

<b>Acknowledgement</b> . . . . .	<b>2</b>
<b>Abstract</b> . . . . .	<b>3</b>
<b>Contents</b> . . . . .	<b>4</b>
<b>List of Figures</b> . . . . .	<b>7</b>
<b>Chapter 1 Introduction</b> . . . . .	<b>11</b>
1.1 Statement of the Problem . . . . .	11
1.2 Seismic Data Processing . . . . .	12
1.3 Post-Stack Inversion . . . . .	13
1.4 Generalized Linear Inversion . . . . .	14
<b>Chapter 2 Principles</b> . . . . .	<b>18</b>
2.1 Forward Model . . . . .	18
2.2 Inverse Problem . . . . .	20
2.3 Inversion for the Reflection Coefficient Sequence . . . . .	24
2.4 Model Parameterization . . . . .	24
2.5 Vertical Resolution . . . . .	26
2.6 Energy and Correlation Coefficient . . . . .	28
<b>Chapter 3 Methodology</b> . . . . .	<b>30</b>
3.1 Data Processing . . . . .	30
3.1.1 Introduction . . . . .	30
3.1.2 Trace Editing and Geometry Editing . . . . .	31
3.1.3 True Amplitude Recovery and Trace Muting . . . . .	31
3.1.4 Prefilter (25 Hz high pass filter) . . . . .	32
3.1.5 Deconvolution . . . . .	33
3.1.6 Field Static Corrections . . . . .	34
3.1.7 Interactive Velocity Analysis (IVA) . . . . .	34
3.1.8 NMO Corrections and Autostatics . . . . .	35

3.1.9	Constant Velocity Stacking (CVS)	36
3.1.10	Trim Statics	37
3.1.11	Stacking, Trace Equalization and Filtering	38
3.1.12	F-K Analysis and F-K Filtering	39
3.1.13	Migration	40
3.2	Use of Logging and Coring Information	42
3.2.1	Introduction	42
3.2.2	Mechanical Log Editing	43
3.2.3	Interpretative Log Editing	43
3.2.4	Modelling Well Log Editing	43
3.2.5	Depth-Time Reconciliation	44
3.3	Inversion Procedure	44
3.3.1	Introduction	44
3.3.2	Initial Guess for the Earth Model	45
3.3.3	Wavelet Extraction	46
3.3.4	Wavelet Parameterization	47
3.3.5	Initial Boundary Inversion	50
3.3.6	Wavelet Inversion	51
3.3.7	Boundary Inversion	51
3.3.8	Acoustic Impedance Inversion	53
3.3.9	Inversion of Adjacent Traces	54
3.3.10	Summary	55
<b>Chapter 4</b>	<b>A Synthetic Model</b>	<b>56</b>
4.1	A 1-D Synthetic Model without Noise	56
4.1.1	Introduction	56
4.1.2	Wavelet Parameters	57
4.1.3	Boundary Locations	60
4.1.4	Acoustic Impedance and Gradients	65
4.2	A 1-D Synthetic Model with White Noise	70
4.2.1	Introduction	70
4.2.2	Wavelet Inversion	70
4.2.3	Boundary Locations	71
4.2.4	Acoustic Impedance and Gradients	72
4.3	Summary	73

<b>Chapter 5</b>	<b>British Coal's Dataset</b>	<b>75</b>
5.1	Introduction	75
5.2	Systematic Study at Thorny Plantation	76
5.2.1	Comparison of the Two Different Processed Sections	76
5.2.2	Time Shift for the Extracted Wavelet	77
5.2.3	Identification of the Main Coal Seams	77
5.2.4	Construction of Initial Guess for the Earth Model	79
5.2.5	Estimation of Wavelet Parameters	82
5.2.6	Inversion of the Trace at the Borehole	83
5.3	Systematic Study at Pillbox	84
5.4	Inversion for the Whole Section	89
5.4.1	Introduction	89
5.4.2	From Thorny Plantation to Pillbox	90
5.4.3	From Pillbox to Thorny Plantation	95
5.5	Summary	96
<b>Chapter 6</b>	<b>Conclusions and Suggestions for Future Work</b>	<b>98</b>
6.1	Conclusions	98
6.2	Suggestions for Future Work	100
<b>References</b>		<b>101</b>
<b>Appendix</b>	<b>Computer Software</b>	<b>107</b>

## List of Figures

**Figure 2.1** Continuous discrete interval parameterization.

**Figure 2.2** The amplitude spectrum of the cosine-tapered-box-car wavelet.

**Figure 2.3** The effect on a zero-phase wavelet of changing the constant phase  $\varphi_0$  in steps of - 15 degrees.

**Figure 2.4** The effect on a zero-phase wavelet of changing  $\varphi_1$  in steps of - 0.1 deg/Hz.

**Figure 2.5** The effect on a zero-phase wavelet of changing  $\varphi_2$  in steps of - 0.001 deg/Hz<sup>2</sup>.

**Figure 3.1** The migrated seismic section processed by British Coal.

**Figure 3.2** The processing sequence table used by British Coal.

**Figure 3.3** The original recorded data from shot No. 85.

**Figure 3.4** The same dataset as Fig. 3.3 but with editing and muting.

**Figure 3.5** The same dataset as Fig. 3.4 with pre-filter applied.

**Figure 3.6** The same dataset as Fig. 3.5 with deconvolution applied.

**Figure 3.7** Fully interactive velocity analysis displays.

**Figure 3.8** CDP gathers 999 and 1000: (a) without NMO corrections; (b) with NMO corrections applied.

**Figure 3.9** Comparison of the stack: (a) without autostatics; (b) with autostatics applied.

**Figure 3.10** CDP gathers 999-1000: (a) without trim statics; (b) with trim statics applied.

**Figure 3.11** Stacked section with all above procedures carried out.

**Figure 3.12** F-K analysis for picking of F-K filter polygons.

**Figure 3.13** The stacked section with F-K filter applied.

**Figure 3.14** The migrated section reprocessed with ProMAX.

**Figure 3.15** Original sonic log at Thorny Plantation borehole.

**Figure 3.16** Original sonic log at Pillbox borehole.

**Figure 3.17** Lithology profile (part) of Thorny Plantation borehole.

**Figure 3.18** Lithology profile (part) of Pillbox borehole.

**Figure 3.19** Edited sonic log at Thorny Plantation borehole.

**Figure 3.20** Acoustic impedance plotted against two-way travel time at Thorny Plantation.

**Figure 3.21** Acoustic impedance plotted against two-way travel time at Pillbox.

**Figure 4.1** Synthetic inversion results for wavelet parameters and earth model with correct initial guess.

**Figure 4.2** Synthetic inversion results for a badly wrong initial guess for the boundary locations with inversion for the reflection coefficient sequence applied prior to GLI with parameterization.

**Figure 4.3** Synthetic inversion results for errors in the initial guess for all types of earth model and wavelet parameters.

**Figure 4.4** Synthetic inversion results with 15 % white noise on the input trace and errors in the initial guess for the boundary locations

**Figure 4.5** Synthetic inversion results with 15 % white noise on the input trace and errors in the initial guess for all types of earth model and wavelet parameters.

**Figure 5.1** Relationship between the time shift and error energy for all 31 positions of the desired output when extracting the wavelet at Thorny Plantation borehole.

**Figure 5.2** All the extracted 31 wavelets at Thorny Plantation borehole.

**Figure 5.3** Contributions of the various coal seams to reduction of the error energy following inversion at CDP 940, the nearest CDP to Thorny Plantation borehole.

**Figure 5.4** Amplitude and phase spectra of the extracted wavelet at CDP 940, close to Thorny Plantation borehole.

**Figure 5.5a** Inversion results for all parameters at CDP 940.

**Figure 5.5b** Inversion results for all parameters at CDP 1230, the nearest CDP to Pillbox borehole.

**Figure 5.6a** Inversion for boundary locations with the extracted wavelet obtained from Thorny Plantation borehole using 0.5/0.5 weights for establishing the initial guess model.

**Figure 5.6b** Inversion for boundary locations with the extracted wavelet obtained from Thorny Plantation borehole using 1.0/0.0 weights, i.e. initial guess based only on the interpreted structural information.

**Figure 5.6c** Inversion for boundary locations with the extracted wavelet obtained from Thorny Plantation borehole using 0.0/1.0 weights, i.e. initial guess based only on the previous trace inversion.

**Figure 5.7a** Inversion for boundary locations with 8-parameter wavelet of Table 5.4 and the initial guess earth model of Table 5.2.

**Figure 5.7b** Inversion for boundary locations and four frequency parameters with 8-parameter wavelet of Table 5.4 and the initial guess earth model of Table 5.2.

**Figure 5.7c** Inversion for boundary locations and all eight parameters with 8-parameter wavelet of Table 5.4 and the initial guess earth model of Table 5.2.

**Figure 5.7d** Inversion for boundary locations with the initial guess taken as the parameters shown in Table 5.5.

**Figure 5.8a** Inversion for boundary locations of the two main coal seams (the Deep Main and Parkgate/Tuption) with the extracted wavelet from Thorny Plantation borehole.

**Figure 5.8b** Same inversion as Fig. 5.8a except that twice as many iterations were applied.

**Figure 5.9a** Inversion for boundary locations with the 7-parameter wavelet shown in Table 5.11.

**Figure 5.9b** Inversion for boundary locations and four frequency parameters with the 7-parameter wavelet shown in Table 5.11.

**Figure 5.10a** Inversion for boundary locations from Pillbox to Thorny Plantation with extracted wavelet obtained from Pillbox borehole and initial guess earth model of Table 5.7.

**Figure 5.10b** Inversion for boundary locations from Pillbox to Thorny Plantation with 8-parameter wavelet of Table 5.9 and initial guess earth model of Table 5.7.

**Figure 5.10c** Inversion for boundary locations from Pillbox to Thorny Plantation with the wavelet extracted from Thorny Plantation borehole and the same acoustic impedance values as in Table 5.2.

**Figure 5.11a** Inversion for boundary locations and four frequency parameters of the 8-parameter wavelet shown in Table 5.9.

**Figure 5.11b** Inversion for boundary locations and all eight parameters of the 8-parameter wavelet shown in Table 5.9.

# 1 Introduction

## 1.1 Statement of the Problem

In the 1970s, seismic interpretation was still mainly limited to structural and stratigraphic interpretation of the subsurface. With the advent of better recording and processing techniques, preserving the amplitude information in the seismic data, attention has subsequently focused on linking subsurface rock and fluid parameters to the seismic amplitudes. 3-D seismic surveys, which have uniform areal coverage and obvious application to field appraisal and development, pushed this requirement further.

During recent years there has been an increasing demand for an integrated approach to reservoir characterization for the most effective recovery of in-place hydrocarbons (Archer et al., 1993). The characterization of reservoirs requires the integration of different data types to define a reservoir model. Geological, well log and core data are traditionally the most commonly used data sets in reservoir model-building (e.g. Raymer and Burgess, 1980). Well log data and core data provide detailed information about the vertical variation of many reservoir properties, but they are restricted to regions adjacent to the borehole. More recently, seismic data have played an increasingly important role in describing reservoirs away from the wellbore (e.g. Martinez et al., 1992). Because of their excellent lateral resolution, seismic data can contribute to a well-defined geometric description of structural and stratigraphic aspects of the reservoir (Graebner et al., 1981).

Classically, seismic exploration consists of three main stages: data acquisition, data processing and geological interpretation. Inversion is the link between the last two stages and is one of the most active areas of current research in exploration seismology.

This thesis is concerned with the inversion of seismic reflection data from Coal Measures. The techniques developed are applied to synthetic data and also tested on real seismic and borehole data from the Belvoir Coalfield. British Coal has long experience of acquiring high resolution data of excellent quality to delineate faults for mine planning (Ziolkowski and Lerwill, 1979; Fairbairn et al., 1986). In the UK, there has also been much recent discussion about the potential for the development of coalbed methane (e.g. Cardy, 1995), which has led to a limited amount of drilling in coal basins traditionally exploited by mining (Creel, 1995). This gives rise to the requirement for high resolution seismic data, processed to identify the fine structures in the coal seams (i.e. washouts, faults and pinchouts) because coalbed methane is exploited by in-seam wells. Thus the ultimate goal of the work presented in this thesis is to develop inversion techniques for seismic data acquired from Coal Measures strata for application both in coal mining and in exploitation of coalbed methane.

## 1.2 Seismic Data Processing

Data processing is a sequence of operations which are carried out according to a pre-defined programme to extract useful information from a set of raw (normally observational) data (see Al-Sadi, 1980). The introduction of the digital computer in the early 1960s opened a new world in data processing. The great processing capabilities of computers have stimulated amazing technical advances in acquisition and interpretation as well as processing itself, leading to seismic reflection datasets whose quality and quantity could hardly have been imagined 30 years ago.

According to Yilmaz (1987), there is a well-established sequence for standard seismic data processing. The three principal processes, deconvolution, stacking and migration, make up the foundation of routine processing. There are also some auxiliary processes that help improve the effectiveness of the principal processes.

Data processing is done to correct for statics, to suppress horizontally travelling noise, to correct the amplitude for spherical divergence and attenuation, to reduce distortions due to ghosts and reverberations, to broaden the bandwidth of the signal, to overcome the earth's attenuation, to suppress multiples and improve the signal-to-noise ratio by stacking, and to present stacked and migrated seismic sections that can be interpreted in terms of the underlying geology that produced the seismic response.

These procedures are general and basic in routine data processing. According to Yilmaz (1987), even when starting with the same raw data, the result of processing done by one organization seems to be different from that done by another organization. The differences often stem from differences in the choice of parameters and the detailed aspects of implementation of processing algorithms. This means that there is no single correct result for data processing, but the aim is to produce a seismic section which represents the subsurface geology as truly and clearly as possible for interpretation.

Based on the migrated section, inversion can be applied as an aid to interpretation.

### 1.3 Post-Stack Inversion

Post-stack inversion techniques have greatly developed since the beginning of the 1980s. At present they can be mainly divided into three categories. One category is wave equation inversion which includes the Born inversion method (Cohen and Bleistein, 1979; Bleistein et al., 1985); inversion by the generalized Radon transform (Beylkin, 1984;

Miller et al., 1987); and the generalized pulse-spectrum technique (Chen, 1985). Another category is seismic tomography which includes ray travel time imaging (Aki, 1981); diffraction tomography (Dines and Lytle, 1979; Pan and Kak, 1983), and both in combination (Pratt and Gouly, 1991). The third category is generalized linear inversion (Bamberger et al., 1982; Cooke and Schneider, 1983; Oldenburg et al., 1983).

There are some other kinds of inversion techniques in the research stages, e.g. simulated annealing inversion (Sen and Stoffa, 1991) and genetic inversion (Stoffa and Sen, 1991). The classical recursive inversion technique (Lavergne and Willm, 1977; Lindseth, 1979) should be mentioned, but it is intrinsically unstable in the presence of noise.

For wave equation inversion, even though it uses all the information (travel times and waveforms) and has a strict mathematical derivation, there are still some shortcomings in its application: weak scattering assumption in the Born approximation and expensive computational time. For seismic tomography, the 2-D or 3-D images are computed very fast, but its disadvantages for surface seismic reflection data are that it generally uses only travel time information and the source-receiver geometry is far from optimum.

#### 1.4 Generalized Linear Inversion

The category of generalized linear inversion methods is a very wide category. All the linear inversion methods can be drawn into it. The theory is described by Backus and Gilbert (1967, 1968), Sabatier (1977a, 1977b), Aki and Richards (1980) and Tarantola and Valette (1982). Previous work on it has been reported by Cooke and Schneider (1983), Oldenburg, et al. (1983), Cornish and King (1988) and Brac et al. (1992).

Oldenburg, et al. (1983) proposed that the inversion for acoustic impedance could be supplemented by two construction methods to find the missing high and low frequencies.

However, they said that the reflection response to a thin bed was a situation which would prevent them from obtaining a unique solution. Cooke and Schneider (1983) presented a least-squares inversion method with the introduction of the block earth model which corresponds to the method of Oldenburg et al. (1983). Furthermore, they introduced parameterization of the wavelet in the frequency domain which makes it possible to invert the effective wavelet simultaneously. But they had to put some constraints on the errors in initial guess model in order to ensure the solution was within the region of convergence. Even though both papers contained results from synthetic and field studies, they did not consider inversion if there was no well log information available. And most importantly they all did not try to solve the nonuniqueness of the inversion for acoustic impedance in sections containing thin beds.

Cornish and King (1988) presented a broadband constrained inversion by using a stochastic algorithm. Its application was shown by Martinez et al. (1992) for reservoir characterization. Brac et al. (1992) demonstrated their work for integrated stratigraphic interpretation. All these authors concentrated on the acoustic impedance, because they assumed the boundary locations were correct from a priori information obtained by structural and stratigraphic seismic interpretation. However, in thin bed cases such as coal seams, the boundary locations and acoustic impedance values are not independent (Widess, 1973).

I have been unable to find any published research about the GLI method being applied in thin bed exploration. Also there is no case history published using GLI based on the work of Cooke and Schneider (1983). In this thesis I investigate the application of the GLI method based on Cooke and Schneider (1983) to seismic sections in the Coal Measures. Previous published work (Cooke and Schneider, 1983) has failed to quantify inversion errors satisfactorily, apart from some simple error estimations made on synthetic examples (Weber, 1986), so a particular aim is to quantify the accuracy of the inversion results.

I adopt the forward convolutional model (Treitel and Robinson, 1966) used by both Cooke and Schneider (1983) and Oldenburg et al (1983). However, I do not think the reflectivity function produced by Cooke and Schneider (1983) is necessary or appropriate for post-stack datasets. In their article, they generated a reflectivity function in the Z-domain by recursive application of the following formula (Cooke, 1981):

$$R_j(x, Z) = \frac{C_j + R_{j+1}(x, Z)Z}{1 + C_j R_{j+1}(x, Z)Z} \quad (j=n-1, n-2, \dots, 1, 0) \quad (1.1)$$

Using the above algorithm, one can generate a one-dimensional synthetic seismic trace that includes all multiples and transmission losses for a given digitized impedance log and a source wavelet considered to be a plane wave. However, for some inverse problems, such as the post-stack inversion reported in this thesis, it will not be suitable because deconvolution, NMO corrections and stacking have been applied; a principle aim in applying these processing techniques is to suppress the multiples.

In my research, an improved GLI inversion method is presented and tested using a 2D seismic line passing through two logged boreholes. A post-stack dataset from British Coal, which was reprocessed using ProMAX to preserve amplitudes correctly (Yu, 1985; Mazzotti and Mirri, 1988), was used by applying the inversion to the stacked trace for the common depth point (CDP) gather located at one well. For this case, not only the acoustic impedance but also the lithology were known. Then the inversion result from the first trace was partly used as the starting model for next trace combined with some interpretative structure information. Upon reaching the CDP gather located at the other well, the inverted trace was compared with the known well logs. Their similarities and differences are analysed and the errors are quantified.

To avoid the conflict between the linear problem (amplitudes of reflection coefficients) and non-linear problem (locations of boundaries) presented by van Riel and Berkhout

(1985), in my improved GLI inversion an alternative two-step iterative inversion method (Redanz, 1988) is used.

Another problem in some previous work with the GLI method (e.g. Oldenburg et al., 1983) is that there has been no inversion of the extracted wavelet. To do this, I unwrap the phase spectrum of the wavelet (Shatilo, 1992) after extracting it as a Wiener shaping filter. Then the wavelet is defined in the frequency domain by eight parameters: four frequencies, a constant phase value plus linear and quadratic phase terms as functions of frequency, and an amplitude scaling factor.

To overcome the constraint on the accuracy of boundary locations in making the initial guess model (Cooke and Schneider, 1983), I adopt a two-part strategy. Firstly, an inversion for the reflection coefficient sequence in which the Jacobian matrix is calculated analytically (Dahl and Ursin, 1991) is used, if it is needed. Secondly, separate inversion steps are carried out for the boundary locations, acoustic impedance values, and the wavelet parameters.

For the thin beds encountered in coal exploration, which is the most difficult case for the inversion, I applied my inversion method to investigate which parameters are most sensitive to noise and which should be constrained for the inversion. Before the field data are inverted, some synthetic examples are studied.

## 2 Principles

### 2.1 Forward Model

A description of the least-squares inversion method begins with a definition of the forward problem. The forward model is used to calculate the seismic response of an earth model, in which  $x$  is the lateral coordinate and  $t$  is elapsed time. The seismic response depends on the seismic excitation characterised by an effective wavelet  $w(x,t)$  injected at the surface with onset at time zero. Here the mathematical model used for calculating the surface seismic response  $S(x,t)$  is the standard convolutional model:

$$S(x,t) = \int_0^{\infty} r(x,t-\tau)w(x,\tau)d\tau \quad (2.1)$$

where  $r(x,t)$  is the primary reflectivity distribution of the medium, approximately related to the acoustic impedance distribution,  $A(x,t)$ , by

$$r(x,t) \approx -\frac{1}{2} \partial/\partial t[\ln A(x,t)]. \quad (2.2)$$

The convolutional model gives an alternative and complementary look at the seismic reflection method (Treitel and Robinson, 1966) compared to the wave propagation model, which describes the reflection method in terms of the laws of classical physics, i.e., Hooke's law and Newton's second law. It has produced an increased understanding of the relationship between geological features, such as pinchouts, facies changes, reefs and sand lenses, and the seismic response to such features. In addition to providing a basis for

interpretation of seismic data in terms of fine subsurface detail, the convolutional model has led directly to deconvolution and other time-sequence processing procedures.

The convolution model is a simplistic mathematical way to describe the physical phenomenon as well. Seismic theory in the early 1950s regarded a seismic trace as an entity that resulted from the solution of the wave equation with complicated initial and boundary conditions. As Robinson (1983) said: " Earthquake seismologists had obtained solutions in the case of very simple boundary conditions, but no comparable solutions had been obtained by exploration seismologists for any practical situation."

The convolutional model allows the impedance to be continuous, piecewise continuous, or discrete, and the earth's impedance is never discrete. With continuous impedance, the major reflections come from those impedance distributions in the earth that have periods that match the period of the effective seismic pulse. In effect, as the seismic pulse travels into the earth, it seeks out those impedance distributions to which it is tuned, i.e., those that have the same period as the effective pulse. One of the most significant results from the convolutional model is its demonstration that tuned events are most prominent, and this has laid to rest the fallacy that the largest reflections on seismic data are from discrete layering (White and Sengbush, 1987).

In this thesis, a discrete earth model is used to simplify the inversion problem. In discrete form the convolutional model of equation (2.1) may be written for a single trace as:

$$S = r * w \quad (2.3)$$

where  $S$  is the digital seismogram of length  $m+n+1$  samples,  $r$  is the reflection coefficient sequence of length  $n+1$  samples, and  $w$  is the effective wavelet of length  $m+1$  samples. Then the following summation is a general expression for the coefficients of  $S$ :

$$S_i = \sum_{j=0}^i r_j w_{i-j}, \quad i=0, 1, 2, \dots, m+n. \quad (2.4)$$

The discrete acoustic impedance distribution corresponding to the discrete reflectivity consists of a stack of  $n$  layers, in which the two-way travel times equal the time sample interval, bounded above and below by half spaces (Goupillaud, 1961). Thus the reflection coefficients for particle displacement may be expressed in terms of the acoustic impedance values as

$$r_j = \frac{A_j - A_{j+1}}{A_j + A_{j+1}}, \quad j=0, 1, 2, \dots, n. \quad (2.5)$$

## 2.2 Inverse Problem

Actually, we are interested in the inverse problem. Given the recorded surface seismic section, we want to know the acoustic impedance distribution of the medium. A standard way of proceeding is to use least squares. Given a recorded digital seismogram  $S^{\text{rec}}$  of length  $N$  from the processed surface section, the aim is to minimise

$$\begin{aligned} \Phi &= |F(\mathbf{A}) - S^{\text{rec}}|^2 \\ &= \sum_{i=1}^N [F_i(\mathbf{A}) - S_i^{\text{rec}}]^2 \end{aligned} \quad (2.6)$$

where  $F(\mathbf{A})$  is the forward-modelled seismogram. The vector  $\mathbf{A}$  represents the set of  $M$  'model parameters'.

For example, the acoustic impedance values in equation (2.5) could be treated as the  $M$  unknown model parameters. Then, assuming that the wavelet is known (having been estimated previously), the forward-modelled seismogram can be calculated using equations (2.4) and (2.5) with an initial guess for the acoustic impedance values. In

practice, the forward-modelling schemes used in this thesis are variants on this scheme, for reasons given below, but the following algebraic development is general in that it allows for some non-linearity in the dependence of  $\mathbf{F}$  upon  $\mathbf{A}$ . Having guessed an initial model  $\mathbf{A}^0$ , we linearize the relation between data and model by putting

$$\mathbf{F}(\mathbf{A}) \approx \mathbf{F}(\mathbf{A}^0) + \mathbf{G}\mathbf{a}, \quad (2.7)$$

where

$$\mathbf{G}_{ij} = \left( \frac{\partial F_i}{\partial A_j} \right)_{\mathbf{A}=\mathbf{A}^0}, \quad (2.8)$$

and

$$\mathbf{a} = \mathbf{A} - \mathbf{A}^0. \quad (2.9)$$

Putting  $\mathbf{d} = \mathbf{S}^{\text{rec}} - \mathbf{F}(\mathbf{A}^0)$ , we get

$$\Phi \approx |\mathbf{d} - \mathbf{G}\mathbf{a}|^2.$$

Minimizing  $\Phi$ , the least-squares solution is found (Aki and Richards, 1980)

$$\mathbf{a}^L = (\mathbf{G}^T\mathbf{G})^{-1}\mathbf{G}^T\mathbf{d}, \quad (2.10)$$

where  $\mathbf{G}^T$  is the transpose of matrix  $\mathbf{G}$ .

The standard linearization-iteration proceeds by constructing the second model  $\mathbf{A}^1 = \mathbf{A}^0 + \mathbf{a}^L$ , revising the linear relation by putting

$$\mathbf{F}(\mathbf{A}) \approx \mathbf{F}(\mathbf{A}^1) + \mathbf{G}\mathbf{a}, \quad (2.11)$$

where now

$$\mathbf{G}_{ij} = \left( \frac{\partial F_i}{\partial A_j} \right)_{\mathbf{A}=\mathbf{A}^1}, \quad (2.12)$$

and repeating the minimization process.

In practice, the above process may not converge (Hartley, 1961). A remedy is to construct the second model as

$$\mathbf{A}^1 = \mathbf{A}^0 + K\mathbf{a}^L, \quad (2.13)$$

where  $0 < K \leq 1$ . Even with small  $K$ , failure to converge is not uncommon.

An entirely different approach is the gradient method, in which the direction of most rapid change of  $\Phi$  is obtained in the model space. Since the equation of a plane tangent to the surface  $\Phi = \text{constant}$  at  $\mathbf{A} = \mathbf{A}^0$  is given by

$$\sum_j \frac{\partial \Phi}{\partial A_j} (A_j - A_j^0) = 0, \quad (2.14)$$

the direction of most rapid change is normal to the plane, and is given by the vector  $\mathbf{a}^G$ , with components  $(-\partial\Phi/\partial A_1, -\partial\Phi/\partial A_2, \dots, -\partial\Phi/\partial A_M)$ , evaluated at  $\mathbf{A} = \mathbf{A}^0$ .

From (2.6),

$$\frac{\partial \Phi}{\partial A_j} = 2 \sum_r (S_i^{\text{rec}} - F_i(\mathbf{A})) \frac{\partial F_i}{\partial A_j}$$

$$\begin{aligned}
&= 2 \sum_{\tau} d_i \frac{\partial F_i}{\partial A_j} \\
&= 2 \sum_{\tau} G_{ij} d_i,
\end{aligned} \tag{2.15}$$

and  $\mathbf{a}^G$  is parallel to  $\mathbf{G}^T \mathbf{d}$ .

Adjustment of a model by the gradient method can always be made to converge towards a minimum for  $\Phi$ . The convergence, however, may be very slow. On the other hand, the least-squares iteration converges very rapidly when it does converge. The vectors  $\mathbf{a}^G$  and  $\mathbf{a}^L$  are often nearly 90 degrees apart from each other.

It therefore seems reasonable to take an intermediate direction between  $\mathbf{a}^G$  and  $\mathbf{a}^L$ . Marquardt (1963) shows that the damped least-squares solution,

$$\mathbf{a}^M = (\mathbf{G}^T \mathbf{G} + \epsilon^2 \mathbf{I})^{-1} \mathbf{G}^T \mathbf{d} \tag{2.16}$$

points in such an intermediate direction. In fact, when  $\epsilon^2=0$ ,  $\mathbf{a}^M = \mathbf{a}^L$ ; and when  $\epsilon^2 \rightarrow \infty$ , the direction of  $\mathbf{a}^M$  approaches that of  $\mathbf{G}^T \mathbf{d}$ , and therefore of  $\mathbf{a}^G$ . For a small  $\epsilon^2$ , the process may diverge, and for a large  $\epsilon^2$ , the convergence may be too slow. After a few trials, an optimal  $\epsilon^2$  may be found for rapid convergence.

In (2.16),  $\mathbf{G} = \partial F_i / \partial A_j$  is called the sensitivity matrix or Jacobian matrix,  $\epsilon^2$  the damping factor, and  $\mathbf{I}$  is the identity matrix. The damping factor  $\epsilon^2$  can be calculated analytically as discussed by Marquardt (1963), or it can be chosen in an empirical manner as was done by Cooke and Schneider (1983). The empirical method searches for the  $\epsilon^2$  that minimises the root-mean-square (rms) error between the data being inverted and the synthetic seismogram generated from the corrected initial guess. The corrected guess, and thus the associated synthetic, is a function of  $\epsilon^2$  according to equations (2.9) and (2.16). This method is also known as the Generalised Linear Inversion method (GLI).

### 2.3 Inversion for the Reflection Coefficient Sequence

The simplest least squares scheme for inverting the observed seismograms is to use equation (2.4) to invert directly for the reflection coefficients. This requires that an estimate of the effective wavelet is available, so the wavelet coefficients are fixed. In this case the relationship between the reflection coefficients and the observed seismic trace is linear. With the notation of equation (2.4), equation (2.12) can be rewritten as

$$G_{ij} = \left( \frac{\partial S_i}{\partial r_j} \right) = w_{i-j}. \quad (2.17)$$

Then the reflection coefficient sequence  $r$  can be found by using equations (2.16) and (2.9). Because the problem is linear, the inversion is carried out once only (without iteration), unless it is desired to try different values of the damping parameter  $\epsilon^2$ .

This simple scheme does not itself invert for the acoustic impedance function. However, in some circumstances, it is useful for obtaining an initial guess acoustic impedance model before inverting for a parameterized wavelet and parameterized earth model, as described in the following section. It is equivalent to designing a Wiener shaping filter, corresponding to the reflection coefficient sequence, which does the best job in a least-error-energy sense of shaping the wavelet into the observed trace.

### 2.4 Model Parameterization

The earth's impedance is a continuous function in depth or time (as it is measured here). It is advantageous to approximate this function as a restricted number of layers in order to

**Figure 2.2** The amplitude spectrum of the cosine-tapered-box-car wavelet.

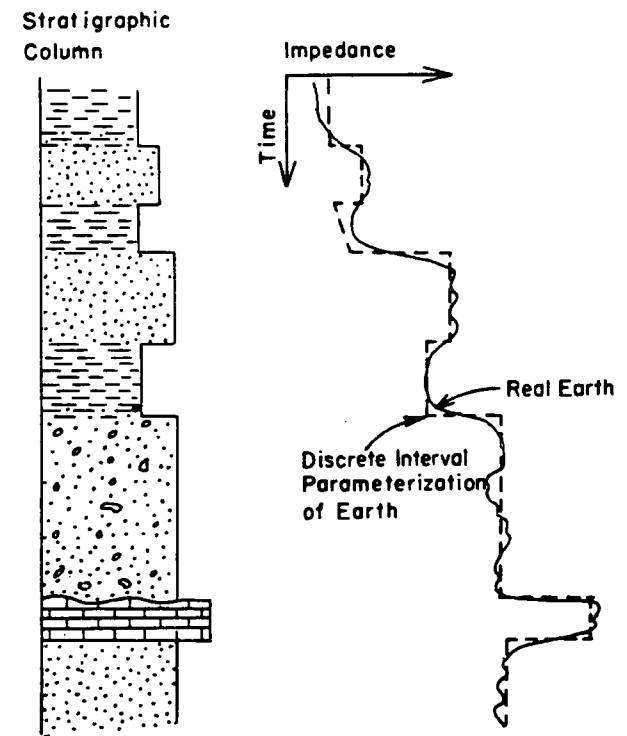
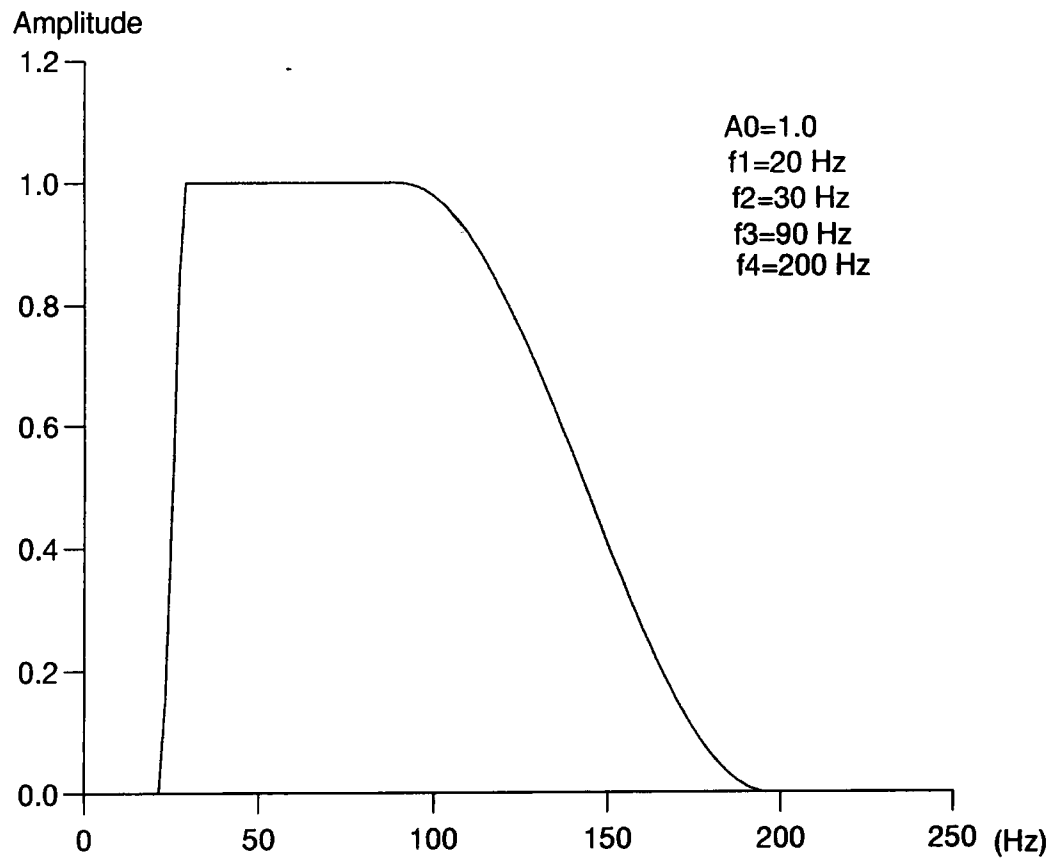


**Figure 2.1** Continuous discrete interval parameterization.

avoid problems such as (1) singular matrices or instability in inversion; (2) excessive costs in computer time and storage; (3) underconstrained inversion when extra model parameters are added; and (4) vertical resolution problems caused by non-linearity in boundary locations, which will be discussed in next section. The parameterization used in this thesis includes both the earth model and the wavelet. The principle for the parameterization is to use as few parameters as possible to represent the main features in the seismic response.

The parameterization describes the earth in terms of separate blocks or lithologies and is termed "discrete interval parameterization". Each lithic unit has assigned to it (a) a variable two-way time at the bottom of the block; (b) a variable impedance value at the top of the block; and (c) a variable linear rate of change of the impedance within the block (the impedance gradient). Figure 2.1 demonstrates this discrete interval parameterization method with the continuous earth model. Theoretically, the introduction of the impedance gradient makes it possible to restore the low-frequency trend of the impedance, whereas other methods can only get it by other means (from velocity analysis or by interpolation between wells) and not from the inversion itself. That is to say, the possible advantage of this inversion method is that it could widen the bandwidth.

In the above section on the forward model, it is assumed that one knows the effective wavelet that is to be convolved with the reflectivity function. This is not the case with real seismic data, so the effective wavelet must be treated as an unknown and solved for in the same manner as the impedance. The unknown wavelet is parameterized in the frequency domain where it is described by the four frequencies that constitute a band-pass filter (Fig. 2.2), up to three phase parameters and an amplitude. The form of the wavelet phase spectrum adopted here is

$$\Phi(f) = \varphi_0 + \varphi_1 f + \varphi_2 f^2. \quad (2.18)$$

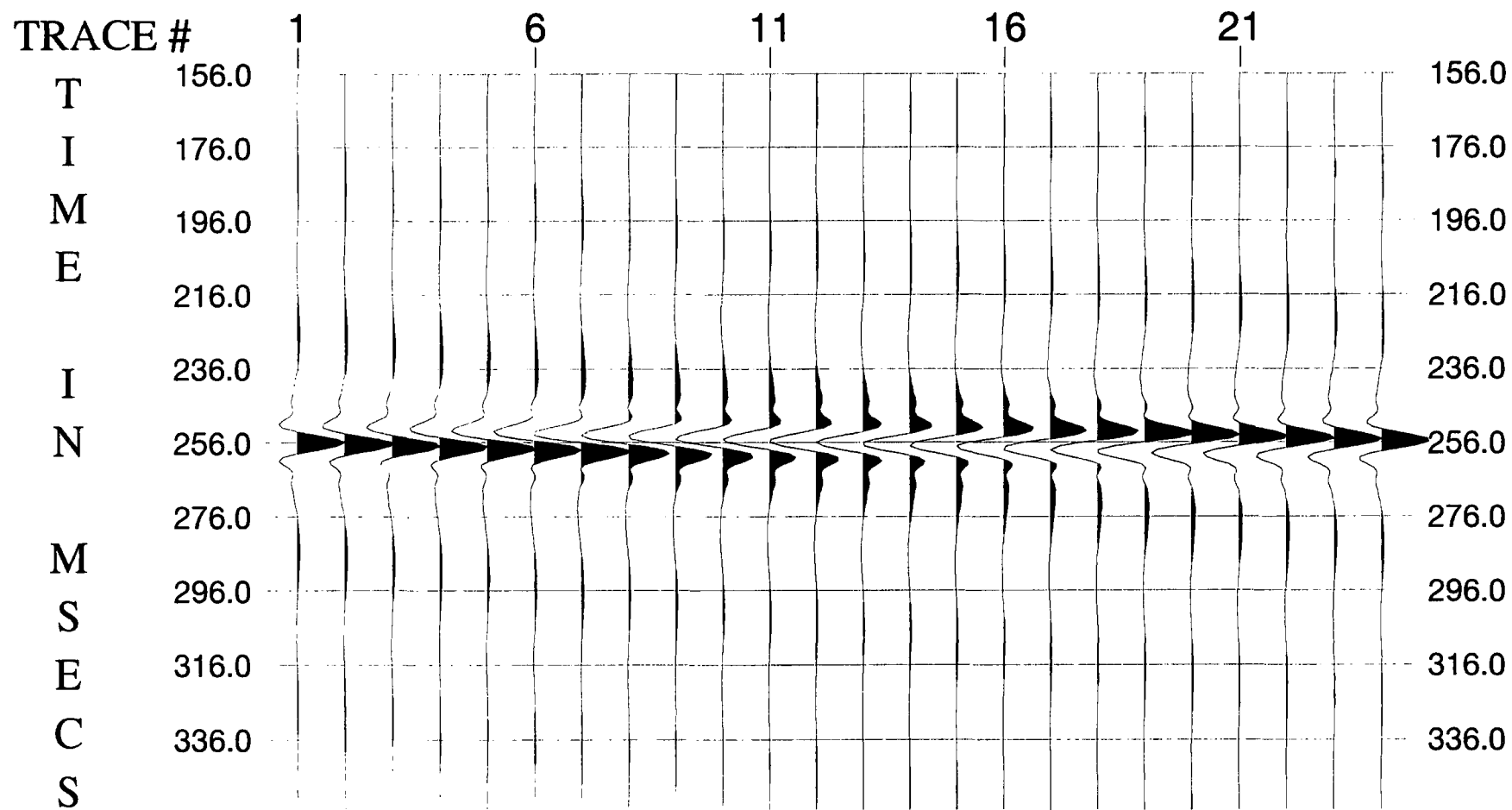


**Figure 2.3** The effect on a zero-phase wavelet of changing the constant phase  $\varphi_0$  in steps of - 15 degrees.

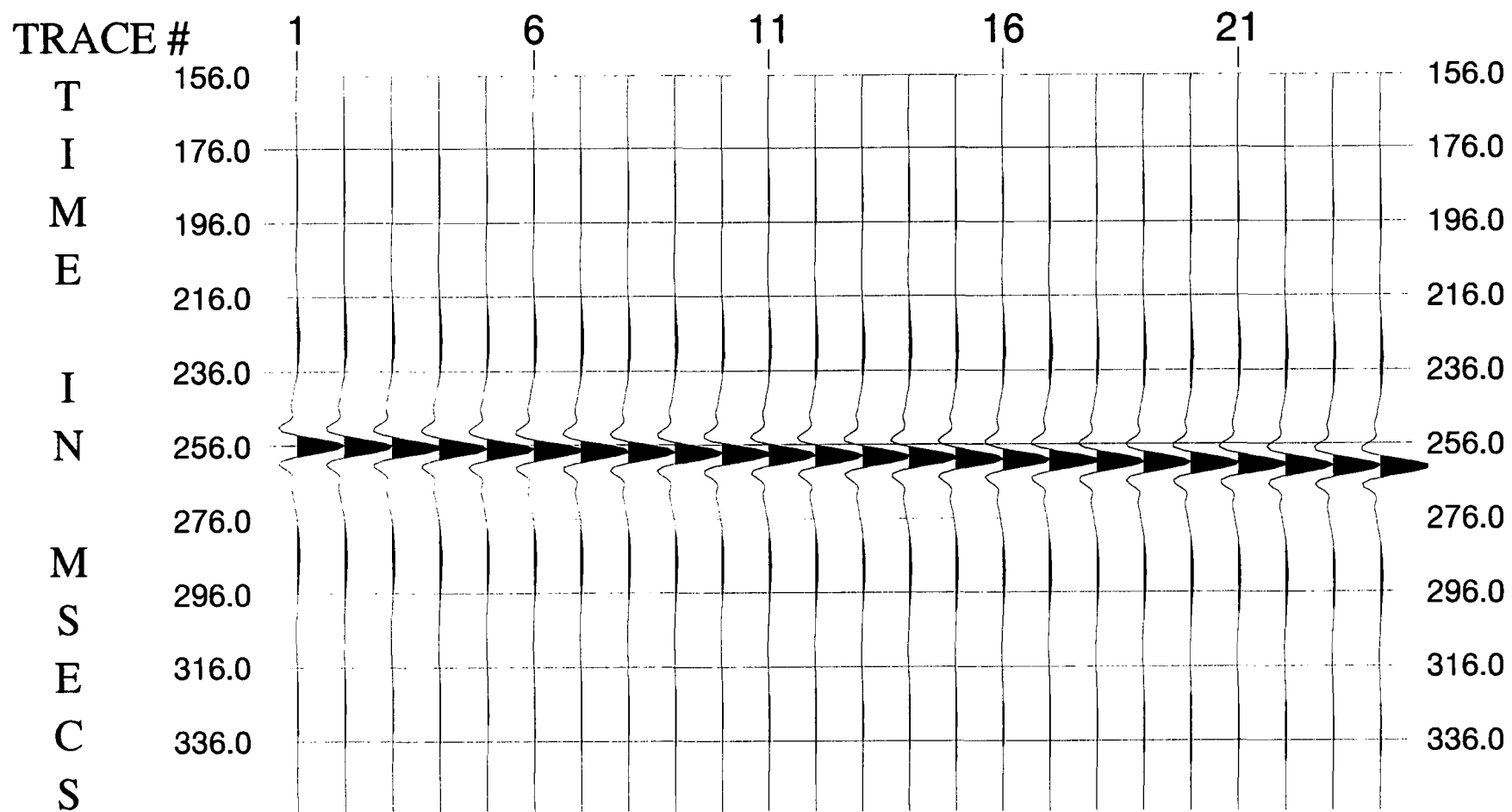
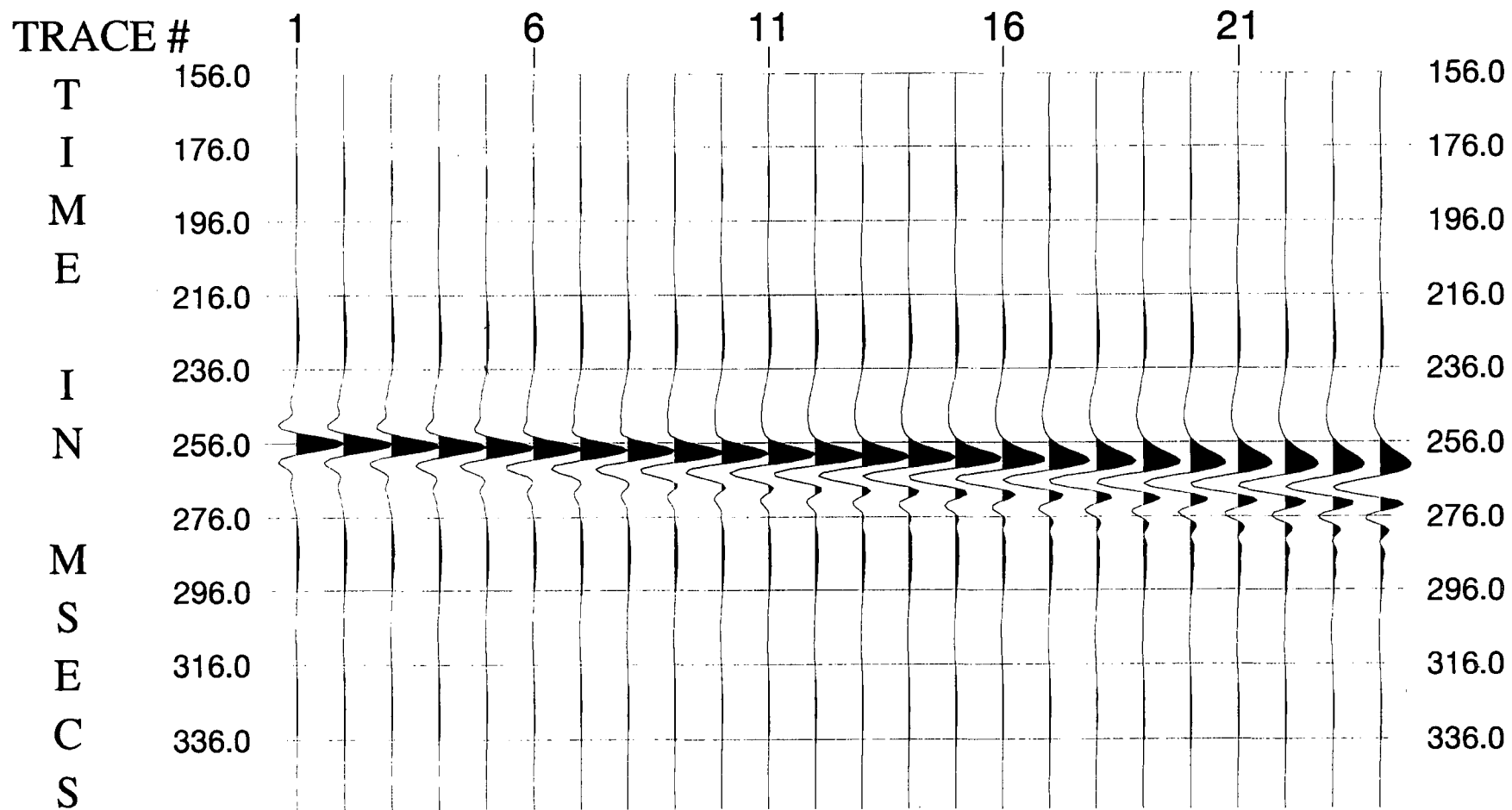


Figure 2.4 The effect on a zero-phase wavelet of changing  $\varphi_1$  in steps of - 0.1 deg/Hz.



**Figure 2.5** The effect on a zero-phase wavelet of changing  $\varphi_2$  in steps of  $-0.001$  deg/Hz<sup>2</sup>.

The family of wavelets used here have amplitude spectra which are cosine-tapered box-cars defined by four frequencies (Bracewell, 1978). The cosine tapers have the effect of suppressing the side-lobes at the cut-off frequencies in the time domain. This type of wavelet is commonly used in seismic modelling.

The following three figures demonstrate the effect of varying each phase parameter independently. Figure 2.3 shows how the shape of the wavelet changes as the constant phase value at all frequencies,  $\varphi_0$ , is incremented in steps of -15 degrees starting with zero phase. Figure 2.4 shows the effect of changing the value of  $\varphi_1$  in increments of -0.1 degree/Hz, which simply shifts the wavelet in the time domain. Figure 2.5 shows the effect of changing the value of  $\varphi_2$  in increments of -0.001 degree/Hz<sup>2</sup>. The amplitude of the wavelet enables us to scale the forward-modelled trace with the observed trace.

Because these parameters are implicit in equation (2.12), it is impossible to calculate the Jacobian matrix analytically. This problem will be discussed in Chapter 3. GLI using this type of model is called GLI with parameterization.

## 2.5 Vertical Resolution

The convolutional model of equation (2.1) may be rewritten for a discrete reflectivity model as

$$\begin{aligned} S(t) &= w(t) * r(t) \\ &= \sum_{j=1}^n r_j w(t - \tau_j) \end{aligned} \quad (2.19)$$

where  $r(t)$  is the reflectivity model consisting of  $N$  reflectors:

$$r(t) = \sum_{j=1}^n r_j \delta(t - \tau_j) \quad (2.20)$$

with reflection coefficients  $r_j$  and corresponding boundary locations (i.e. two-way times)  $\tau_j$ . We can see that  $S(t)$  depends linearly on the values of  $r_j$ , but nonlinearly on the values of  $\tau_j$ .

According to the analysis by Van Riel and Berkhout (1985), the solution obtained by generalized linear parametric inversion is usually superior to the resolution obtained by inversion with a convolutional inverse filter, or at least equal to it in the worst case. In parametric inversion the reflectivity function is represented as a parameterized earth model with a limited number of reflectors (blocks) as fewer unknowns, whereas in wavelet inverse filtering the reflectivity function is a regularly sampled function where every sample point represents an unknown, so there are many more unknowns. Of course, to formulate an initial guess for a parametric model, a priori information is required. This information may be available from various sources, e.g., log data, data on regional geology, or results from petrophysical analysis. The reason for the improved resolving power of the parametric approach is that a priori information is explicitly used. The effort of collecting sufficient a priori information is the cost of increasing resolution beyond that offered by wavelet inverse filtering.

GLI with model parameterization and least squares inversion for the reflection coefficient sequence correspond to these two different inversion methods. I found each method useful in different circumstances, and in different positions in the inversion sequence. Because inversion for the reflection coefficient sequence has lower vertical resolution, but no prior earth information is required, it is used to search for a guess model for boundary locations when the guess model obtained by inverting the previous trace is not suitable. It is necessary that an estimate of the effective wavelet is available. Circumstances where it could be used are where there is a fault or a stratigraphic change (e.g. pinchout), or even

in some area with a low signal-to-noise ratio (SNR). After inverting for the reflection coefficient sequence, the approximate boundary locations for each block can be obtained by analysing the reflectivity function. The previous acoustic impedance values for each layer are used to form the new guess model, on the assumption that there are no gross sudden lateral changes in lithology. Then this guess model is used to continue the inversion by GLI with model parameterization.

Recent research by Okaya (1995) shows that the spectral amplitude response of thin beds has bands and notches whose periodicities are directly related to layer thickness. An "optimally" tuned reflection occurs when the fundamental spectral amplitude band in the reflectivity response is excited by a seismic source. Distinct (resolved) reflections from the two interfaces occur when at least the fundamental and second amplitude bands are preserved. These considerations are directly relevant to my work as coal seams are the predominant reflecting horizons, as well as being the target horizons, and they are most certainly thin beds in terms of their reflection response to the seismic source.

Gochioco (1992) concluded that, "High-resolution seismic surveys applied to coal exploration indicated the existence of complex problems associated with interference reflections in the recorded wavefield data". He showed how two dominant coal seams and a rider seam could easily affect the resulting reflection by their thickness, separation distance, and sequence layering.

## 2.6 Error Energy and Correlation Coefficient

In order to measure the quality of the least-squares inversion between the forward-modelled trace  $S(t)$  and the observed trace  $X(t)$ , an error energy function was defined by

$$E = \left\{ \frac{\sum_i [S(i) - X(i)]^2}{\sum_i [X(i)]^2} \right\} \times 100\% \quad (2.21)$$

If E equal to 0 that means two traces are exactly the same, which shows that this error energy also can measure the quality of the match between them. Apart from this, a correlation coefficient is defined to describe the similarity of these two traces, especially when they are not normalised:

$$C = \frac{[\sum_i S(i)X(i)]^2}{\sum_i S^2(i) \sum_i X^2(i)} \quad (2.22)$$

It is easy to see that  $0 \leq C \leq 1$ . When C equals to 1 that means two traces looks exactly the same, but may have a constant factor difference. These two concepts are useful for later discussions.

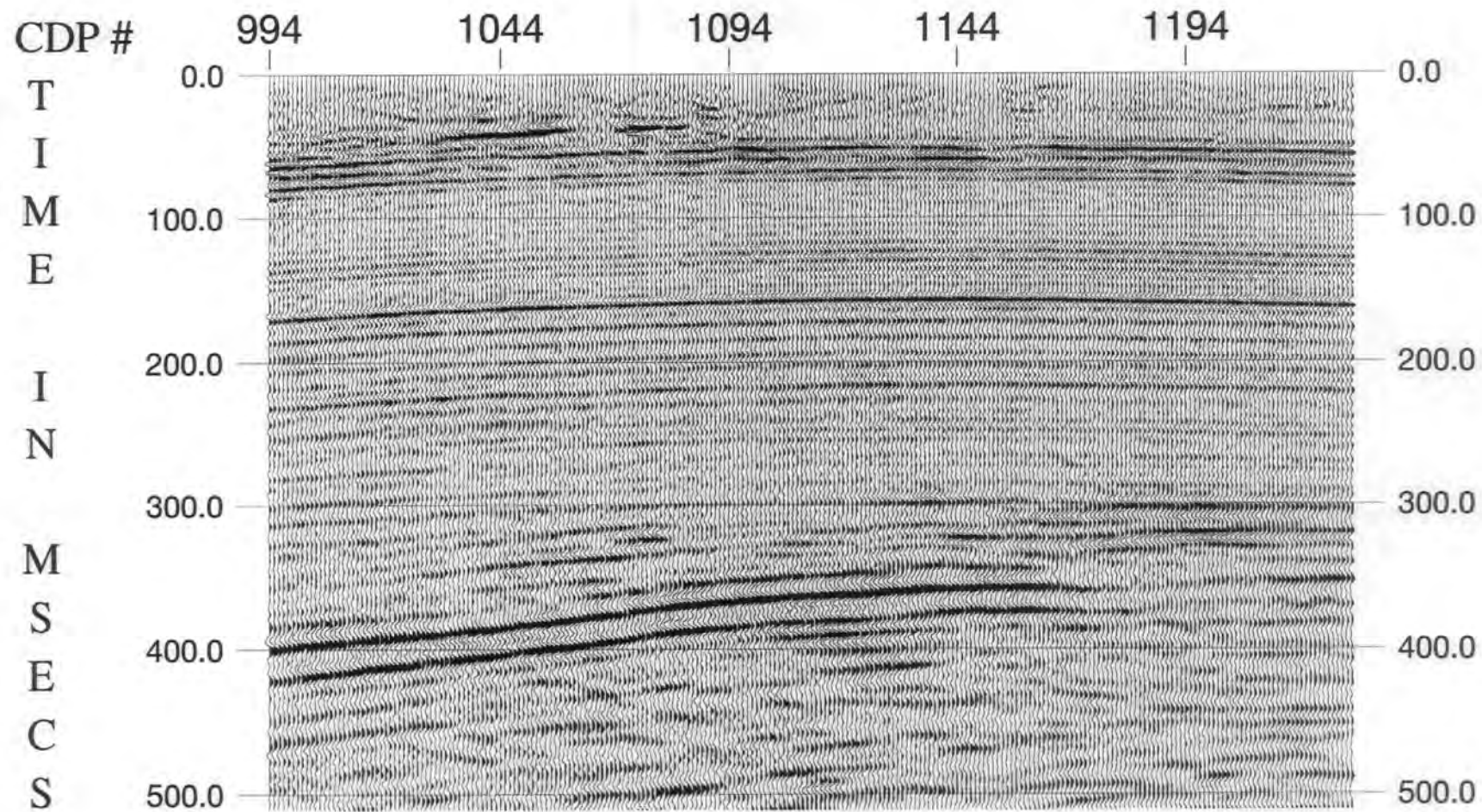


**Figure 3.1** The migrated seismic section processed by British Coal.

**LINE 87-AFY-04 MIGRATED STACK  
PROCESSING SEQUENCE**

PROCESSED DURING JULY-DECEMBER 1987

PROCESSING SAMPLE RATE 1 MS

PROCESSING LENGTH 1.5 SECS

XX

- 1 DEMULTIPLEX AND POLARITY REVERSAL
- 2 SPHERICAL DIVERGENCE AND GAIN CORRECTION
- 3 TRACE EDIT
- 4 CDP GATHER
- 5 FIRST BREAK SUPPRESSION MUTE
- 6 SYSTEM RESPONSE FILTER
- 7 PREFILTER (25-OUT HZ HIGH PASS FILTER)
- 8 TIME INVARIANT DECONVOLUTION (TYPE-WHITENING)  
OPERATOR LENGTH 51 MSECS  
DESIGN GATE :-  
ZERO METERS OFFSET: 70 MS -- 1000 MS  
580 METERS OFFSET : 400 MS -- 1000 MS
- 9 FIELD STATIC CORRECTIONS CALCULATED USING UPHOLE  
STATIC METHOD (DATUM: CURVED SEE HEADSTRIP)
- 10 VELOCITY ANALYSIS
- 11 AUTOMATIC RESIDUAL STATIC CORRECTIONS  
SURFACE CONSISTENT STATICS (MAXIMUM STATIC: +/- 4MS)  
3 TRACE PILOT CORRELATION GATES: 25 - 450 MS
- 12 VELOCITY ANALYSIS WITH 30 CDP CONSTANT VELOCITY STACK
- 13 AUTOMATIC RESIDUAL STATIC CORRECTIONS  
SURFACE CONSISTENT STATICS (MAXIMUM STATIC: +/- 4MS)  
3 TRACE PILOT CORRELATION GATES: 45 - 500 MS
- 14 NORMAL MOVEOUT CORRECTIONS
- 15 NORMAL MOVEOUT STRETCH MUTING
- 16 TIME INVARIANT EQUALIZATION
- 17 CDP STACK
- 18 TIME VARIANT DIGITAL BANDPASS FILTER  
FILTER LENGTH : 401 MS  
SP RANGE : 109-867  
0 - 200 MS            60 - 200 HZ  
300 MS                40 - 160 HZ  
500 - 600 MS        30 - 140 HZ  
1000 - 1500 MS      25 - 100 HZ  
LOCUT SLOPE 4DB/HZ    HICUT SLOPE 2DB/HZ
- 19 TIME VARIANT EQUALIZATION ( 6 BALANCE GATES)
- 20 F-K FILTER
- 21 FD MIGRATION (65 DEGREE DIP)

XX

**Figure 3.2** The processing sequence table used by British Coal.

### 3 Methodology

#### 3.1 Data Processing

##### 3.1.1 Introduction

The seismic dataset I used is line ASFORDBY 87-AFY-04 from the Belvoir coalfield, acquired by the British Coal Corporation who kindly supplied me with the raw data and a fully processed section (Fig. 3.1). Its processing sequence is tabulated in Fig. 3.2.

The quality of British Coal's processing is high, but their objective was to maximize SNR and resolution for interpretation, and not to pre-condition the stacked data for inversion. For example, they used a time-variant digital bandpass filter after stack to improve SNR, which will definitely have changed the amplitude spectrum along the trace, but the wavelet should be constant for inversion based on the convolutional model. Consequently I decided to reprocess the dataset from the field records using ProMAX in the Department of Geological Sciences, University of Durham.

The dataset has a total of 190 shots and each shot has 116 traces with a group spacing of 5 m. The record length is 3 seconds and the sample interval is 1 ms. CDP gathers are numbered from 206 to 1804 with a spacing of 2.5 m.

There are two boreholes on the line named Thorny Plantation and Pillbox, located at CDPs 994 and 1230, so I concentrated on the section over this range in order to compare the inversion results with the well logs. That is to say, only about 500 CDPs (851-1350)

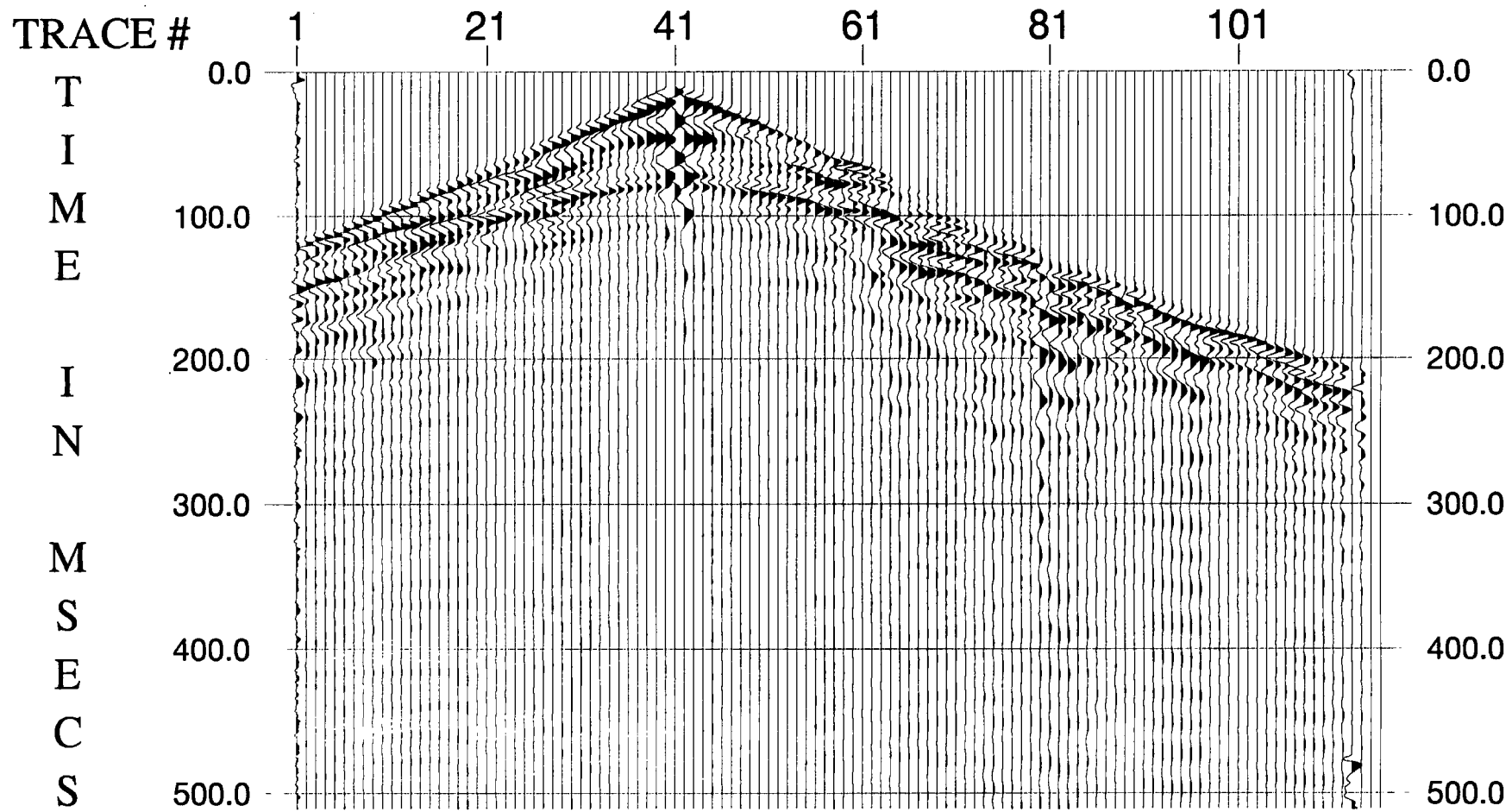


**Figure 3.3** The original recorded data from shot No. 85.

comprise the study area for testing the inversion methodology. Since the main coal seams are all above 500 ms, the processing length I chose was 512 ms.

### 3.1.2 Trace Editing and Geometry Editing

First all the recorded data in SEG-Y format were input from a 8 mm data cartridge. The "Screen Display" was used to edit out noisy traces (traces 1 and 113) and reverse traces (trace 41) with the wrong polarity as shown in Fig. 3.3 for shot number 85. "Trace Kill" and "Trace Reverse" were used to edit these traces.

"Geometry Editing" involves several files to edit. The files should contain information about the elevations of sources and receivers, hole depths, uphole times and the statics at source and receiver locations. The generating file is `geom_file` which can also be edited without interpolation.

The next step is "Geometry Installation" to set up the database and initialize it with all of the necessary geometry information. There are four steps: (1) "Header Fixup" (correct channel number and end-of-ensemble problems in trace headers); (2) "Initialize" (initialize a dataset and the database); (3) "Load Geometry" (load the geometry specified in '`geom_file`' to the database); (4) "Load Headers" (load geometry info from the database to the dataset trace headers). The "Header Fixup" step is optional, and should only be used when problems exist. The other steps are required, and should be run one at a time or run all together by choosing "Combination".

### 3.1.3 True Amplitude Recovery and Trace Muting

True amplitude recovery applies a single time-variant gain function to traces to compensate for loss of amplitude due to spherical divergence (wavefront spreading), transmission losses and anelastic attenuation.

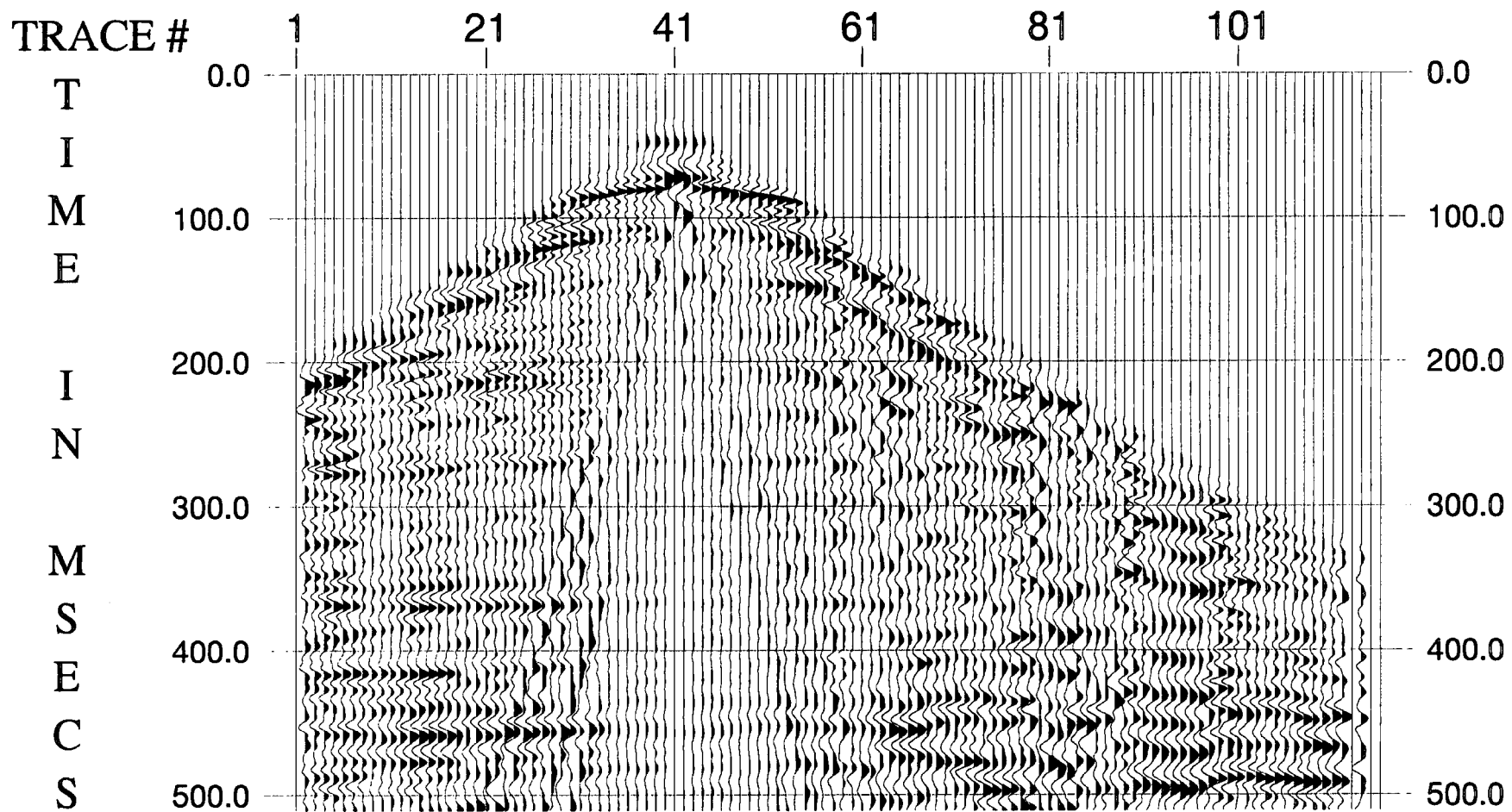


Figure 3.4 The same dataset as Fig. 3.3 but with editing and muting.

Spherical divergence corrections may be based on the reciprocal of the distance that the wavefront has travelled, using the "1/dist" option. Alternatively, corrections may be based on a function of travel time and velocity (assuming a layered earth). The actual function used is  $1/(\text{time} \times \text{velocity})^2$ . The velocity function is input using an editor, so that it may be varied to suit the area. To choose between these two options, see Newman (1973).

"Trace Muting" has three different types of mute available: top, surgical and bottom. While only one type of mute can be specified per call to this module, many mutes may appear in any one processing flow. All data samples that are muted are set to zero. A mute ramp is also provided to smooth the transition from live data to muted data samples. Ramping is done to prevent undesirable side effects from the mute process, especially following the application of filters. The trace mute file is created interactively on the "Screen Display" of the data and is then retrieved from the database when it is to be applied during the processing flow.

-v

Figure 3.4 shows the results of this procedure with the 85 shot gather.

#### 3.1.4 Prefilter (25 Hz high pass filter)

A prefilter is needed to remove the effects of ground roll at shot 85 (Fig. 3.4). Since ground roll is characterised by low frequency and strong amplitude, a high pass filter was applied.

The process applies a frequency filter to each trace that is input. Filters are four-frequency Ormsby or Butterworth (low frequency-low slope-high frequency-high slope) and may be zero phase or minimum phase. In my processing, a single bandpass filter was chosen and four "corner" frequencies (20-30-500-500) were specified for the standard bandpass filter. The four values represent sequentially the 0% and 100% points of the low-

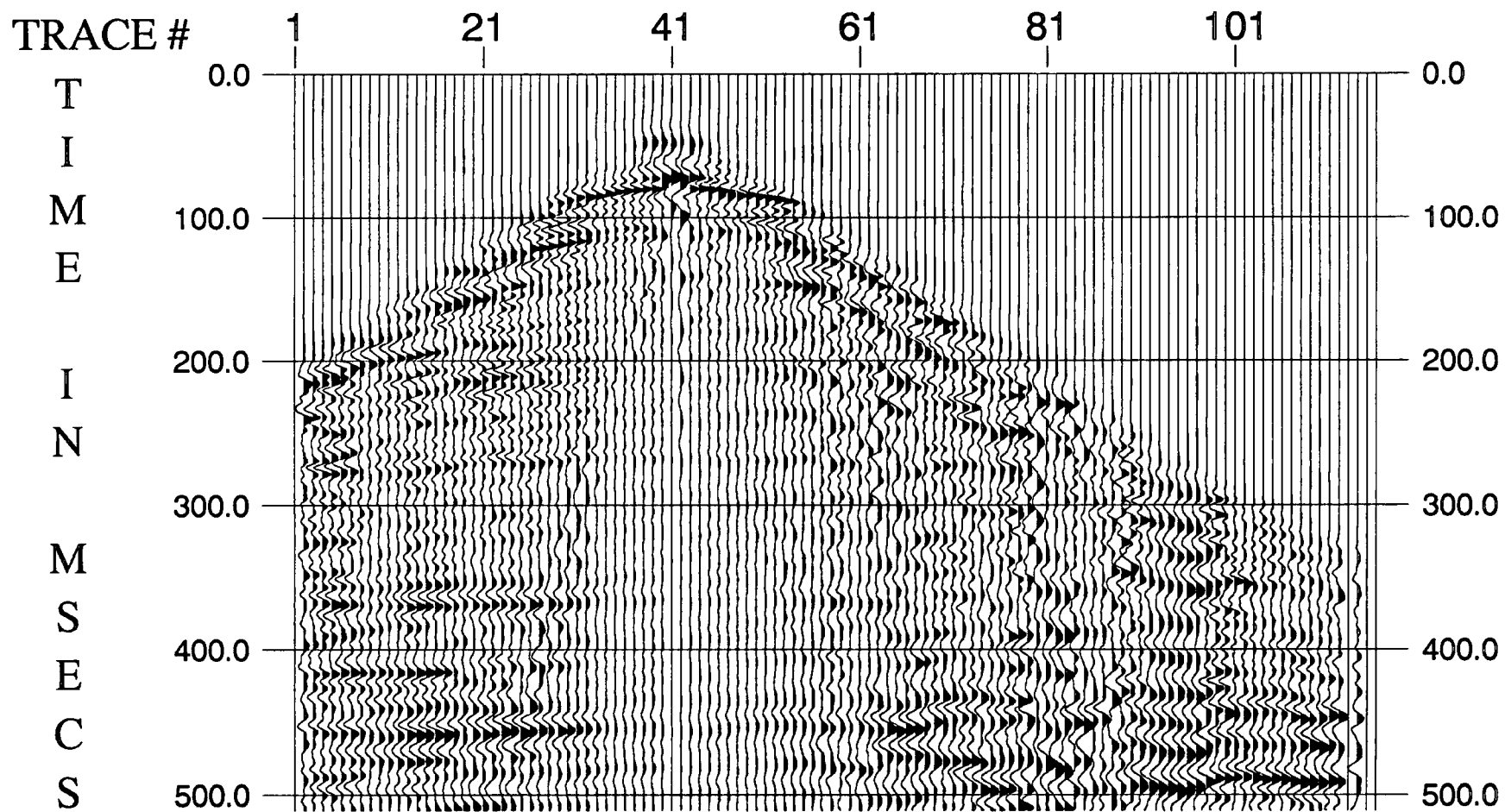
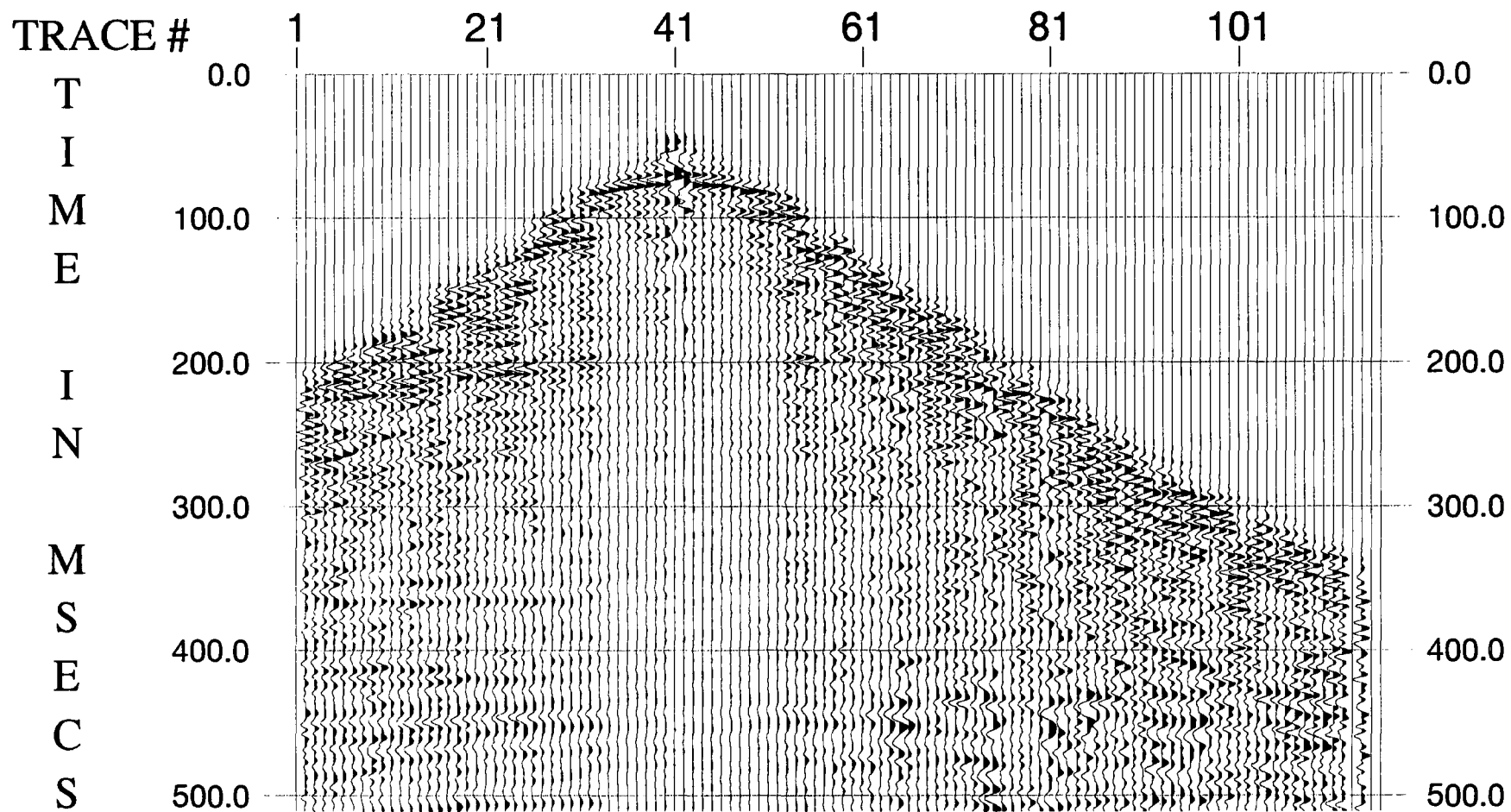


Figure 3.5 The same dataset as Fig. 3.4 with pre-filter applied.



**Figure 3.6** The same dataset as Fig. 3.5 with deconvolution applied.

cut ramp, and the 100% and 0% points of the high-cut ramp (in Hz). These ramps are formed by Hanning (cosine) tapers in the frequency domain. Figure 3.5 shows the results after applying the prefilter to the same shot point gather as Fig. 3.4.

### 3.1.5 Deconvolution

Prestack deconvolution is aimed at improving temporal resolution either by compressing the effective source wavelet to a spike (spiking deconvolution) or, less ambitiously, by truncating it (gapped or predictive deconvolution) (Robinson and Treitel, 1980).

ProMAX has a "Decon Parameter Stack Test" which creates multiple CDP stacks with user-specified pre-stack deconvolution applied, plus one stack with no deconvolution applied as a control. This was used to choose the optimum parameters: operator lengths, prediction distances and white noise levels can be varied.

Then "Ensemble Deconvolution" was used to compute a single deconvolution operator for all of the traces in the input ensemble. This ensemble could be a shot record (in my case), or a CDP or receiver gather. Minimum phase spiking was used for the pre-stack deconvolution. The operator length was 51 samples and the design gate was from 70 ms to 700 ms for zero offset and from 400 ms to 700 ms for 580 m offset. Since spiking deconvolution broadens the spectrum of seismic data, traces contain much more high-frequency energy after deconvolution. Because both high-frequency noise and signal are boosted, the data need filtering with a wide band-pass filter after deconvolution. The bandwidth was 20-30-200-250 Hz.

Figure 3.6 shows the result of deconvolution for the field record acquired at the same shot gather as above.

### 3.1.6 Field Static Corrections

In order to obtain a seismic section which shows seismic reflectors representing the actual geological structure, the reflection times must be reduced to a defined reference time. This is normally taken to correspond to a horizontal plane fixed at a certain known elevation above mean sea level. The static correction is essentially a time shift applied to each trace to reduce the observed reflection time to the datum plane.

The value of the total static correction depends on the following factors: (1) the perpendicular distance of the source from the datum plane; (2) the surface topography, i.e. the perpendicular distance of the detector from the datum; (3) the velocity variation of the surface layer along the seismic line; and (4) the thickness variation of the surface layer.

Field statics were provided by British Coal, so in ProMAX either "User-defined Statics", which gets the input from the geometry specification, or "Hand Statics", which gets the input from the flow input, can be used to apply them.

Though I have tried many times, "User-defined Statics" still will not work properly, which I suspect is due to bug in the ProMAX system. Eventually, I found I could apply the field statics using "Hand Statics", provided that "Elevation Statics" was applied first. Even though the values of the elevation statics were zero, they were required to create headers for "Hand Statics".

### 3.1.7 Interactive Velocity Analysis (IVA)

In addition to providing an improved SNR, multifold coverage yields velocity information about the subsurface. Velocity analysis is performed on selected CDP gathers or groups of gathers. The output from each velocity analysis is a table of numbers as a

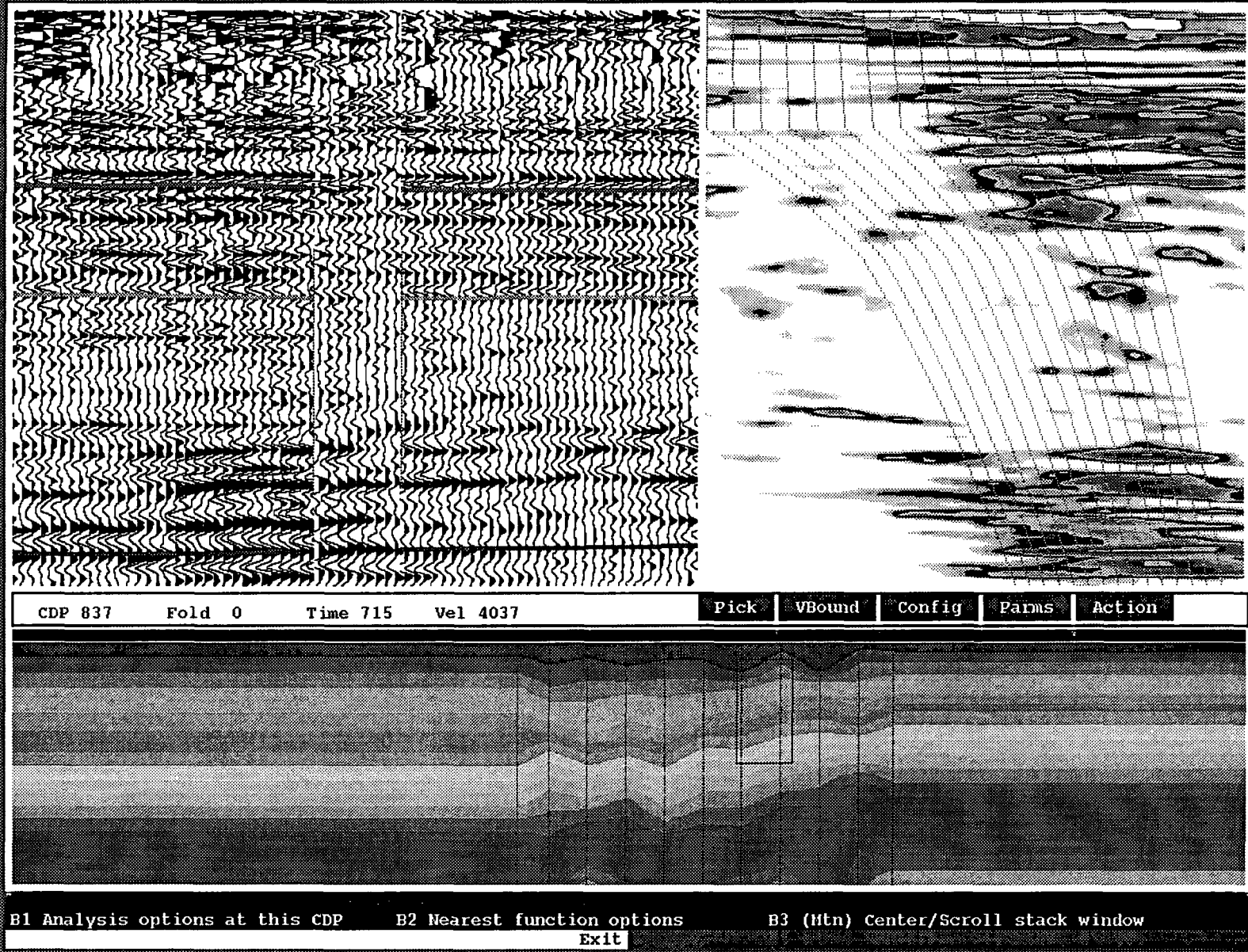


Figure 3.7 Fully interactive velocity analysis displays.

function of velocity versus two way zero-offset time. These numbers represent some measure of signal coherency along hyperbolic trajectories governed by velocity, offset, and travel time.

The "Interactive Velocity Analysis" tool in ProMAX provides comprehensive interactive velocity analysis, velocity quality control, velocity field modification capabilities, mute analysis, and autostatics-compatible horizon picking. In my processing, the "Fully Interactive" option was used. In this mode, the screen is divided into three windows: the upper left hand corner is a stack display; the upper right hand corner is a semblance display; and across the bottom is an iso-velocity contour display. Therefore one can decide which stacking velocity is suitable for the CDP according to all three displays (Fig. 3.7). At the same time, choosing "Yes" for "Provide Horizon Data Table" allows us to select an autostatics-compatible horizon table for the next processing stage.

### 3.1.8 NMO Corrections and Autostatics

Normal moveout corrections are applied according to the following formula:

$$T_x = \sqrt{T_0^2 + (X/V)^2} \quad (3.1)$$

where  $T_x$  is the actual reflection time of the seismic event;  $T_0$  is the zero offset reflection time of the seismic event;  $X$  is the actual source-receiver offset distance and  $V$  is the NMO or stacking velocity for this reflection event (Sheriff and Geldart, 1983).

This process applies NMO corrections from a space-variant velocity field. Velocities are interpolated for each CDP. In addition, "Direction for NMO Application" specifies whether to apply the correction for normal moveout (FORWARD), or to remove a previously applied correction (INVERSE) which makes it possible to repeat the velocity analysis and autostatics processes. The stretch mute percentage was set to 30.0. The

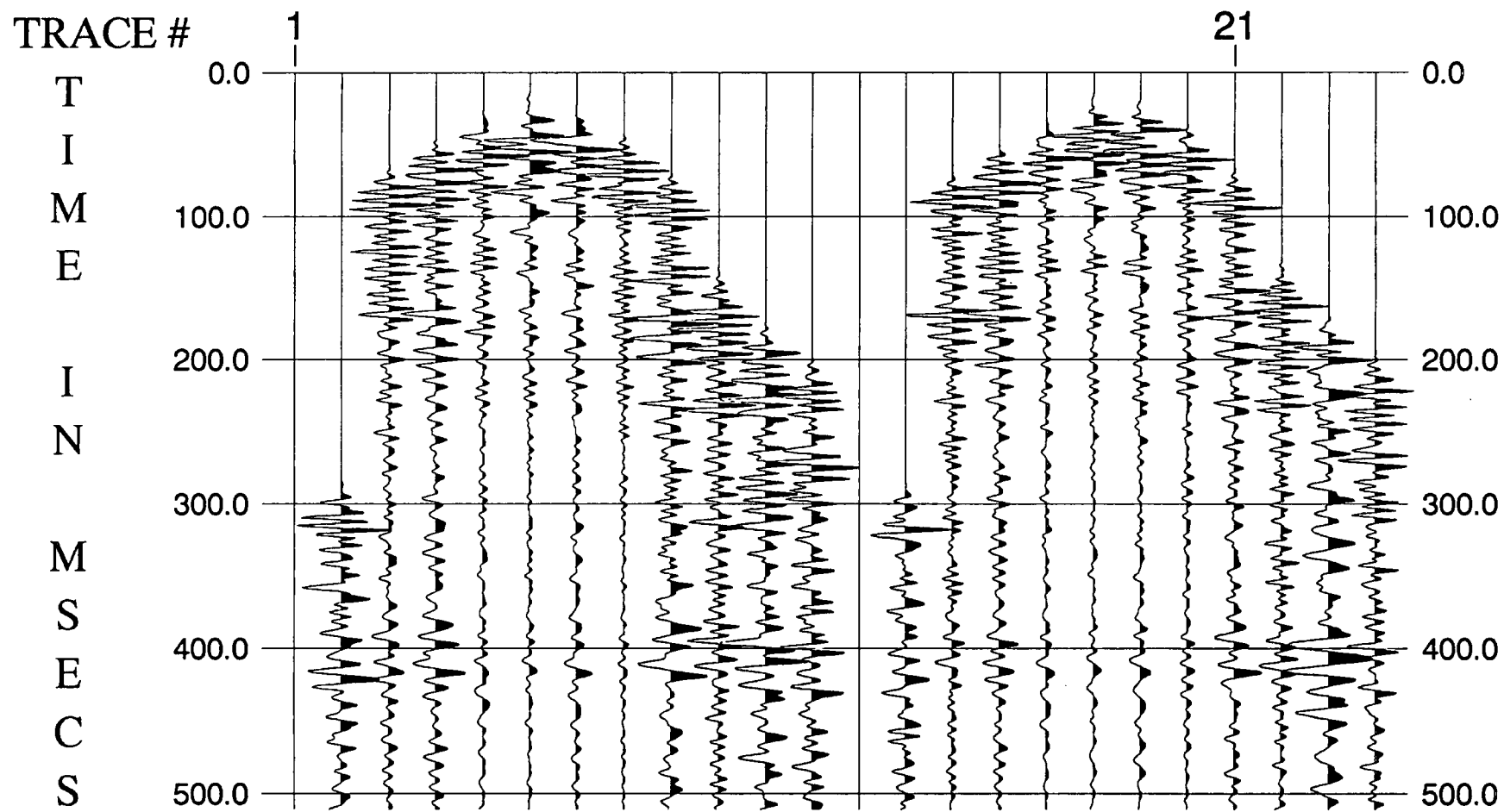


Figure 3.8 CDP gathers 999 and 1000: (a) without NMO corrections.

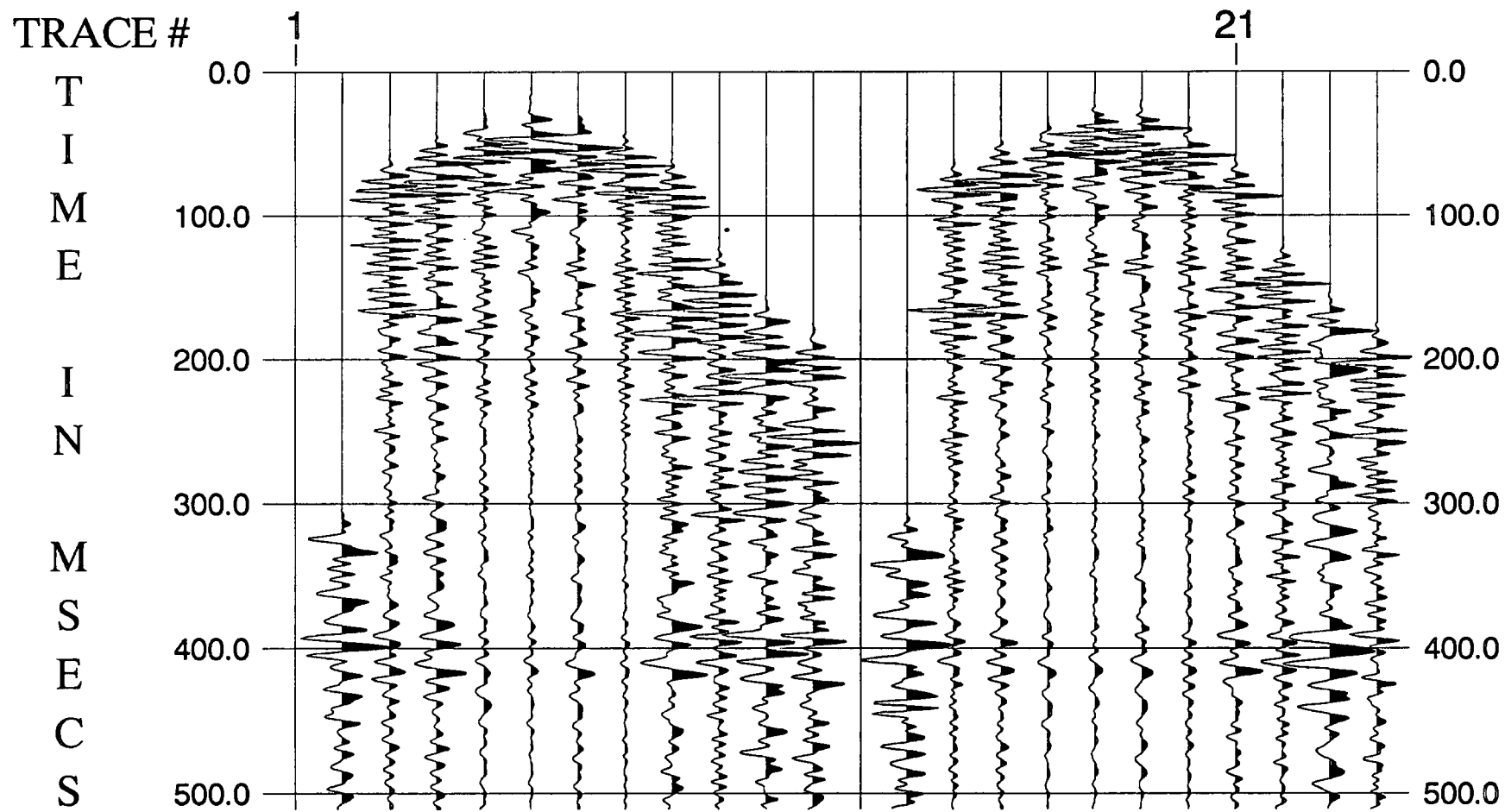


Figure 3.8 CDP gathers 999 and 1000: (b) with NMO corrections applied.

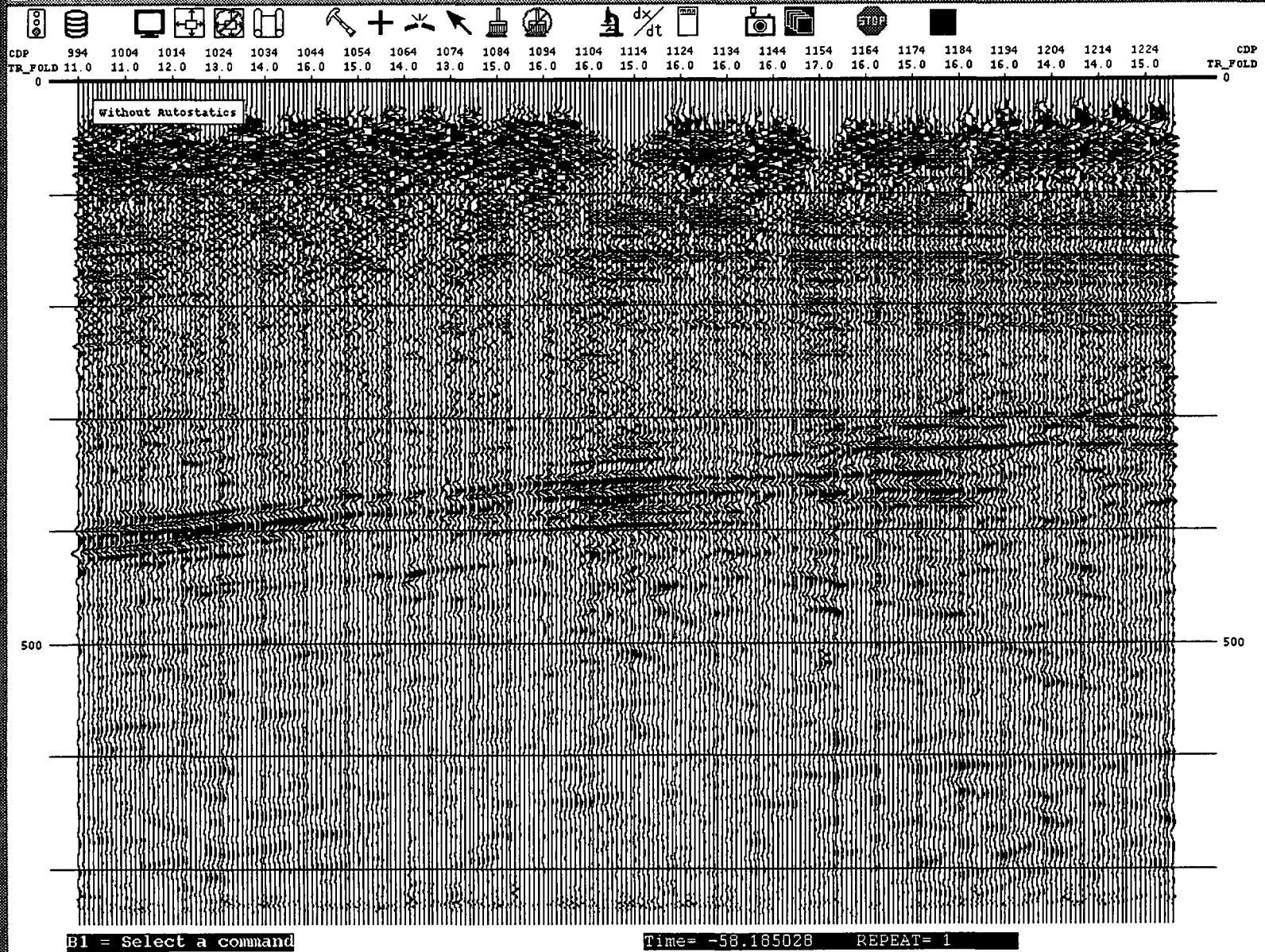


Figure 3.9 Comparison of the stack: (a) without autostatics.

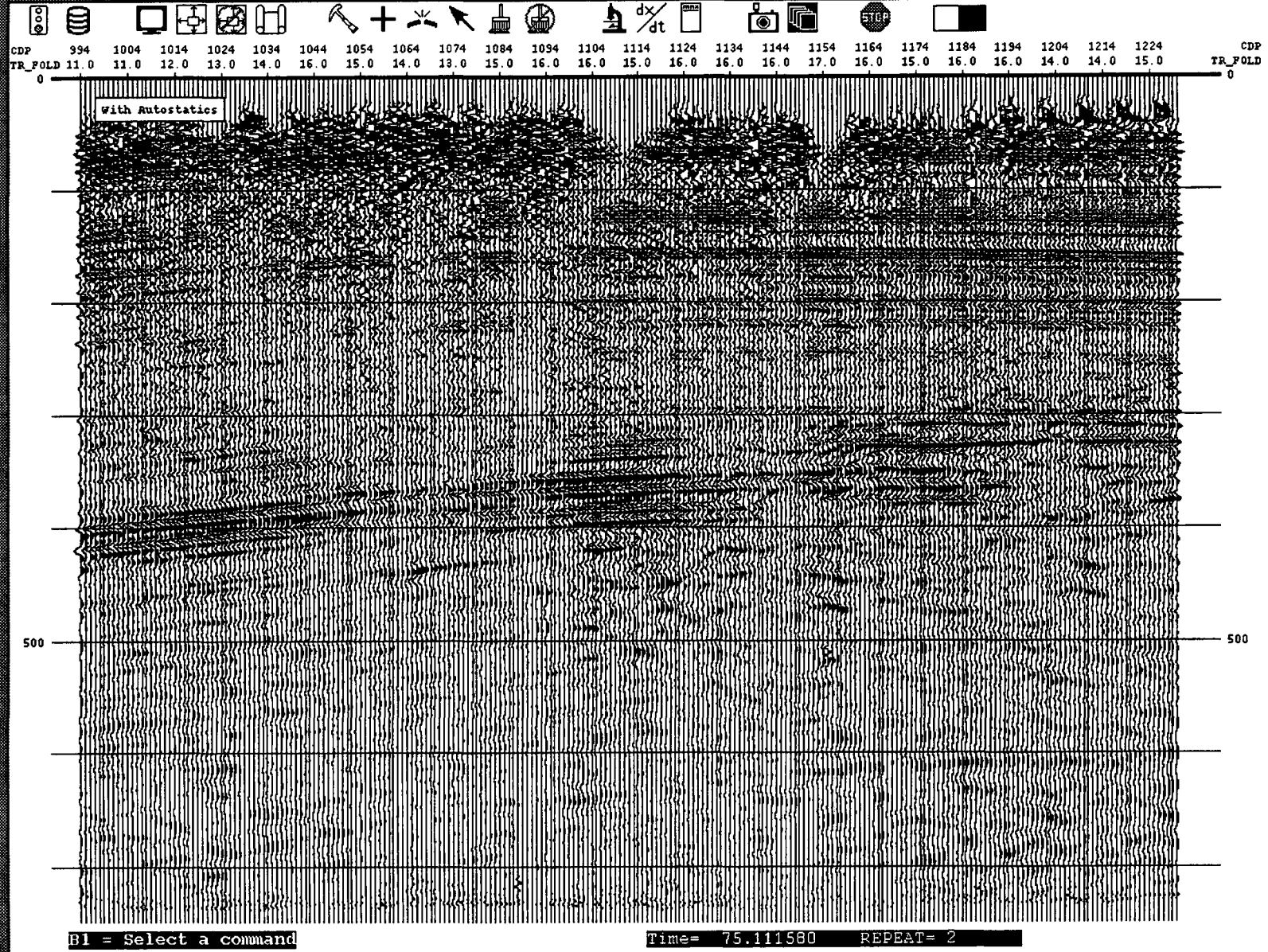


Figure 3.9 Comparison of the stack: (b) with autostatics applied.

comparison of NMO corrections applied between CDPs 999-1000 are shown in Fig. 3.8a (before) and Fig. 3.8b (after).

Reflection times are commonly affected by irregularities in the near-surface. To improve stacking quality, residual statics (autostatics) corrections are needed on the moveout-corrected CDP gathers. This is done in a surface-consistent manner; i.e. time shifts are dependent only on shot and receiver locations, not on the raypaths from shots to receivers. The estimated residual corrections are applied to the original CDP gathers with no NMO corrections applied. Velocity analysis may then be repeated to improve the velocity picks.

There are currently five automatic statics options available in ProMAX. All of these, except "CDP Correlation Trim Statics", are surface-consistent solutions: "Maximum Power Autostatics", "Model-Based Correlation Autostatics", "Differential Autostatics", and "Summed Differential Autostatics". The Model-Based Correlation Autostatics was applied to the data in my case. This process measures time shifts relative to a model, and uses a modified Gauss-Seidel method to partition these time shifts into source and receiver statics. It also performs a horizon velocity analysis as part of the estimation of the residual NMO term, and writes these results to the database. The method is relatively insensitive to moderate velocity errors in good quality data (Wiggins et al., 1976).

The maximum static shift allowed was set to 4 ms. The "Compare Autostatics Stack" MACRO process was used to demonstrate the improvement due to autostatics by creating two CDP stacks, one without (Fig. 3.9a) and one with (Fig. 3.9b) autostatics applied.

### 3.1.9 Constant Velocity Stacking (CVS)

The method of "Constant Velocity Stacking" of certain CDP gathers is an alternative technique for velocity analysis. The most important reason for obtaining a reliable velocity function is to get the best quality stack of signal. Therefore, stacking velocities are often

estimated from data stacked with a range of constant velocities on the basis of stacked event amplitude and continuity.

This 'process' is actually a macro consisting of following process:

Apply AGC (optional)

Constant Velocity Stacks

Screen Display (for the user to pick the CVS panel)

The velocity input option was chosen as "Calculated" for creating stack panels. This "Calculated" option results in a set of velocities which are sampled more finely at low velocities in order to give approximately equal increments in NMO.

After CVS, the "Model-Based Correlation Autostatics" process was applied again using this new velocity table to improve the SNR.

#### 3.1.10 Trim Statics

After all efforts have been made to obtain the optimum statics and velocity solutions, it is a good idea to perform a final pass of non-surface-consistent CDP trim statics. Trim statics are used to optimize trace alignment within a CDP gather. The traces within a CDP gather are cross-correlated against a smoothed version of the corresponding stacked trace. The cross-correlations are used to pick time shifts which will best align the CDP gather traces with the reference stacked trace.

ProMAX provides this tool which computes these trace-by-trace trim statics and loads their values into the database. The resulting statics can be loaded from the database into the trace headers and applied before CDP stacking. To do this, use the "Database/Header Transfer Tool", followed by the "Header Statics Tool".

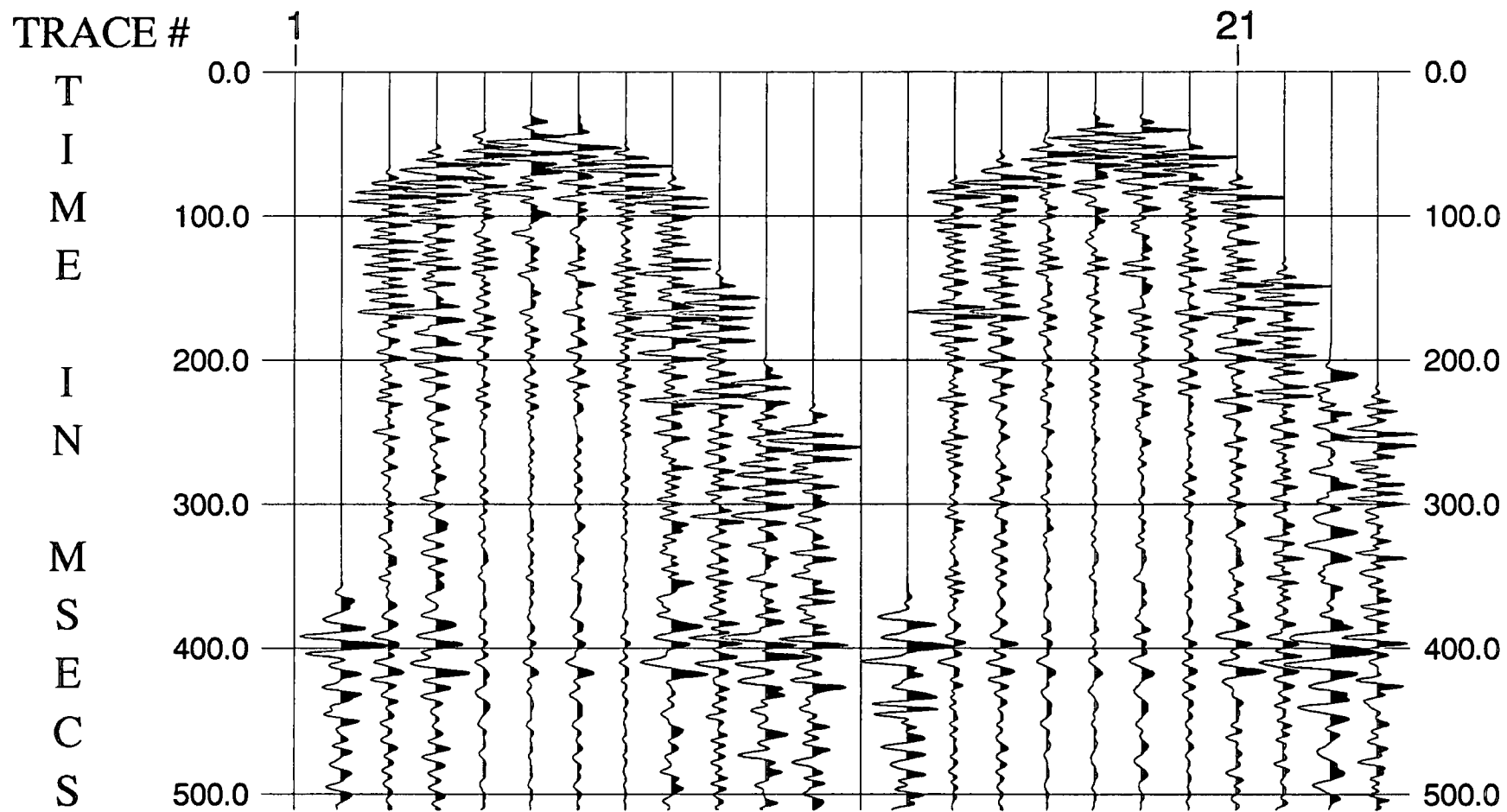


Figure 3.10 CDP gathers 999-1000: (a) without trim statics.

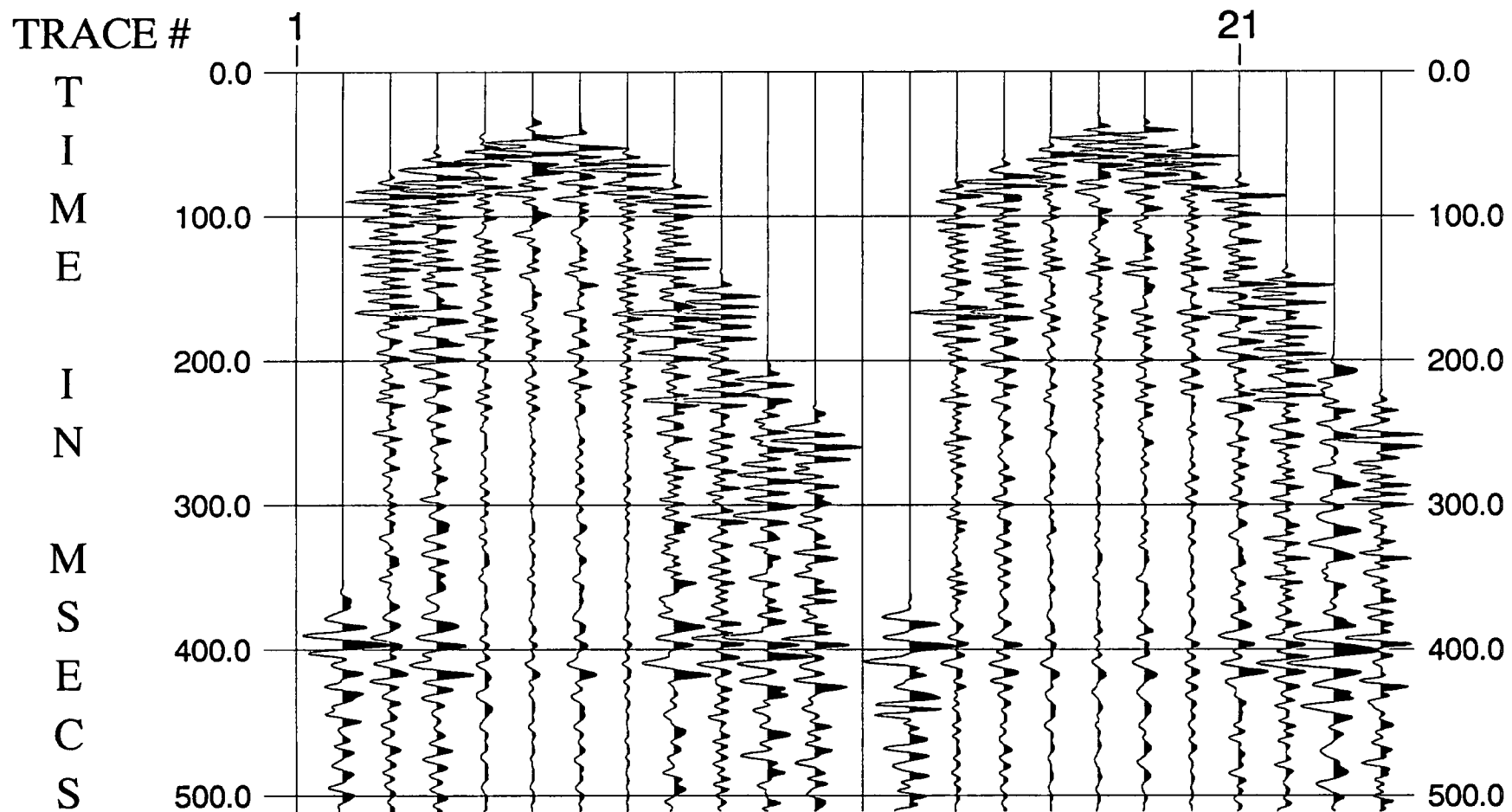


Figure 3.10 CDP gathers 999-1000: (b) with trim statics applied.

The maximum static shift allowed was set to 4 ms and a horizon file was generated from IVA process. It was found that trim statics performed better if the process was applied twice, rather than only once, judging by the stacking results. Figures 3.10a (without trim statics) and 3.10b (with trim statics) show the comparison. IVA was carried out for a second time in order to get an up-to-date horizon table between the two applications of trim statics.

### 3.1.11 Stacking, Trace Equalization and Filtering

In order to get a better quality of stack, a trace equalization was applied to the traces in each CDP gather. This means that all the traces contribute equally in a CDP gather. The details of this process will be discussed later.

The "CDP/Ensemble Stack" process vertically stacks input ensembles of traces. Vertical stack algorithms include: (1) straight mean; (2) header value weighted; (3) sign bit stack; (4) minimum/maximum; (5) sample value exclusion stack; (6) diversity sum; (7) median and (8) alpha-trimmed mean.

The straight mean stack was applied, which sums the sample values and divides by the number of samples summed raised to a user-supplied power. The value of 0.5 was normally chosen to scale by the square root of the number of samples.

This time a Butterworth bandpass filter (Oppenheim and Schaffer, 1975) was used in which low frequency, low slope, high frequency and high slope was specified. The Butterworth ramps defined in the frequency domain are formed by

$$R=1/\sqrt{1 + (F/FMID)^{2P}} \quad (3.2)$$

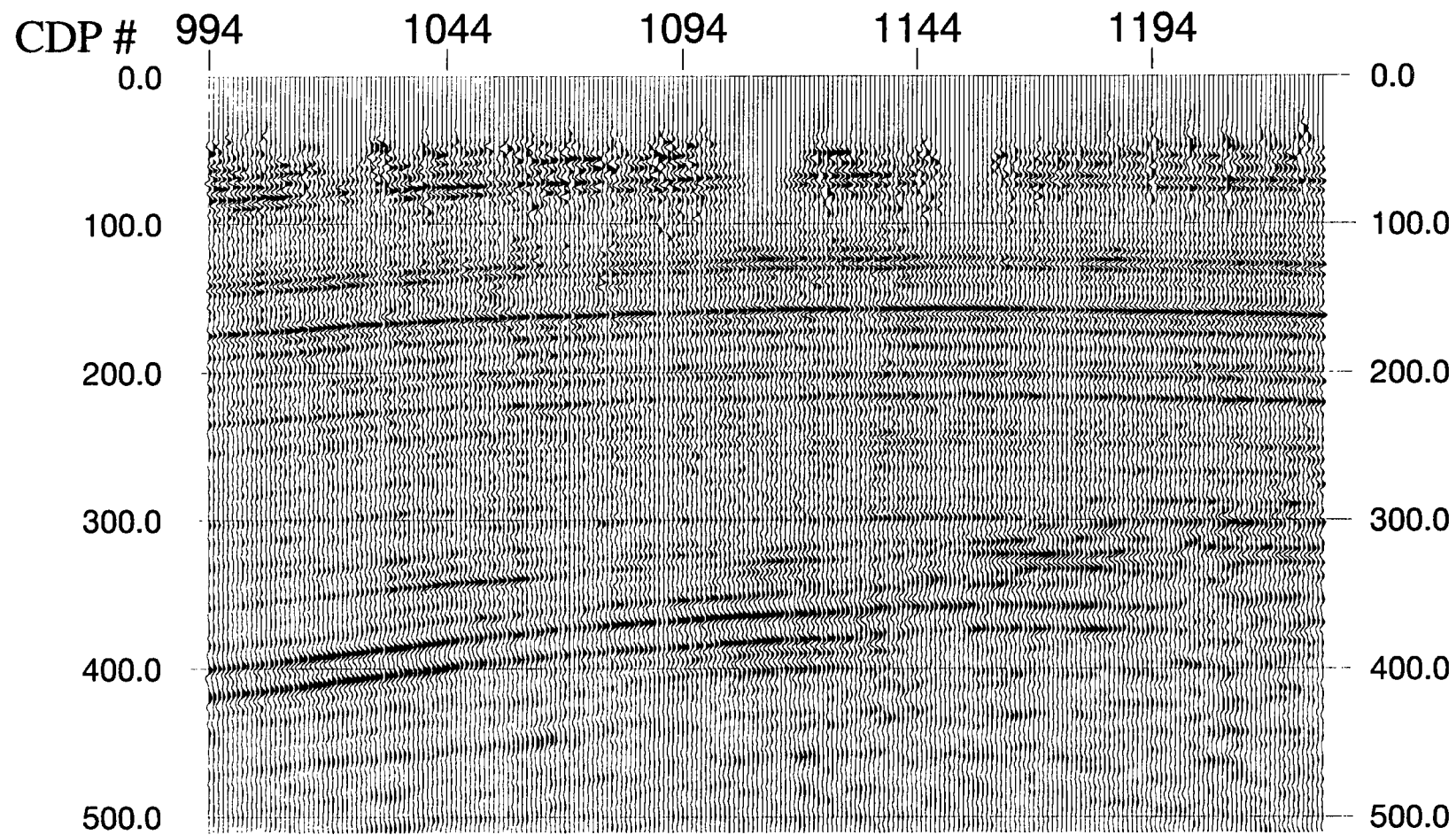


**Figure 3.11** Stacked section with all above procedures carried out.

where FMID is the centre frequency of the pass band and P is computed for the lower and upper slopes to get the correct db/octave rolloff. The parameters were chosen as: low cut - 30 Hz, 10 db/octave; high cut - 200 Hz, 20 db/octave. A Butterworth bandpass filter was chosen to match British Coal's processing in order to make a fair comparison. However, the lower and upper slopes are different (See Fig. 3.2).

For the purpose of the later inversion, "Trace Equalization" was performed here. This is a trace-to-trace amplitude balancing function. This program uses a single time window for each trace, which may be spatially varied by a primary and a secondary key. The amplitude in the window is computed, and a scalar calculated to convert this amplitude to a constant value. This scalar is then applied to the entire trace. In this way, variations in amplitude between traces are reduced.

The time gate parameter was set as 851:70-500/1350:60-500/ which means that at CDP 851 the time gate was between 70 ms and 500 ms, and at CDP 1350 the time gate was between 60 ms and 500 ms. The parameters were interpolated for other CDPs between these two. The result of this processing is shown in Fig. 3.11.

It should be pointed that in the British Coal's processing of the data, the time-variant digital bandpass filter and time-variant trace equalization applied at this stage in processing were different from the time-invariant one applied here.

### 3.1.12 F-K Analysis and F-K Filtering

Multichannel processes can be useful in discriminating against noise and enhancing signal on the basis of a criterion that can be distinguished from trace to trace, such as dip or moveout. The 2-D Fourier transform is a basis for both analysis and implementation of multi-channel processes.

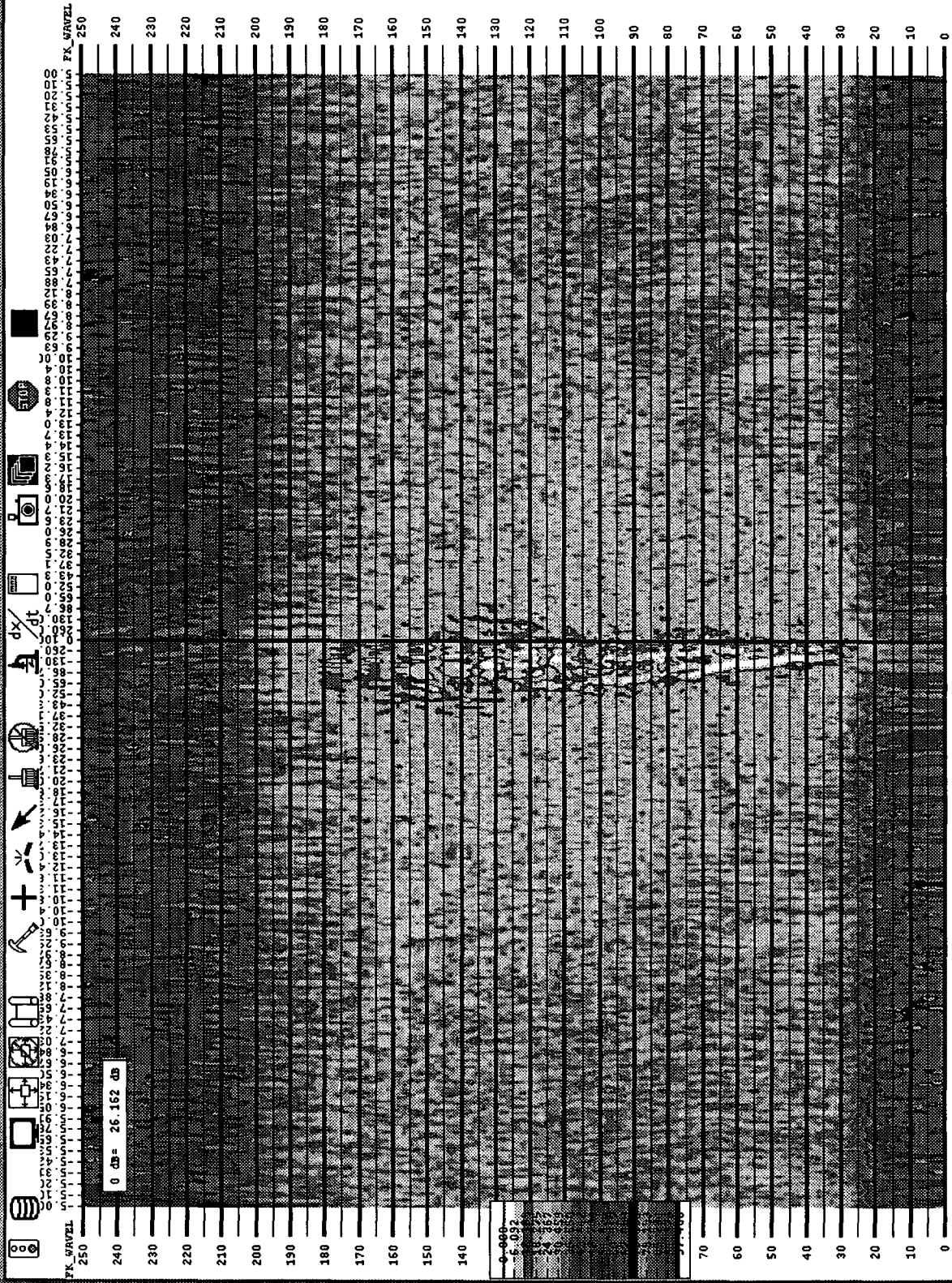


Figure 3.12 F-K analysis for picking of F-K filter polygons.

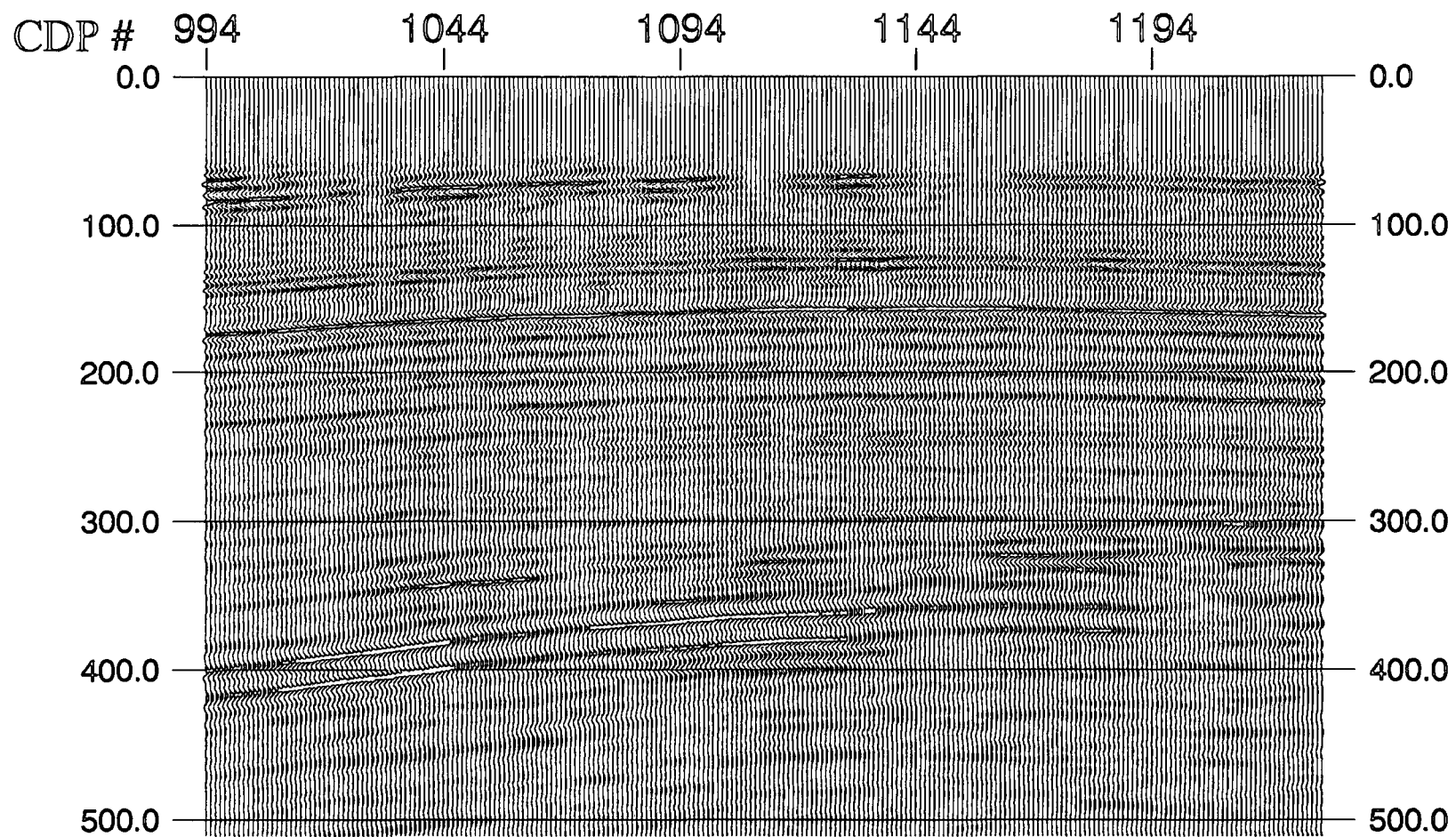


Figure 3.13 The stacked section with F-K filter applied.

Events that dip in the (t,x) plane can be separated in the (f,k) plane by their dips. This allows us to eliminate certain types of unwanted energy from the data. In particular, coherent linear noise (in the form of ground roll), guided waves, and side-scattered energy commonly obscure the genuine reflections that may be present in recorded data. These types of noise usually are isolated from the reflection energy in (f,k) space (Yilmaz, 1987).

Before F-K filtering, the "F-K Analysis" was run. This transforms the data from time and space (t,x) sample values to frequency and wavenumber (f,k) values and displays the results. The displays supported interactive picking of F-K filter polygons (Fig. 3.12).

For F-K filtering, the fan or pie-slice filters are specified by frequency and velocity limits. The program allows data to be passed or rejected within the selected windows. The maximum attenuation and the portion of the zone to be passed at 100% are also under user control. The parameters I chose are: (1) Type of filter: fan filter; (2) Panel width in traces: 256; (3) Fan filter parameters: -2500,4000,30,200 (velocity1-velocity2-frequency1-frequency2); (4) Mode of filter operation: accept; (5) Percent flat for accept zones: 90; (6) Minimum filter attenuation level: 0.001.

The result of the F-K filter is shown in Fig. 3.13. Comparing with Fig. 3.11, it is easy to see that the noise appearing between 250 and 350 ms on the right hand of the section is completely removed from the section.

### 3.1.13 Migration

Migration is the process of converting the seismic response on stacked sections into its true structure; diffractions are migrated back to their diffraction points at faults, multibranch reflections are migrated into their true synclinal shapes, anticlines are slimmed down, and apparent dips are converted to true dips. For 2D data, migration can only work

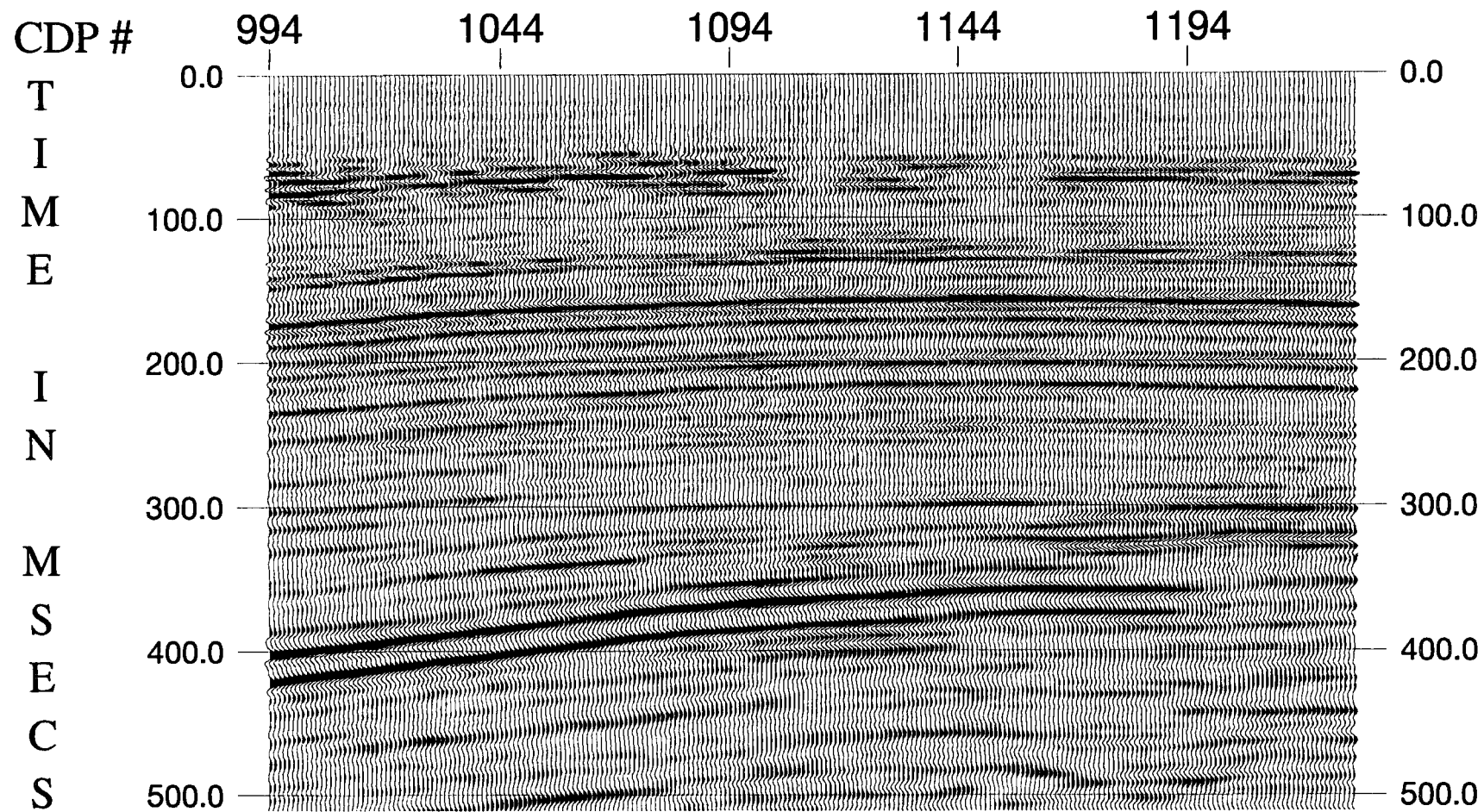


**Figure 3.14** The migrated section reprocessed with ProMAX.

correctly if the line is oriented in the dip direction. Otherwise out-of-plane events will be present on the section.

Since the formal solution of the acoustic wave equation in inhomogeneous media is generally an impossibility, resort has been made to numerical methods. In particular, these methods may be based on calculation of finite differences, and "Steep Dip FD Time Migration" was chosen for the processing. This process performed a post-stack time migration on an input stack section using a finite difference algorithm capable of improved accuracy at steep dips. The migration algorithm is implemented in the frequency-space domain, i.e.  $(f,x,z)$ , requiring that the input stacked section be transformed from time to frequency (Claerbout, 1985).

The parameters were set as: (1) Minimum frequency to migrate (in Hz): 30; (2) Maximum frequency vs. depth to migrate: 0-200,2000-160 (Depth1-Max. Frequency1, Depth2-Max. Frequency2); (3) Percent velocity scale factor: 50; (4) Time attenuation factor (dB/sec): 0.2; (5) Largest angle to be properly migrated: 65 (migrated to 65 degrees).

Figure 3.14 showed the migrated section. Comparing Figs 3.1 and 3.14, the differences between the data processed by British Coal and the reprocessed data can be seen.

Firstly, there are some obvious differences in the shallow area. In my reprocessed section, there are no reflections above 50 ms, whereas British Coal's section contains some strong reflections there, and the continuity of the events above 100 ms is not as good as British Coal's. I found that these differences resulted from the different filters applied in the processing flows. Because a time variant bandpass filter was applied in British Coal's processing, the bandpass between 0 and 200 ms is 60 - 200 Hz whereas mine is 30 - 200 Hz along the whole trace. I have found by testing that if the lowcut frequency is increased, the shallow data in my reprocessed section do look more similar to British Coal's section.

However, the continuity of the target coal seams between 300 ms and 440 ms was worse than Fig. 3.14. Therefore, the bandpass of 30 - 200 Hz was preferred.

Secondly, the SNR of whole section is improved due to the carefully repeated velocity analysis and autostatics. This will be discussed later in Chapter 5 where the improvement is demonstrated by comparing their correlation coefficients with the well log.

Finally, the continuity of the two main coal seams, at 400 ms and 420 ms at CDP 994, in my reprocessed data are better than British Coal's, especially between CDP 1175 and CDP 1196. This will be helpful for the inversion.

## 3.2 Use of Logging and Coring Information

### 3.2.1 Introduction

As is generally known, most formations are altered when a borehole is drilled through them. The more competent formations show an imperceptible change, while the softer formations often suffer significant, obvious alterations. Everyone who has worked quantitatively with well logs recognizes that it is not uncommon for portions of a well log to contain data that may be significantly different from the true, in situ formation properties. This may be due to either log calibration problems or environmental conditions.

Ausburn (1977) suggested that one should use three different levels of log editing, which he called mechanical, interpretative and modelling. These log editing methods should be carried out before time-depth reconciliation.

SK 72 SW		BRITISH COAL NOTTINGHAMSHIRE GROUP			118					
THORNY PLANTATION SURFACE BOREHOLE										
SEAM ANALYSED STRATIGRAPHIC HORIZON	DEPTH (metres)	LITHOLOGY	FAUNA / FLORA	STRATA DESCRIPTION	SEAM DETAILS (cm)	CORE DIP Dip Az B	TRUE DIP	GEOPHYSICAL LOG	DRILLING FORMAT	CASING IN HOLE
Clay Cross SOAM Lower Gynl	500			lt fls / lt fls Coal / IC 24 at 486.15 Flotrio	10 17 2					
BROWN RAKE				fls 16 7 at 504.56						
BLACK RAKE	510			rip tr dr. pyr limestone fls 16 30 at 508.17 16 24 at 508.37 16 9 at 510.52 rip tr dr.						
	520			Coal 1 at 518.35 strong rip						
DEEP MAIN	530			rip IC 5 at 528.82 Coal / IC 258 at 529.51 16 8 at 530.81 16 5 at 530.85	14 7 4 2 39					
	540			pyr tr dr. rip biturb lt Pop dunes						
	550			rip biturb		2°				
PARKGATE/TUPTON	560			pyr Coal 331 at 558.08 Lest Core lt IC 43 at 560.80	40 8 38 15 107 4 119					
THREEQUARTERS				pyr						
YARD YARD FLOOR COAL	570			lt Coal / IC 38 at 573.03 Coal 25 at 574.18	12 31 3 25					

Figure 3.17 Lithology profile (part) of Thorny Plantation borehole.

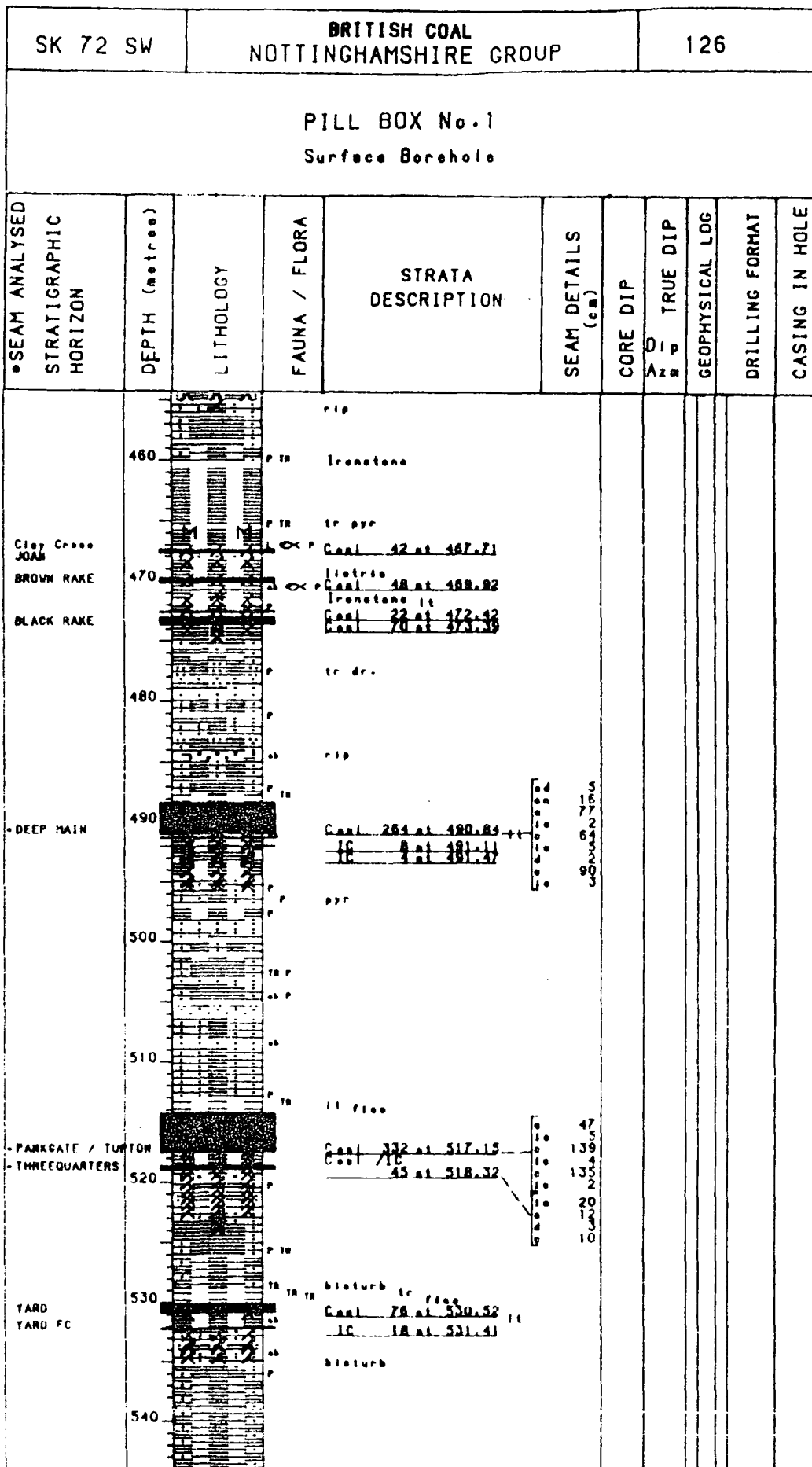


Figure 3.18 Lithology profile (part) of Pillbox borehole.

Figure 3.19 Edited sonic log at Thorny Plantation borehole.

# Edited Sonic Log at TP Borehole

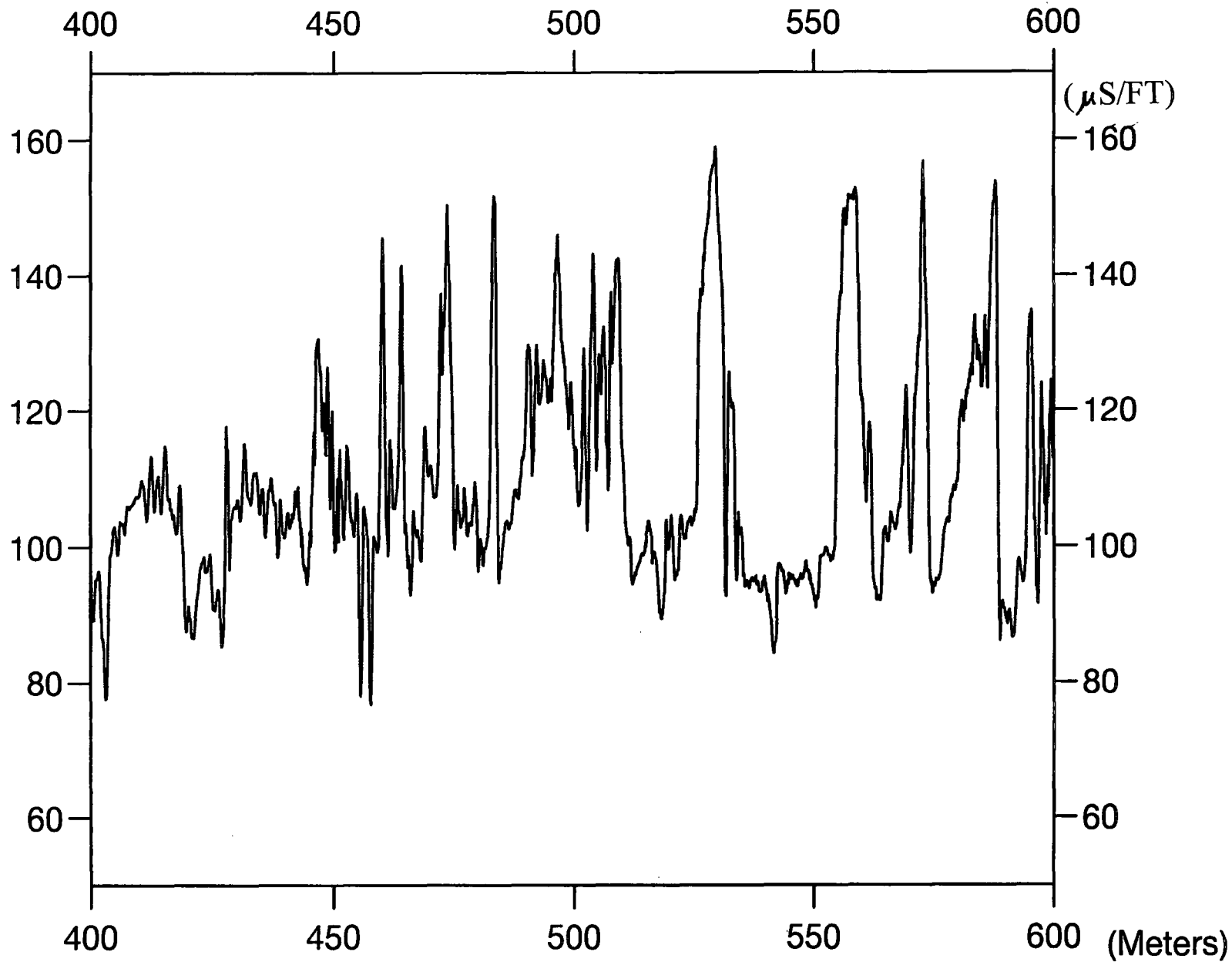
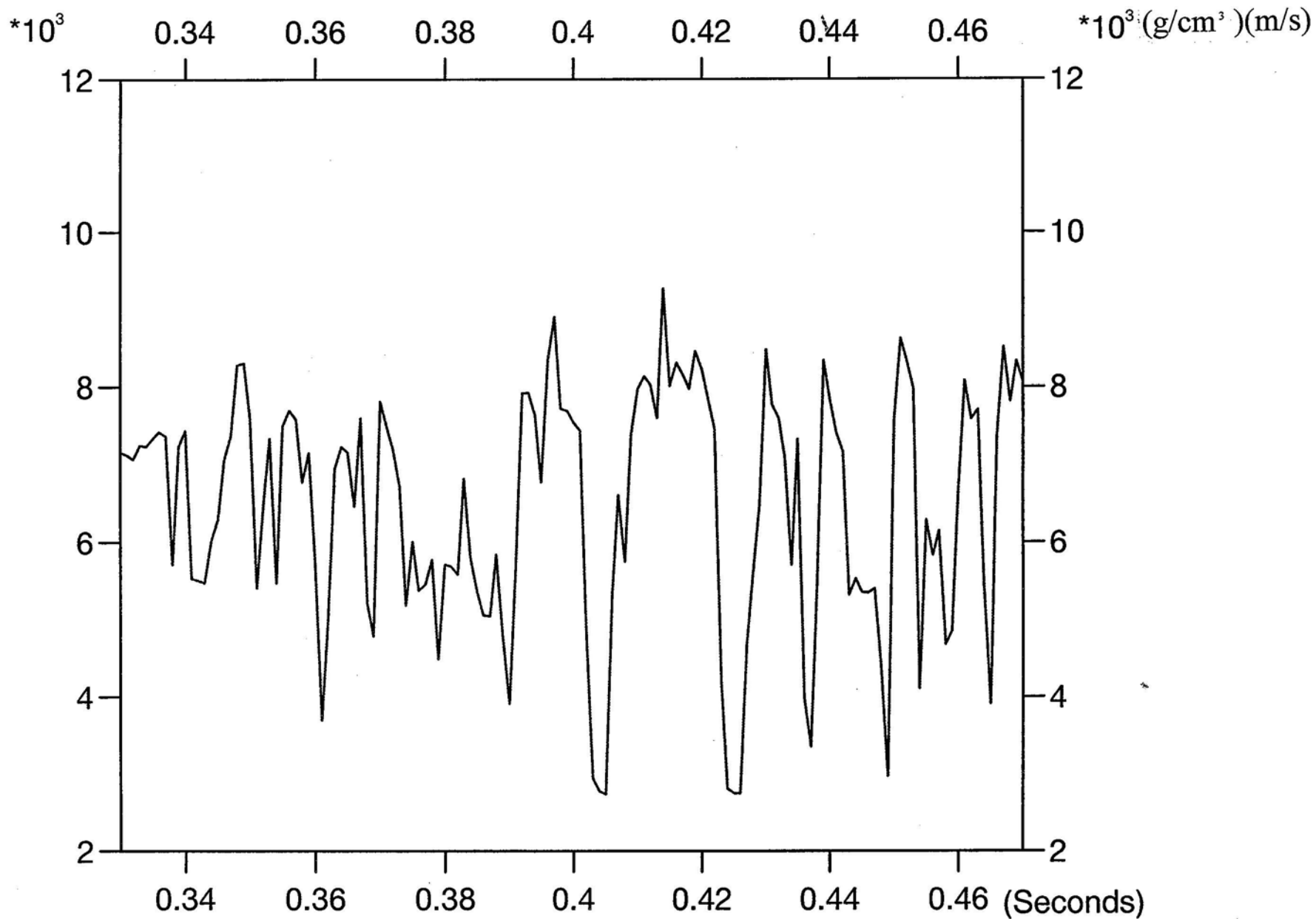


Figure 3.20 Acoustic impedance plotted against two-way travel time at Thorny Plantation.

# Acous. Imp. in Two-way Time at TP



### 3.2.2 Mechanical Log Editing

Due to the compensated sidewall tool used for the density log, the calibration error was supposed to be negligible. Therefore mechanical editing included the detection of obvious instrument/electronic noise (cycle skipping and so on) in the sonic log from Thorny Plantation ( at 515 m and 540 m on Fig. 3.15) and obvious hole-related errors from Pillbox (at about 500 m on Fig. 3.16).

### 3.2.3 Interpretative Well Log Editing

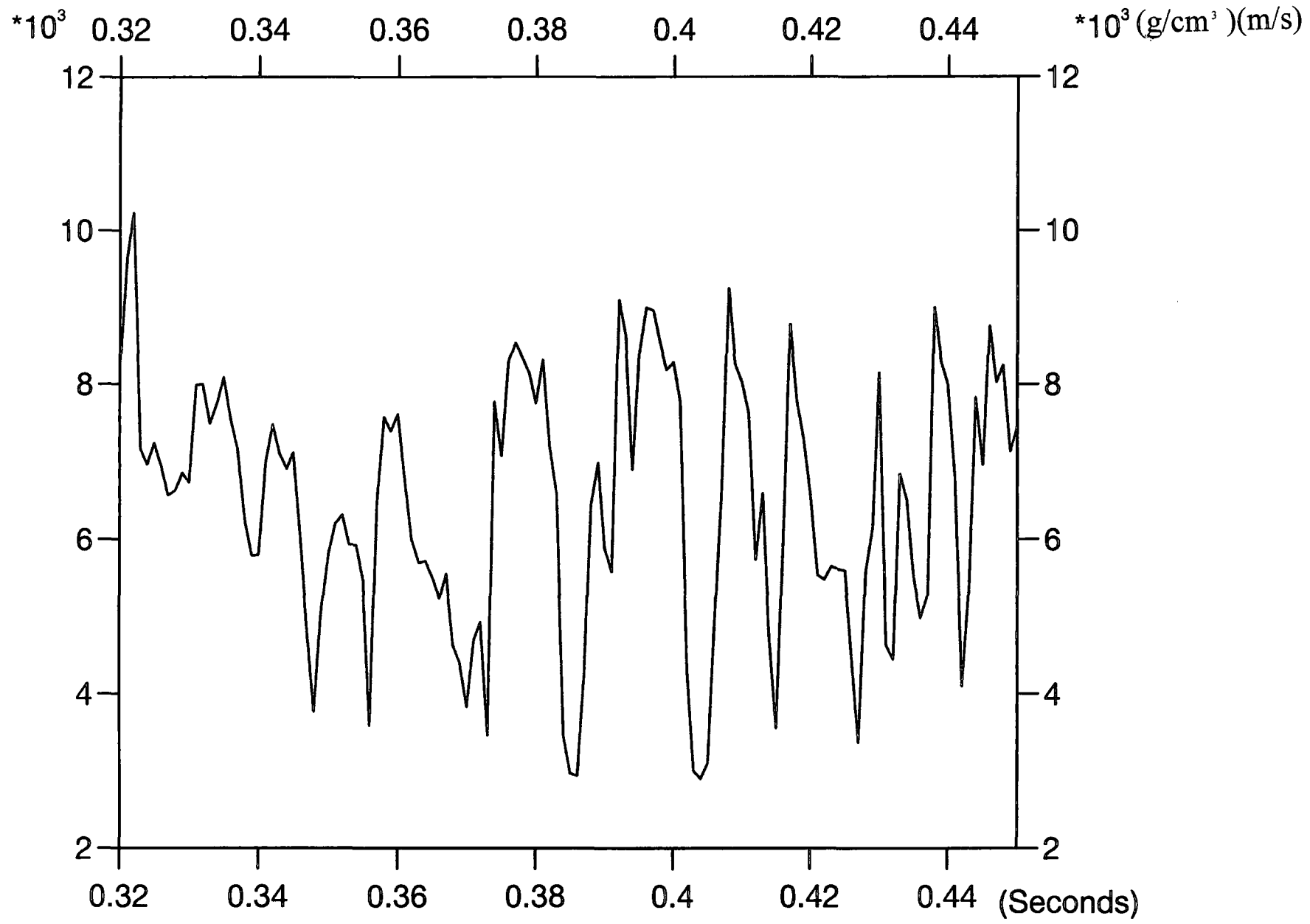
This type of editing included making judgements in both recognizing bad data values and in substituting better ones. Because the lithologies from coring information (Fig. 3.17 for Thorny Plantation and Fig. 3.18 for Pillbox), and other logs are available (neutron and gamma, etc.), it is not too difficult to identify the lithology and estimate corresponding sonic or density values. Figure 3.19 shows the edited sonic log data from Thorny Plantation. Some smoothing was also applied in this process based on interpretative judgement using the other available information.

### 3.2.4 Modelling Well Log Editing

After the above two editing procedures, the forward model (seismic response) based on the edited acoustic impedance to compare with the observed data (seismic information) can be calculated. It can be shown whether the editing has improved the correlation or not by using the correlation coefficient defined by equation (2.20)<sup>2</sup>. If the edited model produces a better result, it is accepted; otherwise some further editing is required. For example, there are some very high sonic values giving the appearance of a thick coal seam at about 490 m depth on the well log at Thorny Plantation borehole (Fig. 3.15), but on the lithology profile at the corresponding depth there is only a thin (0.24 m) coal seam (Fig.

Figure 3.21 Acoustic impedance plotted against two-way travel time at Pillbox.

# Acous. Imp. in Two-way Time at PB



3.17). I corrected these high values to the same lower values as the surrounding rocks. The corrections were accepted because the correlation coefficient is increased following corrections.

This so-called modelling method is totally different from Ausburn's (1977). He used either theoretical relationships or empirical observations of the saturated rocks to calculate the formation density and wave velocity. In my editing, the values of real density and velocity are more important than knowing precisely the lithological composition. This is because his objective was to interpret the well logs in terms of lithology, whereas I am attempting to invert seismic data.

### 3.2.5 Depth-Time Reconciliation

In order to get an acoustic impedance log in terms of two-way travel time for the purpose of inversion, a depth-time transformation has to be applied. There is a major difference between this reconciliation and time-depth transformation in seismic reflection interpretation. In the well log, the depth interval is very fine (1 cm), so interpolation is not required. Here the fraction of the depth interval and average value of velocities for the integer sample period should be considered instead. The results are shown in Figs 3.20 (Thorny Plantation) and 3.21 (Pillbox).

## 3.3 Inversion Procedure

### 3.3.1 Introduction

In Cooke and Schneider's (1983) GLI method some constraints were required. Firstly, in the initial guess model the location of each boundary must lie within a distance  $X$  of the solution. The distance  $X$  is defined as one-half of the central lobe width of the source

wavelet (normally less than 4 samples in the time domain). That is difficult to realise for the reflected events in a recorded trace. Secondly, the polarity at each impedance contrast should have the same polarity as the corresponding arrival on the seismic trace to be inverted. This is also not easy to do, especially if there is no prior knowledge about the wavelet. This, in my opinion, directly led to their conclusion that residual wavelet effects are negligible, allowing them to assume a zero-phase wavelet in all cases.

A modified GLI method using a parameterized wavelet as well as a parameterized earth model is developed here to overcome these faults. The initial guess for the model parameters is best obtained using well data, but an alternative method based solely on the seismic trace, which inverts for the reflection coefficient sequence, has also been implemented.

### 3.3.2 Initial Guess for the Earth Model

After well log editing, I have got the acoustic impedance as a function of two-way travel time. Based on this acoustic impedance information and the post-stack section from field seismic data, an inversion window and the number of layers (blocks) can be selected. Of course, this task is not an easy one and will be discussed in a systematic study of the real dataset in Chapter 5.

Then the initial guess parameters for the earth model can be established. Starting at the top of the model, each layer needs three parameters to describe it: the location of the bottom boundary in two-way travel time  $\tau$ , the acoustic impedance  $p$  at the bottom of the layer, and the gradient of acoustic impedance  $g$ . In the  $j$ th layer, the acoustic impedance at each sample is given by

$$e_i = p_j + g_j(\tau_j - i) \quad (\tau_{j-1} \leq i \leq \tau_j). \quad (3.3)$$

According to equation (2.5), the reflection coefficient sequence  $r$  in discrete form at each sample is expressed by

$$r_i = \frac{e_{i-1} - e_i}{e_{i-1} + e_i} \quad (3.4)$$

The first trace to be inverted should be at the nearest CDP to the well on which the guess model is based.

### 3.3.3 Wavelet Extraction

To solve those problems mentioned in §3.3.1, the first step is to extract a fairly accurate wavelet by applied a Wiener shaping filter (Robinson and Treitel, 1980) using the observed trace and prior knowledge about the acoustic impedance, which in my case comes from the well logs.

The Wiener shaping filter  $w$  is the best  $(m+1)$ -length filter, in the least-error energy sense, which may be convolved with the  $(n+1)$ -length input reflection coefficient sequence  $r$  (derived from edited well logs) to match an  $(m+n+1)$ -length desired output  $d$ , which is the observed trace at the well.

The normal equations are:

$$\sum_{i=0}^m w_i a_{j-i} = g_j \quad (j=0, 1, 2, \dots, m), \quad (3.5)$$

where the unknown  $w_i$  are the weighting coefficients of the Wiener shaping filter, the known  $a_{j-i}$  are the autocorrelation coefficients of the input  $r$ , and the known  $g_j$  are the cross-correlation coefficients between the desired output  $d$  and the input  $r$ . The Levinson recursion was used to solve the normal equations.

In order to get the best filter (wavelet estimate), the desired output had to be shifted to and fro in time. For each time shift, the error energy defined in (2.18) between the actual output and the desired output was calculated. The best filter was chosen according to the minimum error energy and the corresponding time shift was then applied to the observed trace. There are several sources of error contributing to this time shift, some resulting from the fact that the well logs and seismic section are referred to different datum levels. It is assumed that this time shift will be present in all the traces along the section.

### 3.3.4 Wavelet Parameterization

In my inversion, the wavelet is to be defined by a maximum of eight parameters in the frequency domain (see §2.4). The best-fitting values of these eight parameters need to be found for the wavelet extracted by the Wiener shaping filter. These values then define the initial guess of the wavelet parameters prior to GLI.

The amplitude spectrum  $A(f)$  of the extracted wavelet  $w(t)$  is studied for obtaining the frequency parameters. If  $f_{\max}$  is the frequency corresponding to the maximum value  $A_{\max}$  of amplitude spectrum, then four frequency parameters are defined as follows. First,  $f_2$  is the largest frequency less than  $f_{\max}$  such that  $A(f_2) = 0.8 A_{\max}$ . Secondly,  $f_3$  is the smallest frequency greater than  $f_{\max}$  such that  $A(f_3) = 0.8 A_{\max}$ . Similarly,  $f_1$  is the largest frequency less than  $f_{\max}$  such that  $A(f_1) = 0.2 A_{\max}$ ; and  $f_4$  is the smallest frequency greater than  $f_{\max}$  such that  $A(f_4) = 0.2 A_{\max}$ .

In order to fit the quadratic polynomial for the phase spectrum given in equation (2.18), it is necessary to unwrap the phase spectrum of the extracted wavelet. This can be done in the frequency domain, as described by Shatilo (1992), using the polynomial fitting technique (User's Manual of NAG Fortran Subroutines).

The initial phase spectrum of the extracted wavelet  $w(t)$  may be written as

$$\Phi_{in}(f) = \arctan\{\text{Im}[W(f)]/\text{Re}[W(f)]\}, \quad (3.6)$$

where  $W(f)$  is the complex spectrum of  $w(t)$ , for  $(-\pi/2) \leq \Phi_{in}(f) \leq \pi/2$ . Transformation from  $\Phi_{in}(f)$  to  $\Phi_{pr}(f)$  for  $-\pi \leq \Phi_{pr}(f) \leq \pi$  can be done by analysis of the sign combination of  $\text{Re}[W(f)]$  and  $\text{Im}[W(f)]$ .  $\Phi_{pr}(f)$  is the main (or principal) value of the phase spectrum  $\Phi(f)$ , given by traditional spectral analysis of the phase spectrum alone. Since the true value of the phase spectrum  $\Phi(f)$  lies between  $-\infty$  and  $+\infty$ ,  $\Phi(f)$  and  $\Phi_{pr}(f)$  are related by the expression

$$\Phi(f) = \Phi_{pr}(f) + 2\pi n, \quad (3.7)$$

where  $n$  is an integer. The transition from  $\Phi_{pr}(f)$  to  $\Phi(f)$  is called phase unwrapping (or phase restoration).

Phase unwrapping should remove discontinuities in the phase spectrum  $\Phi_{pr}(f)$ . Two types of discontinuity have been defined (Poggiagliolmi et al., 1982). The first is a discontinuity of  $2\pi$  caused by a complex vector transition from one sheet in the Riemann surface to another, and the second is a discontinuity of  $\pi$  at the frequency where the wavelet amplitude spectrum  $A(f)$  is equal to zero. The second one does not occur within the signal bandwidth of the extracted wavelet in my examples. Therefore I adopted the phase restoration presented by Shafer (1969), in which he proposed taking the phase increment  $\Delta\Phi_{pr}(\Delta f)$  between two adjacent frequency points  $\Delta f = f_i - f_{i-1}$

$$\Delta\Phi_{pr}(\Delta f) = |\Phi_{pr}(f_i) - \Phi_{pr}(f_{i-1})|, \quad (3.8)$$

It is assumed that a discontinuity of  $2\pi$  exists if  $\Delta\Phi_{\text{pr}}(\Delta f)$  exceeds  $\pi$ . The unwrapping process starts at zero frequency and it is repeated for each consecutive harmonic. And the sign of this  $2\pi$  is the same as the sign of  $\Phi_{\text{pr}}(f_i) - \Phi_{\text{pr}}(f_{i-1})$ .

Then I approximate the phase spectrum as defined in (2.18). Because  $\Phi$  is known, it is possible to find  $\varphi_0$ ,  $\varphi_1$  and  $\varphi_2$  by polynomial fitting. In order to get a better match for the wavelet, I fit the phase spectrum only in the range between  $f_2$  and  $f_3$ . However, the subroutine E02ACF from the NAG Fortran Library treats  $f_2$  as a coordinate origin in order to get an intersection value with ordinate axis. Therefore a simple transformation of the frequency coordinate (abscissa) is needed. After fitting, the reverse coordinate transformation is carried out.

The wavelet is defined in the frequency domain as

$$W(f)=A(f)\exp[-i\Phi(f)], \quad (3.9)$$

where  $A(f)$  is the amplitude spectrum to be approximated by the tapered boxcars (Fig. 2.2) defined by four frequency values,  $f_1$ ,  $f_2$ ,  $f_3$ ,  $f_4$ , and an amplitude scaling factor. The wavelet has three phase parameters, one amplitude and four frequencies; therefore it is called the 8-parameter wavelet.

Because my program always calculates the forward-modelled trace in the frequency domain, it is easy to apply this 8-parameter wavelet in this domain. However, sometimes if the inversion for the reflection coefficient sequence is used, it is necessary to transform this 8-parameter wavelet into a wavelet of chosen length in the time domain. In my case, it is a 32-length digital wavelet. The inverse Fourier transform and cosine tapers over 5 samples at each end in the time domain are used to get the 32-length wavelet.

### 3.3.5 Initial Boundary Inversion

The boundary locations must be solved for independently of the impedance because GLI is a procedure that minimizes the error between the observed seismic trace and the synthetic seismic response. If a given boundary has the correct impedance contrast but the wrong location, there are two ways to reduce the error: (1) move the location of the boundary; or (2) change the impedance contrast. The non-linear relationship between boundary locations and seismic response effectively means, as discussed in §2.5, that boundary locations and acoustic impedance values are not independent model parameters. If one tries to invert for these parameters together, each will try to reduce the error energy independently of the other, so the change in model parameters will overshoot instead of finding the minimum. To avoid this, the impedance are solved for only after all the boundary locations are known.

Inversion for the boundary locations therefore has to be done independently of the other model parameters. For the trace closest to the borehole, the first application of GLI is to estimate the boundary locations using the extracted wavelet in the time domain. During this first step, the wavelet was fixed; also the acoustic impedance and their gradients are all fixed at their 'initial guess' values obtained from well log information.

In the inversion, the Jacobian matrix of partial derivatives must be computed. These derivatives can be determined by formal differentiation if the model is simple enough. But where the model parameters do not appear directly in the forward formula due to the discrete parameterization, the partial derivatives may be approximated by finite differences (Lines and Treitel, 1984). This can be computationally expensive since it is necessary to determine the complete model responses for a change in each parameter. Then the simplest finite difference formula is used to approximate the partial derivative by

$$\frac{\partial F(A)}{\partial A} = \frac{[F(A + \Delta A) - F(A)]}{\Delta A} \quad (3.10)$$

### 3.3.6 Wavelet Inversion

The initial guess for the 8-parameter wavelet was obtained by fitting a polynomial to the phase spectrum and by making an empirical approximation to the amplitude spectrum. Therefore the next step following the initial inversion for the boundary locations is to invert for the wavelet parameters by GLI before any further inversion for the earth model is carried out. When the unwrapped phase spectrum is close to linear, a 7-parameter wavelet can be defined for inversion, with  $\varphi_2$  set to be zero. The amplitude of the wavelet scales the forward-modelled trace with the observed trace. The program also has alternative choices for the shape of the amplitude spectrum other than the boxcar-with-cosine-tapers shape.

After this first inversion to optimise the wavelet parameters, one can choose to fix the wavelet for inverting the earth model parameters along the seismic section. This would be logical if one had grounds for believing the effective wavelet in the seismic data is constant (e.g. from consistent wavelet estimates at different boreholes). Otherwise, one can proceed by iteratively inverting for the boundary locations, acoustic impedance values (both the constant values at the top of each layer and the gradient in each layer, simultaneously), and the wavelet parameters.

### 3.3.7 Boundary Inversion

Previous work (Cooke and Schneider, 1983) has only mentioned that the boundaries should be inverted first because of the interference between the boundary locations and acoustic impedance values. I have found, moreover, that it is better to invert for the wavelet and acoustic impedance parameters separately, which does not cause any significant extra computational cost. One of the reasons is that these different kinds of

parameters have different orders of the optimum damping factors. Another reason is to avoid interference with each other. For instance, the amplitude spectrum of the wavelet obviously affects the amplitude of the forward-modelled trace, but the same effect can be achieved by changing all the acoustic impedance values such that all the reflection coefficients are scaled by the same factor.

The inversion proceeds exactly as in §3.3.5, except that the wavelet is now the 7-parameter or 8-parameter wavelet.

Alternatively, if the previous inversion has become lost (e.g. on meeting a fault), another procedure for obtaining the initial guess instead of using the inversion result from the previous trace is introduced. In this case, my strategy is to take the last reliable estimate of the effective wavelet as a 32-length digital wavelet in the time domain. This wavelet can be an extracted wavelet or a parameterized frequency-domain wavelet which should be first transformed to time domain. The wavelet is fixed and least squares is used to find the reflection coefficient sequence in the time domain which gives the best fit to the observed trace.

This estimated reflection coefficient sequence will, in general, have non-zero values at every sample. In order to proceed using GLI with parameterization, it is necessary to limit the number of non-zero reflection coefficients to some arbitrary number of boundaries chosen for the parameterized acoustic impedance model. The program can automatically locate this arbitrary number of boundaries according to the relative amplitudes in the estimated reflection coefficient sequence. Of course, some constraints should be put on this choice, e.g. maximum difference from the previous boundary location; otherwise another relatively large value will be chosen within this constraint.

Then the acoustic impedance for this new model in every layer are kept the same as for the previous inversion result, although this does require some interpretative judgement on the correlation between layers.

### 3.3.8 Acoustic Impedance Inversion

Theoretically, it is not difficult to invert for the relative amplitudes of acoustic impedance when the locations of boundaries are correct and the thicknesses of the layers are greater than the dominant wavelength in the data. In order to invert for the true values of acoustic impedance, it is necessary to fix the known acoustic impedance value of at least one layer .

If the acoustic impedance above a boundary is  $e_i + \Delta e_i$ , and the acoustic impedance under the boundary is  $e_i - \Delta e_i$ , then according to the equation (3.4), the reflection coefficient is

$$r_i = \frac{\Delta e_i}{e_i} . \quad (3.11)$$

As long as  $\Delta e_i \ll e_i$  for all the interfaces, it can be assumed that the sample values of the synthetic trace are linearly related to the acoustic impedance values.

For the real data from the Belvoir Coalfield, in order to solve the problems, only two lithologies were taken into consideration - coal seams and country rocks (e.g. Dresen and Ruter, 1994). It can be seen from the well logs that the acoustic impedance of coal does not change much along the section, nor even between seams, which makes it reasonable to fix it. For country rocks one has the option to invert for their acoustic impedance or to fix them. In the inversion, maximum and minimum values for the acoustic impedance of the country rocks were set according to the well logs.

Inversion for the gradient of acoustic impedance can be considered as fine tuning of the constant acoustic impedance values found in each layer by the previous procedure. The maximum values for the gradients may be set according to well logs. Inversion of the gradients can be done simultaneously with constant values of acoustic impedance taken at the bottom of each layer.

### 3.3.9 Inversion of Adjacent Traces

The termination of iterations for optimising wavelet parameters and earth model parameters is determined by one of the following factors:

- (1) the error energy between the observed and forward-modelled traces is less than some arbitrary small value;
- (2) the current minimum error energy has remained unchanged after successive iterations;  
or
- (3) the number of iterations reaches some arbitrary maximum value.

After completing the inversion process for the starting trace closest to the borehole, the next seismic trace can be inverted either by using the results from the previous trace as the initial guess model or by basing the initial guess on other interpretive information, as will be discussed in Chapter 5. Inversion then proceeds, trace by trace, along the section. The inversion results for each trace and some useful parameters such as the normalized energy value, are saved and therefore the program can be carried on after interruptions, which is very useful for work with a long computation time.

### 3.3.10 Summary

In general, the boundary locations are the most important parameters to invert in coal exploration because the acoustic impedance of the coal seam is normally stable. The main aim is to determine seam thickness, including the identification of washouts, and also to find any seam splits or small faults. However, boundary locations are the most difficult type of earth model parameter to invert. Furthermore, the wavelet phase parameters and acoustic impedance parameters are all affected by changes in the boundary locations. The difficulties and some methods for resolving them are illustrated on synthetic and real data, respectively, in Chapters 4 and 5.

## 4 A Synthetic Model

### 4.1 A 1-D Synthetic Example without Noise

#### 4.1.1 Introduction

Before the field data from British Coal were processed, some tests were carried out on synthetic data in order to prove that the programs are working. The results of the tests also give some indication of potential problems which might arise when inverting real data. First I consider the situation in which the data are noise-free.

Because there is no scaling problem for the synthetic example, the error energy can be used to measure the quality of the match between the synthetic data trace and the forwarded-modelled trace. In the real data case, the correlation coefficient may be used to describe the similarity between the observed data trace and the forward-modelled trace, and the error energy is used as the criterion for the inversion quality.

In the synthetic example, the sampling interval is 1 ms and the length of the wavelet is 32 ms, as they are for the field data described in Chapter 5. The length of the whole trace is 512 ms. The inversion window is set to be between 300 ms and 470 ms. The wavelet parameters and earth model parameters are listed in Table 4.1. There are nine layers and eight boundaries, i.e., the top and bottom layers are treated as half-spaces. The boundary locations are the bottom of each layer in two-way travel time. The acoustic impedances in each layer are set at values appropriate for the thin coal seams

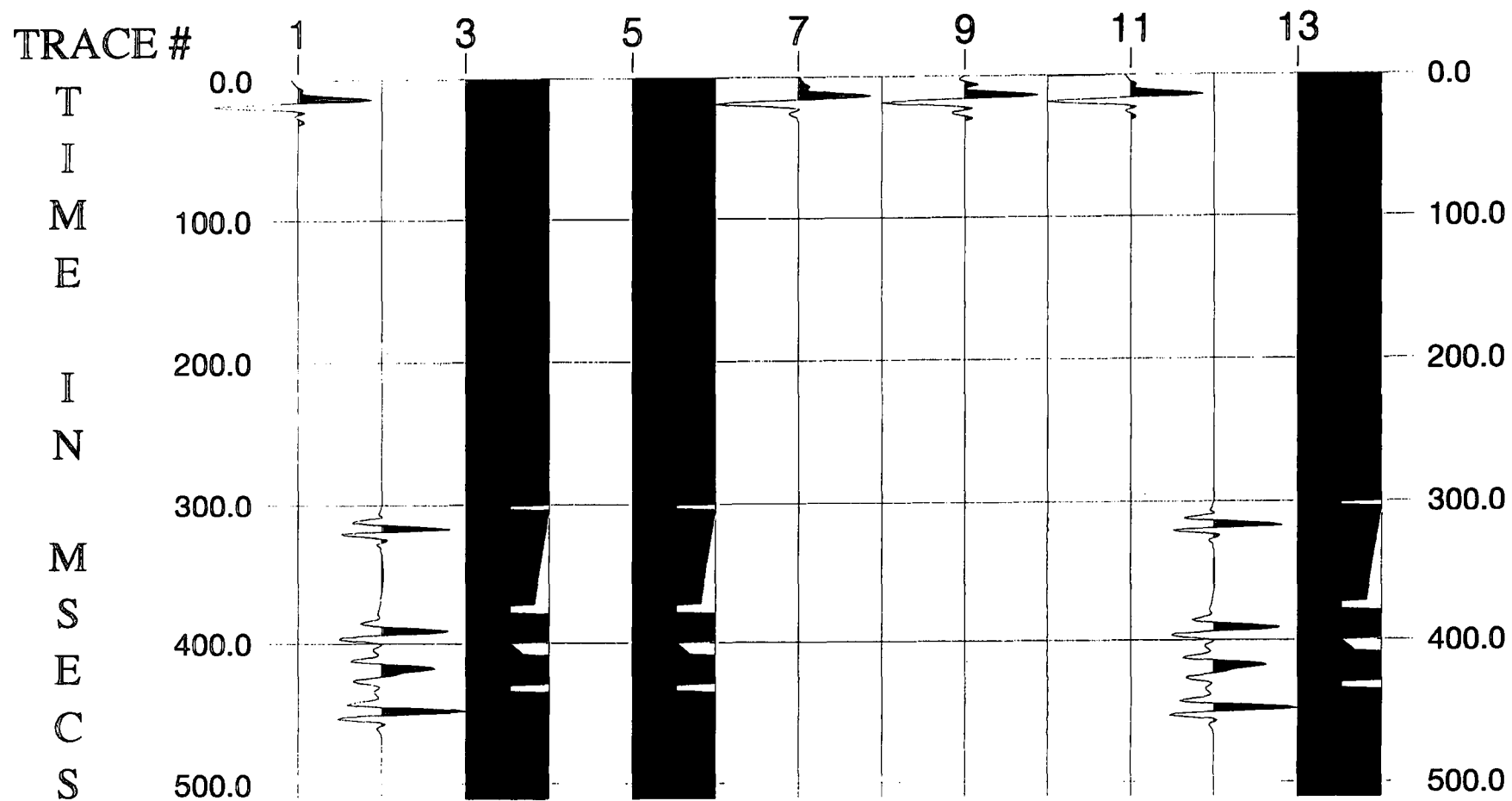


**Figure 4.1** Synthetic inversion results for wavelet parameters and earth model with correct initial guess. Trace 1- synthetic wavelet; trace 2- synthetic trace; trace 3- synthetic earth model; trace 5- initial guess for the earth model; trace 7- extracted wavelet; trace 9- estimated 8-parameter wavelet; trace 10- error between synthetic and forward-modelled traces; trace 11- inverted wavelet; trace 12- forward-modelled trace; trace 13- inverted earth model.

and thick country rocks, at 4.0 and 7.6 (g/cm<sup>3</sup>)(km/s), respectively. The model is shown in Fig. 4.1 (trace 3).

Wavelet	Bound. Locations (ms)	Acous. Impedance (g/cm <sup>3</sup> )(km/s)	Ac. Imp. Gradient (g/cm <sup>3</sup> )(m/s <sup>2</sup> )
f <sub>1</sub> =20 Hz	301	7.6	0.0
f <sub>2</sub> =30 Hz	304	4.0	0.0
f <sub>3</sub> =90 Hz	373	7.6	-0.02
f <sub>4</sub> =200 Hz	379	4.0	0.0
a <sub>0</sub> =1.0	400	7.6	0.0
φ <sub>0</sub> =90 degree	409	4.0	0.15
φ <sub>1</sub> =0.1 deg/Hz	430	7.6	0.0
φ <sub>2</sub> =-0.002 deg/Hz <sup>2</sup>	435	4.0	0.0
		7.6	0.0

Table 4.1 Synthetic wavelet and earth model

#### 4.1.2 Wavelet Parameters

For the first test, the initial guess for the earth model is exactly the same as the real one. After a wavelet was extracted by a Wiener shaping filter, its phase spectrum was unwrapped and an 8-parameter wavelet was defined. Figure 4.1 shows the parameters of the synthetic example, the initial guess and the inversion results, ordered in the following way. Trace 1 is the synthetic wavelet used to generate the synthetic data (trace 2) with the reflection coefficient sequence resulting from the earth model shown on trace 3. Trace 5 shows the initial guess for the earth model. Traces 7 and 9 are the extracted wavelet and the estimate of the 8-parameter wavelet after phase unwrapping. After iterative inversion, trace 10 is the error between the synthetic and forward-

modelled trace. Traces 11 and 12 show the inverted wavelet and the forward-modelled trace. Trace 13 is the inversion result for the earth model.

For the extracted wavelet, the error energy between the synthetic trace and the forward-modelled trace is 0.11%. After phase unwrapping, the estimated values of the 8 parameters for the parameterized wavelet are shown in Table 4.2. For this estimate of the wavelet parameters, the error energy between the synthetic trace and the forward-modelled trace is 2.50 %.

$f_1=14$ Hz	$f_2=25$ Hz	$f_3=121$ Hz	$f_4=172$ Hz
$a_0 = 1.03$	$\varphi_0=89$ degree	$\varphi_1 = 0.12$ degree/Hz	$\varphi_2 = -0.002$ degree/Hz <sup>2</sup>

Table 4.2 The estimate for wavelet parameters  
after phase unwrapping

The inversion result, following optimisation of the 8-parameter wavelet, shows that the inverted wavelet is even better than the extracted wavelet because the final error energy between the synthetic trace and forward-modelled trace after three iterations is equal to 0.01%. The parameters of the inverted wavelet are shown in Table 4.3.

$f_1=16$ Hz	$f_2=33$ Hz	$f_3=92$ Hz	$f_4=200$ Hz
$a_0 = 1.0$	$\varphi_0=90$ degree	$\varphi_1 = 0.10$ degree/Hz	$\varphi_2 = -0.002$ degree/Hz <sup>2</sup>

Table 4.3 Inverted wavelet after three iterations

This test is similar to the one we will carry out on the nearest trace to the well when inverting real data, where the initial guess for the earth model is almost correct based on the edited well log (see next chapter). In that case, before inverting for the wavelet

parameters, an initial inversion for the boundary locations is made using the extracted wavelet. However, for the synthetic test, this process is omitted.

If it is not possible to obtain an extracted wavelet, because no well log data are available, then it may be necessary to start with a guess wavelet, which could be in error. This case does not apply for my real-data example. However, in order to show that problems exist in Cooke and Schneider's (1983) previous work, I give the following example. Consider the arbitrary initial guess for the wavelet parameters shown in Table 4.4. Its initial error energy is 42.63%. After inversion to optimise all the wavelet parameters, the error energy between the synthetic trace and the forward-modelled trace becomes 0.005%. The inverted wavelet parameters are listed in Table 4.5.

8-parameter Guess Wavelet			
$f_1=20$ Hz	$f_2=30$ Hz	$f_3=90$ Hz	$f_4=200$ Hz
$a_0 = 1.0$	$\varphi_0=45.0$ degree	$\varphi_1 = 0.0$ degree/Hz	$\varphi_2 = 0.0$ degree/Hz <sup>2</sup>

Table 4.4 Arbitrary initial guess for wavelet parameters

8-parameter Inverted Wavelet			
$f_1=19$ Hz	$f_2=31$ Hz	$f_3=90$ Hz	$f_4=200$ Hz
$a_0 = 1.0$	$\varphi_0=90$ degree	$\varphi_1 = 0.1$ degree/Hz	$\varphi_2 = -0.002$ degree/Hz <sup>2</sup>

Table 4.5 Inverted wavelet for arbitrary initial guess

From this result one can see that if the error in  $\varphi_0$  between the guess wavelet (Table 4.4) and the synthetic wavelet (Table 4.1) is quite big, GLI still can find the correct answer for  $\varphi_0$  as well as  $\varphi_1$  and  $\varphi_2$ . One can also see that if the  $\varphi_0$  values of the

actual wavelet and guess wavelet are different, the error energy without inversion is rather large and cannot be neglected. That is to say, this shows that Cooke and Schneider's (1983) conclusion (see §3.3.1) is not always correct. In the next section, this will also be shown together with inversion for the boundary locations.

#### 4.1.3 Boundary Locations

Before any further inversion is discussed, it is necessary to see the inversion result for the boundary locations if there is no extracted wavelet available and just a guess wavelet has to be used. The result shows that if there are errors in the guess wavelet, the inversion will try to change the boundary locations to reduce the error energy even when the guess model of the boundary locations is correct. The guess wavelet is that given in Table 4.4. The initial error energy is still 42.63%, but the error energy after inverting for the boundary locations is 14.20% if there is no wavelet inversion. Table 4.6 shows the results of the inversion.

However, if the wavelet inversion is carried out before inverting for the boundary locations, the boundary locations remain unchanged and the error energy is also unchanged at 0.005%. Thus the wavelet plays just as important a role as the other earth model parameters in the inversion. This also shows the interference effects between the boundary locations and the wavelet parameters. Any errors in either guess model will affect the other, but provided one inverts for both wavelet and earth parameters, it may be possible to reach the global minimum.

For the following examples, the guess wavelet will be the same as the inverted wavelet in Table 4.3. Two iterations of the inversion procedure will be carried out in each case. Let us consider the case in which the guess model differs from the real model only in the boundary locations, as shown in Table 4.7.

Wavelet	Bound. Locations (ms)	Acous. Impedance (g/cm <sup>3</sup> )(km/s)	Ac. Imp. Gradient (g/cm <sup>3</sup> )(m/s <sup>2</sup> )
f <sub>1</sub> =20 Hz	300	7.6	0.0
f <sub>2</sub> =30 Hz	303	4.0	0.0
f <sub>3</sub> =90 Hz	372	7.6	-0.02
f <sub>4</sub> =200 Hz	378	4.0	0.0
a <sub>0</sub> =1.0	399	7.6	0.0
φ <sub>0</sub> =45 degree	407	4.0	0.15
φ <sub>1</sub> =0.0 deg/Hz	428	7.6	0.0
φ <sub>2</sub> =0 deg/Hz <sup>2</sup>	434	4.0	0.0
		7.6	0.0

Table 4.6 Inverted boundary locations  
for the guess wavelet of Table 4.4

Wavelet	Bound. Locations (ms)	Acous. Impedance (g/cm <sup>3</sup> )(km/s)	Ac. Imp. Gradient (g/cm <sup>3</sup> )(m/s <sup>2</sup> )
f <sub>1</sub> =16 Hz	301	7.6	0.0
f <sub>2</sub> =33 Hz	305	4.0	0.0
f <sub>3</sub> =92 Hz	370	7.6	-0.02
f <sub>4</sub> =200 Hz	380	4.0	0.0
a <sub>0</sub> =1.0	401	7.6	0.0
φ <sub>0</sub> =90 degree	409	4.0	0.15
φ <sub>1</sub> =0.1 deg/Hz	432	7.6	0.0
φ <sub>2</sub> =-0.002 deg/Hz <sup>2</sup>	435	4.0	0.0
		7.6	0.0

Table 4.7 Initial guess for the boundary locations

The initial error energy is 35.29%. Table 4.8 shows the final results after iterative inversion for boundary locations and wavelet parameters, yielding an error energy of 0.002%. The result is quite satisfactory and all the boundary locations are moved to the correct places.

Wavelet	Bound. Locations (ms)	Acous. Impedance (g/cm <sup>3</sup> )(km/s)	Ac. Imp. Gradient (g/cm <sup>3</sup> )(m/s <sup>2</sup> )
f <sub>1</sub> =16 Hz	301	7.6	0.0
f <sub>2</sub> =32 Hz	304	4.0	0.0
f <sub>3</sub> =91 Hz	373	7.6	-0.02
f <sub>4</sub> =200 Hz	379	4.0	0.0
a <sub>0</sub> =0.99	400	7.6	0.0
φ <sub>0</sub> =90 degree	409	4.0	0.15
φ <sub>1</sub> =0.1 deg/Hz	430	7.6	0.0
φ <sub>2</sub> =-0.002 deg/Hz <sup>2</sup>	435	4.0	0.0
		7.6	0.0

Table 4.8 Inverted boundary locations and wavelet parameters

It is important to estimate the reliability of this method when the differences between the guess and real earth model are increased, e.g. the guess model listed in Table 4.9. In this guess model, the errors in the boundary locations for the third coal seam (400 - 409 ms) are about 10 ms. I call this a "badly wrong" guess model for the boundary locations. In this case, the initial error energy was 82.26%. After inversion for boundary locations and wavelet parameters (Table 4.10), the final error energy was 6.5%.

Wavelet	Bound. Locations (ms)	Acous. Impedance (g/cm <sup>3</sup> )(km/s)	Ac. Imp. Gradient (g/cm <sup>3</sup> )(m/s <sup>2</sup> )
f <sub>1</sub> =16 Hz	301	7.6	0.0
f <sub>2</sub> =33 Hz	305	4.0	0.0
f <sub>3</sub> =92 Hz	370	7.6	-0.02
f <sub>4</sub> =200 Hz	380	4.0	0.0
a <sub>0</sub> =1.0	410	7.6	0.0
φ <sub>0</sub> =90 degree	419	4.0	0.15
φ <sub>1</sub> =0.1 deg/Hz	432	7.6	0.0
φ <sub>2</sub> =-0.002 deg/Hz <sup>2</sup>	435	4.0	0.0
		7.6	0.0

Table 4.9 Badly wrong initial guess for the boundary locations

Wavelet	Bound. Locations (ms)	Acous. Impedance (g/cm <sup>3</sup> )(km/s)	Ac. Imp. Gradient (g/cm <sup>3</sup> )(m/s <sup>2</sup> )
f <sub>1</sub> =20 Hz	301	7.6	0.0
f <sub>2</sub> =32 Hz	304	4.0	0.0
f <sub>3</sub> =85 Hz	373	7.6	-0.02
f <sub>4</sub> =205 Hz	379	4.0	0.0
a <sub>0</sub> =0.99	400	7.6	0.0
φ <sub>0</sub> =111 degree	414	4.0	0.15
φ <sub>1</sub> =-0.39deg/Hz	430	7.6	0.0
φ <sub>2</sub> =-0.002 deg/Hz <sup>2</sup>	435	4.0	0.0
		7.6	0.0

Table 4.10 Inverted boundary locations and wavelet parameters

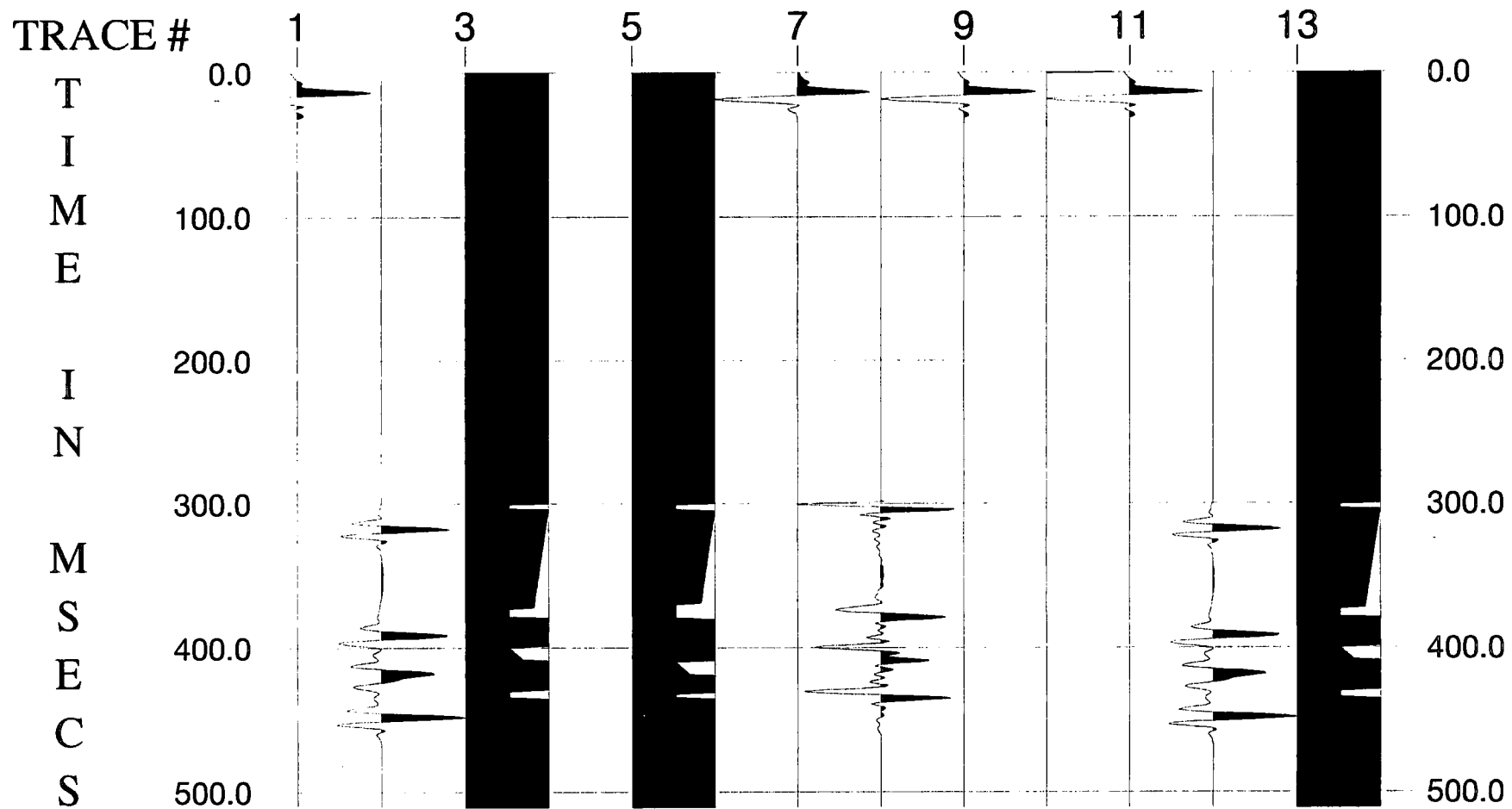


**Figure 4.2** Synthetic inversion results for a badly wrong initial guess for the boundary locations with inversion for the reflection coefficient sequence applied prior to GLI with parameterization.

The inversion failed to get the correct answer for the bottom boundary locations of the third coal seam even though it improved on the initial guess. This indicates that the guess for boundary locations lies outside the "region of convergence" discussed by Cooke and Schneider (1983). This feature of the boundary locations indicates that the boundary locations are the most difficult of all parameters to invert. I will show later that a badly wrong initial guess for the acoustic impedance values can be correctly solved when the boundary locations are correct.

When dealing with real data, large differences between the initial guess and the real acoustic impedance distribution may result from faults, pinchouts, reefs or sand lenses. Normally those features are the exploration targets. Therefore I propose an alternative method for obtaining the initial guess of the acoustic impedance distribution. The first step is to invert for the reflection coefficient sequence directly from the seismic data using the best available wavelet estimate (see § 2.3). Applying this process to the synthetic trace using the inverted wavelet from Table 4.3 gives the spiked reflectivity shown as trace 8 on Fig. 4.2. This is equivalent to deconvolution using an optimum-lag Wiener spiking filter.

After estimating the reflection coefficient sequence (i.e., the spiked reflectivity), the program automatically searches for the eight most significant boundary locations. They are: 302, 305, 374, 380, 401, 410, 431, 436 ms, respectively. Then GLI with parameterization was applied, yielding the results shown in Fig. 4.2 and Table 4.11 with an error energy of 0.002 %. Comparing with the previous result, it is obvious that this method is successful. The advantage of this two-stage inversion procedure is that the boundary locations estimated from the spiked reflectivity, following deconvolution, should lie within the region of convergence for the subsequent application of GLI.

Wavelet	Bound. Locations (ms)	Acous. Impedance (g/cm <sup>3</sup> )(km/s)	Ac. Imp. Gradient (g/cm <sup>3</sup> )(m/s <sup>2</sup> )
f <sub>1</sub> =16 Hz	301	7.6	0.0
f <sub>2</sub> =32 Hz	304	4.0	0.0
f <sub>3</sub> =91 Hz	373	7.6	-0.02
f <sub>4</sub> =200 Hz	379	4.0	0.0
a <sub>0</sub> =1.0	400	7.6	0.0
φ <sub>0</sub> =90 degree	409	4.0	0.15
φ <sub>1</sub> =0.1 deg/Hz	430	7.6	0.0
φ <sub>2</sub> =-0.002 deg/Hz <sup>2</sup>	435	4.0	0.0
		7.6	0.0

Table 4.11 Inverted boundary locations and wavelet parameters following initial inversion for the reflection coefficient sequence

#### 4.1.4 Acoustic Impedance and Gradients

In this section I will show that, if the initial guess for the boundary locations is correct and keep fixed, there will be no limitations on the acoustic impedance guess model because of the approximately linear relationship between the coefficients of the synthetic trace and the acoustic impedance values as expressed in equation (3.11). And even when there are some errors in the guess model for the boundary locations, it is still possible to get a nearly correct solution to the problem.

The guess earth model for the first example is listed in Table 4.12. There are some errors in the initial guess for acoustic impedance. The error energy after inversion for the boundary locations and the acoustic impedance values reduced from 9.20 % to 0.01 %. The final solution is shown in Table 4.13. This means if the guess for the

boundary locations is correct and the error energy for the initial guess is not big (up to, say, 30 %), the correct boundary locations will remain unchanged in the inversion.

Wavelet	Bound. Locations (ms)	Acous. Impedance (g/cm <sup>3</sup> )(km/s)	Ac. Imp. Gradient (g/cm <sup>3</sup> )(m/s <sup>2</sup> )
f <sub>1</sub> =16 Hz	301	7.6	0.0
f <sub>2</sub> =33 Hz	304	4.0	0.0
f <sub>3</sub> =92 Hz	373	8.6	-0.02
f <sub>4</sub> =200 Hz	379	4.0	0.0
a <sub>0</sub> =1.0	400	6.0	0.0
φ <sub>0</sub> =90 degree	409	4.0	0.15
φ <sub>1</sub> =0.1 deg/Hz	430	5.6	0.0
φ <sub>2</sub> =-0.002 deg/Hz <sup>2</sup>	435	4.0	0.0
		7.6	0.0

Table 4.12 Initial guess for acoustic impedance values

In the next test, the initial guess for the acoustic impedance of the third layer was 3.6 instead of 8.6 (g/cm<sup>3</sup>)(km/s). For comparison this guess model can be considered as a "badly wrong" model for the acoustic impedance because the polarities are opposite to the true values for the <sup>c</sup> acoustic impedance contrasts. The initial error energy was 61.36%. The results were almost the same as Table 4.13 with 0.05% error energy but without inversion for the boundary locations. This test shows that even though the acoustic impedance contrasts at the boundaries of the third layer have the wrong polarities, one can still get the correct answer as long as the initial guess for the boundary locations is correct and fixed. If the boundary locations are inverted as well as the acoustic impedance, they will affect each other. Table 4.14 shows the results and the error energy is 4.73%.

Wavelet	Bound. Locations (ms)	Acous. Impedance (g/cm <sup>3</sup> )(km/s)	Ac. Imp. Gradient (g/cm <sup>3</sup> )(m/s <sup>2</sup> )
f <sub>1</sub> =16 Hz	301	7.6	0.0
f <sub>2</sub> =31 Hz	304	4.0	0.0
f <sub>3</sub> =91 Hz	373	7.5	-0.02
f <sub>4</sub> =200 Hz	379	4.0	0.0
a <sub>0</sub> =1.0	400	7.5	0.0
φ <sub>0</sub> =90 degree	409	4.0	0.15
φ <sub>1</sub> =0.1 deg/Hz	430	7.5	0.0
φ <sub>2</sub> =-0.002 deg/Hz <sup>2</sup>	435	4.0	0.0
		7.5	0.0

Table 4.13 Inverted boundary and acoustic impedance for Table 4.12

Wavelet	Bound. Locations (ms)	Acous. Impedance (g/cm <sup>3</sup> )(km/s)	Ac. Imp. Gradient (g/cm <sup>3</sup> )(m/s <sup>2</sup> )
f <sub>1</sub> =18 Hz	300	7.6	0.0
f <sub>2</sub> =34 Hz	304	4.0	0.0
f <sub>3</sub> =83 Hz	373	7.1	-0.02
f <sub>4</sub> =200 Hz	378	4.0	0.0
a <sub>0</sub> =1.0	399	7.6	0.0
φ <sub>0</sub> =84 degree	409	4.0	0.15
φ <sub>1</sub> =0.08 deg/Hz	430	7.4	0.0
φ <sub>2</sub> =-0.003 deg/Hz <sup>2</sup>	435	4.0	0.0
		7.5	0.0

Table 4.14 Inverted boundary and acoustic impedance  
for the badly wrong guess

In the next example, errors in the initial guess for the boundary locations, as in Table 4.7, as well as errors in the guess for the acoustic impedance and their gradients are included. This means that there are errors in all parameter types in the initial guess (Table 4.15). After iterative inversion for the boundary locations, the acoustic impedance and their gradients together, and the wavelet parameters, the error energy is reduced from 45.65% to 0.01% with the results shown in Table 4.16.

Overall, the inversion is fairly successful with no gross errors. However, it should be pointed out that the inverted acoustic impedance values and their gradient values contain some errors compared to the synthetic model, even though the total error energy is quite small. The first possible reason is that the model parameters interfere with each other and make the problem non-unique (or close to non-unique). The second reason for the errors in the acoustic impedance and gradients is the absence of low frequencies in the seismic data.

Wavelet	Bound. Locations (ms)	Acous. Impedance (g/cm <sup>3</sup> )(km/s)	Ac. Imp. Gradient (g/cm <sup>3</sup> )(m/s <sup>2</sup> )
f <sub>1</sub> =16 Hz	301	7.6	0.0
f <sub>2</sub> =33 Hz	305	4.0	0.0
f <sub>3</sub> =92 Hz	370	8.6	0.0
f <sub>4</sub> =200 Hz	380	4.0	0.0
a <sub>0</sub> =1.0	401	6.0	0.0
φ <sub>0</sub> =90 degree	409	4.0	0.0
φ <sub>1</sub> =0.1 deg/Hz	432	5.6	0.0
φ <sub>2</sub> =-0.002 deg/Hz <sup>2</sup>	435	4.0	0.0
		7.6	0.0

Table 4.15 Initial guess for all parameter types

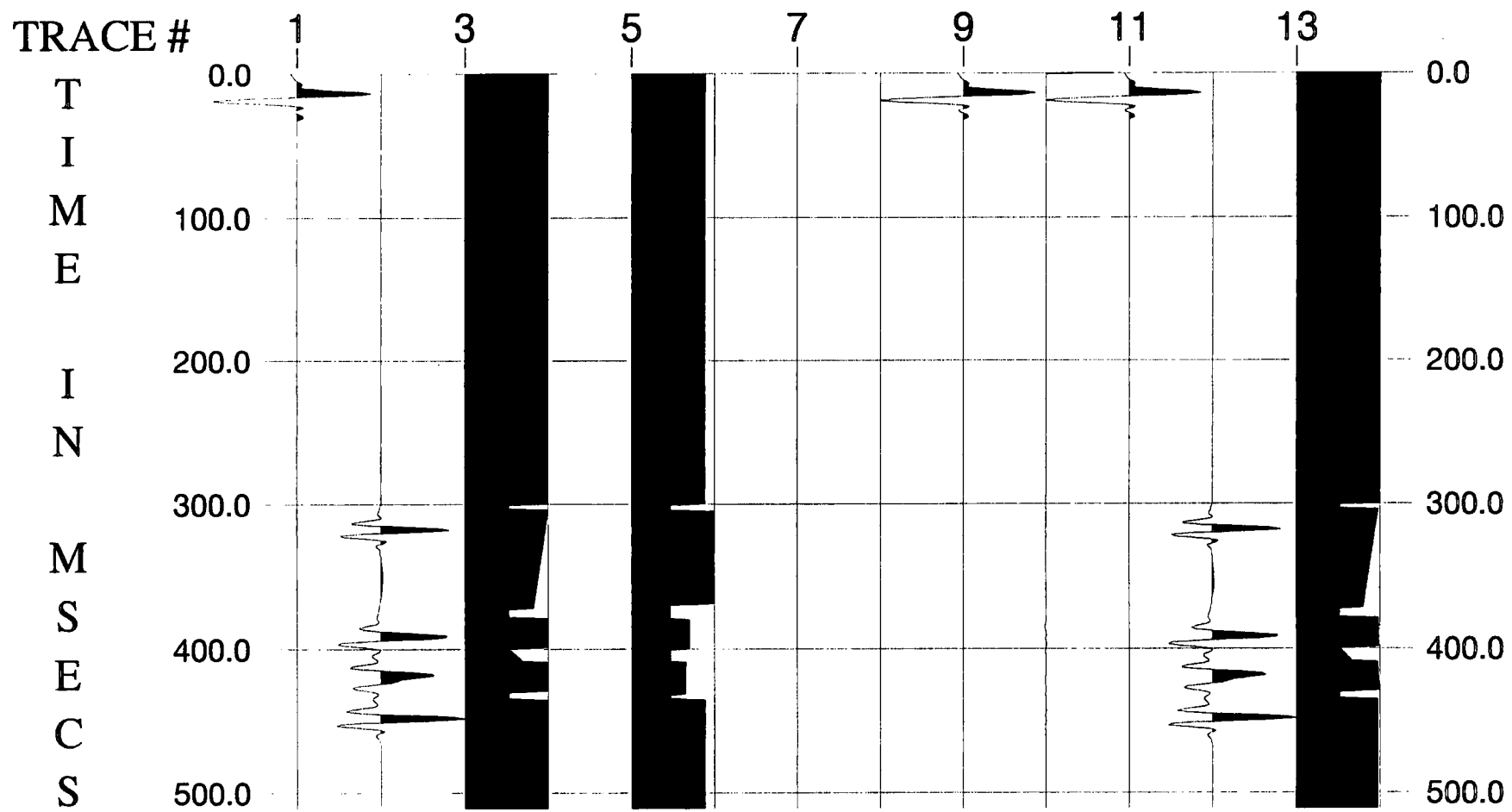


**Figure 4.3** Synthetic inversion results for errors in the initial guess for all types of earth model and wavelet parameters.

Wavelet	Bound. Locations (ms)	Acous. Impedance (g/cm <sup>3</sup> )(km/s)	Ac. Imp. Gradient (g/cm <sup>3</sup> )(m/s <sup>2</sup> )
f <sub>1</sub> =16 Hz	301	7.6	0.0
f <sub>2</sub> =32 Hz	304	4.0	0.0
f <sub>3</sub> =90 Hz	373	7.5	-0.02
f <sub>4</sub> =199 Hz	379	4.0	-0.01
a <sub>0</sub> =1.0	400	7.5	0.0
φ <sub>0</sub> =92 degree	409	4.0	0.13
φ <sub>1</sub> =0.08 deg/Hz	430	7.4	0.01
φ <sub>2</sub> =-0.002 deg/Hz <sup>2</sup>	435	4.0	0.0
		7.4	0.0

Table 4.16 Overall inversion results for initial guess in Table 4.14

Figure 4.3 shows the results of this inversion as a plot. The traces in this plot are ordered as in Fig. 4.1 (see § 4.1.2). A satisfactory feature is that the inverted boundary locations are correct even though there are some boundary location errors in the initial guess. Such errors are bound to exist in the initial guess models for inverting real data, so it is reassuring that the inversion methodology solves for them correctly in this noise-free synthetic data example. As for the errors in the acoustic impedance values and gradients, due to the missing low frequencies, they are not a big problem for inversion of Coal Measures data because the acoustic impedance can be fixed for coal seams. The changes in the thickness of the coal seams are the most interesting effect.

## 4.2 A 1-D Synthetic Model with White Noise

### 4.2.1 Introduction

There is always some noise present on observed seismic traces. Now let us consider the same model as in the previous section with 15% white noise (Gaussian distribution) added. In this section, the error energy will still be used to show the quality of the inversions and to measure the match between the synthetic data trace and the forward-modelled trace.

### 4.2.2 Wavelet Inversion

Following the processes described in §4.1.2, the inverted 8-parameter wavelet found after three iterations is listed in the following Table 4.17:

$f_1=15$ Hz	$f_2=36$ Hz	$f_3=89$ Hz	$f_4=201$ Hz
$a_0 = 1.0$	$\varphi_0=89$ degree	$\varphi_1 = 0.13$ degree/Hz	$\varphi_2 = -0.002$ degree/Hz <sup>2</sup>

Table 4.17 Inverted wavelet after three iterations

For the extracted wavelet, the error energy was 2.05%, but the initial guess for the 8-parameter wavelet gave an error energy of 4.71 %. After three iteration of inversion for the wavelet parameters, the error energy was only reduced to 2.17 %. Unlike the case without noise, the inverted 8-parameter wavelet is not as good as the extracted one. Therefore, it is necessary to look at the extracted wavelet and its spectra to decide whether it is suitable to use an 8-parameter wavelet in real data inversion. I will show in the next section that there are no big differences in the results between using the extracted

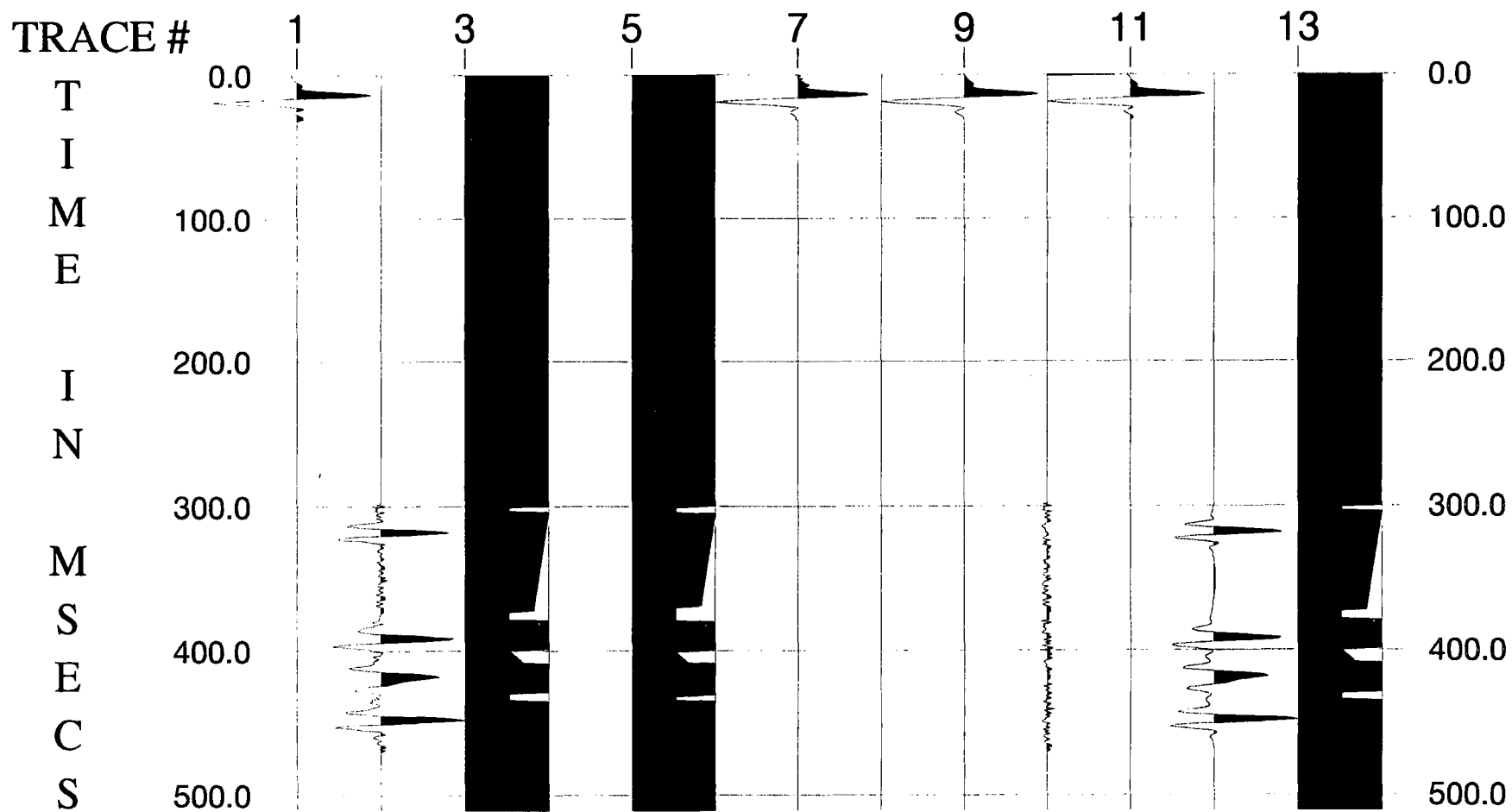


**Figure 4.4** Synthetic inversion results with 15 % white noise on the input trace and errors in the initial guess for the boundary locations

wavelet and the 8-parameter wavelet in my synthetic examples, even though there are some differences in the error energy.

### 4.2.3 Boundary Locations

As in §4.1.3, the initial guess for the constant acoustic impedance values and gradients is the same as for the real forward model. The differences are in the boundary locations as given in Table 4.7. The results after inversion for boundary locations and the 8-parameter wavelet are shown in Table 4.18, with the error energy reduced from 31.59 % to 4.37 %. Figure 4.4 shows plots of the traces, in which the meaning of each trace is the same as described in §4.1.2.

Wavelet	Bound. Locations (ms)	Acous. Impedance (g/cm <sup>3</sup> )(km/s)	Ac. Imp. Gradient (g/cm <sup>3</sup> )(m/s <sup>2</sup> )
$f_1=16$ Hz	300	7.6	0.0
$f_2=34$ Hz	304	4.0	0.0
$f_3=86$ Hz	373	7.6	-0.02
$f_4=204$ Hz	379	4.0	0.0
$a_0=0.96$	400	7.6	0.0
$\varphi_0=89$ degree	409	4.0	0.15
$\varphi_1=0.12$ deg/Hz	430	7.6	0.0
$\varphi_2=-0.003$ deg/Hz <sup>2</sup>	435	4.0	0.0
		7.6	0.0

Table 4.18 Inverted boundary locations and wavelet parameters

Then I fixed the extracted wavelet in the inversion and compared the results. Though the error energy of 2.05% is a little bit better, the boundary locations were almost the

same, i.e. 301, 304, 373, 379, 400, 409, 430, 435 ms. Therefore, for the sake of being able to invert for wavelet parameters on successive traces, an 8-parameter wavelet defined in Table 4.17 is preferred and treated as the guess wavelet for the following inversions.

Comparing these results with §4.1.3, this inversion method shows its ability to invert the boundary locations when 15 % white noise is present on the observed trace, provided that the acoustic impedance values are correct.

#### 4.2.4 Acoustic Impedance and Gradients

Using the same initial guess for the earth model as in Table 4.15 and the initial guess wavelet parameters as in Table 4.17, the final solution obtained by GLI with parameterization is listed in Table 4.19.

Wavelet	Bound. Locations (ms)	Acous. Impedance (g/cm <sup>3</sup> )(km/s)	Ac. Imp. Gradient (g/cm <sup>3</sup> )(m/s <sup>2</sup> )
$f_1=13$ Hz	301	7.6	0.0
$f_2=38$ Hz	305	4.0	0.0
$f_3=88$ Hz	373	7.0	-0.01
$f_4=203$ Hz	379	4.0	-0.1
$a_0=1.0$	400	7.0	0.03
$\varphi_0=96$ degree	409	4.0	0.09
$\varphi_1=-0.08$ deg/Hz	430	6.9	0.02
$\varphi_2=-0.002$ deg/Hz <sup>2</sup>	435	4.0	0.0
		7.2	0.0

Table 4.19 Inverted earth model and the wavelet parameters

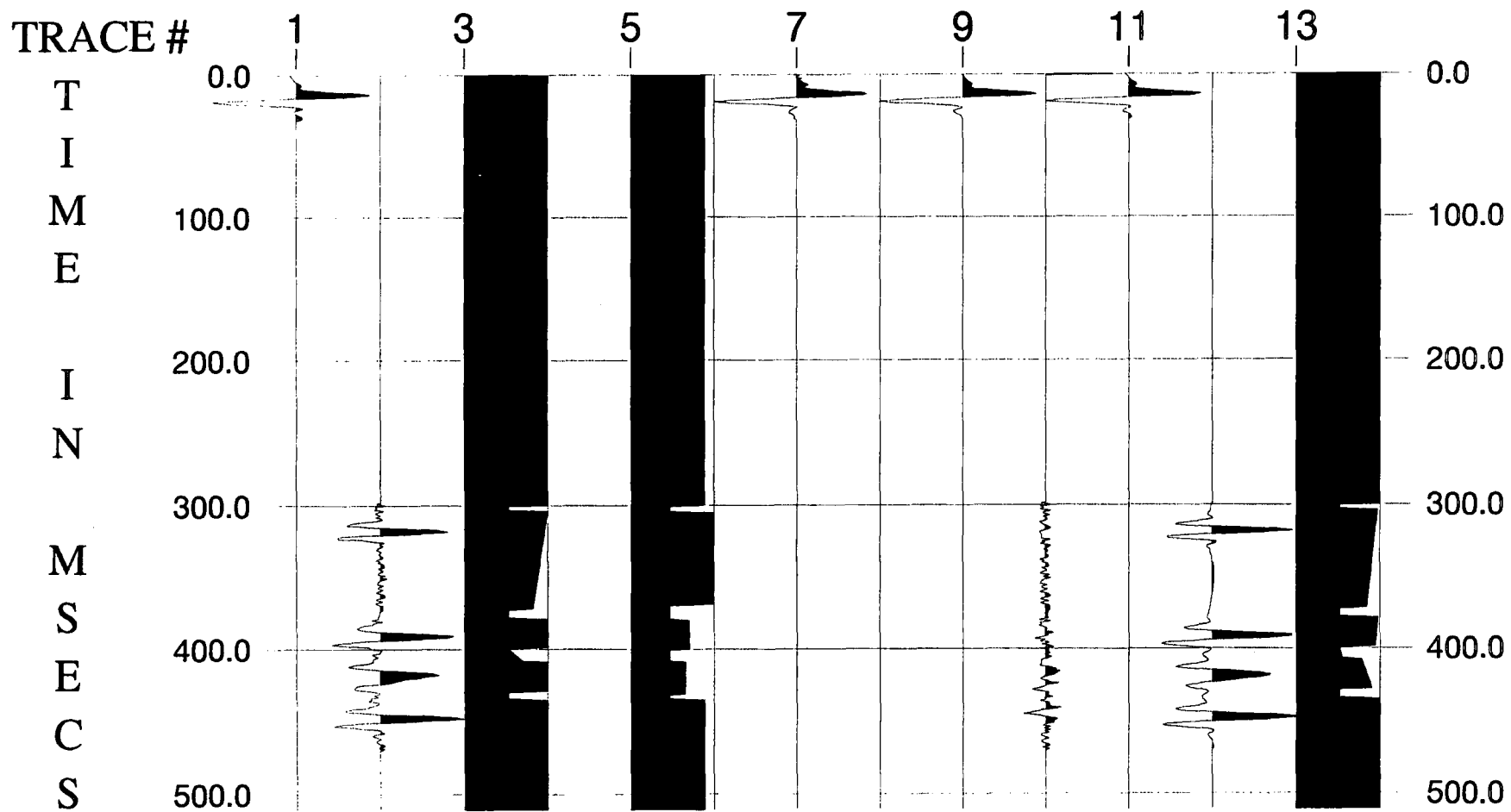


**Figure 4.5** Synthetic inversion results with 15 % white noise on the input trace and errors in the initial guess for all types of earth model and wavelet parameters.

For this inversion, the error energy is reduced from 41.78% to 3.52 %. The results are also shown in Fig. 4.5. Comparing Table 4.19 with Table 4.16, one can see the inversion almost succeeded in locating the boundaries, with only a small error in the boundary at 304 ms, even though 15 % white noise had been added. That is to say, when white noise is present on the observed trace, if boundary locations and acoustic impedances are all in error in the guess model, GLI with parameterization can still find the correct answer for the boundary locations. However, the inverted values of the acoustic impedance and its gradient are worse than the result in the noise-free case. This indicates that acoustic impedance values are more sensitive to white noise on the observed trace than the boundary locations and wavelet parameters are, at least when the SNR is not too poor.

### 4.3 Summary

A number of synthetic examples either with noise-free or with some white noise have been presented. It can be seen that it is possible to use this GLI method to do some inversion on post-stack seismic data in the thin bed area as long as the boundary locations are carefully treated and the noise on the observed traces is not severe. Furthermore, for the badly wrong initial guess for the boundary locations, it is still possible to get the correct answer by applying an inversion for the reflection coefficient sequence and then GLI. For the badly wrong initial guess for the acoustic impedance values, it can obtain the correct solutions only if the initial guess for the boundary locations is correct and fixed.

In this chapter, I have reported results from several different tests on synthetic data. I give a summary table below (Table 4.20) which shows where incorrect parameters were assigned in the initial guess, the inversion procedure applied and the error energy in the result. Corresponding table numbers are given for each test, as available.

Without Noise	Initial Guess Earth	Model Wavelet	Inversion Procedure	Error Energy
Table 4.3	Correct	None	Wavelet extraction and wavelet parameters	0.01 %
Table 4.5	Correct	Wrong	Wavelet parameters only	0.005 %
Table 4.6	Correct	Wrong	Boundary locations only	14.20 %
	Correct	Wrong	Boundary locations and wavelet parameters	0.005 %
Table 4.8	Bdary. locns. wrong	Inverted	Boundary locations and wavelet parameters	0.002 %
Table 4.10	Bdary. locns. badly wrong	Inverted	Boundary locations and wavelet parameters	6.5 %
Table 4.11	Bdary. locns. badly wrong	Inverted	Reflection coefficient sequenc , then as above	0.002 %
Table 4.13	Acoustic imp. wrong	Inverted	Boundary locations and acoustic impedance inversion	0.01 %
	Acoustic imp. badly wrong	Inverted	Acoustic impedance inversion	0.05 %
Table 4.14	Acoustic imp. badly wrong	Inverted	Boundary locations and acoustic impedance inversion	4.73 %
Table 4.16	Everything wrong	Inverted	Bdary. locns., acoustic imp. and wavelet parameters	0.01 %
<b>With 15 % White Noise</b>				
Table 4.17	Correct	None	Wavelet extraction and wavelet parameters	2.05 %
Table 4.18	Bdary. locns. wrong	Inverted	Boundary locations and wavelet parameters	4.37 %
	Bdary. locns. wrong	Extracted	Boundary locations inversion only	2.05 %
Table 4.19	Everything wrong	Inverted	Bdary. locns., acoustic imp. and wavelet parameters	3.52 %

Table 4.20 Brief summary of inversion tests and results  
for a synthetic data example

## 5 British Coal's Dataset

### 5.1 Introduction

In this chapter, I present the results of applying inversion to the reprocessed migrated dataset from British Coal. Due to the complexity of the stratigraphy, it was necessary to start the inversion at a borehole and to do some systematic work to determine the most important model parameters at that borehole. According to the well logs, two different inversion windows were chosen for Thorny Plantation and Pillbox boreholes in order to cover all the coal seams present.

For the real data, the scaling factor between the forward-modelled trace and the observed trace is unknown. Furthermore, for inverting the seismic section, it is necessary to normalise the total energy of the signal in the inversion window on each trace to the same value. Therefore, the acoustic impedance in the coal seams was fixed to provide a consistent scaling for all the acoustic impedance values. Then I calculated the total energy in the chosen window on the observed trace at the borehole and took this value to normalize the total energy in the chosen window for each trace in the section.

In addition, even though I carefully reprocessed the seismic reflection data, the amplitude values of the reflection events on the seismic trace are still not the true relative amplitude values, which are important for thin bed inversion. In the synthetic examples, there are no such problems. I will point out the effect of incorrect relative amplitude values on the inversion for the thicknesses of the coal seams in the following systematic study.

## 5.2 Systematic Study at Thorny Plantation

### 5.2.1 Comparison of the Two Different Processed Sections

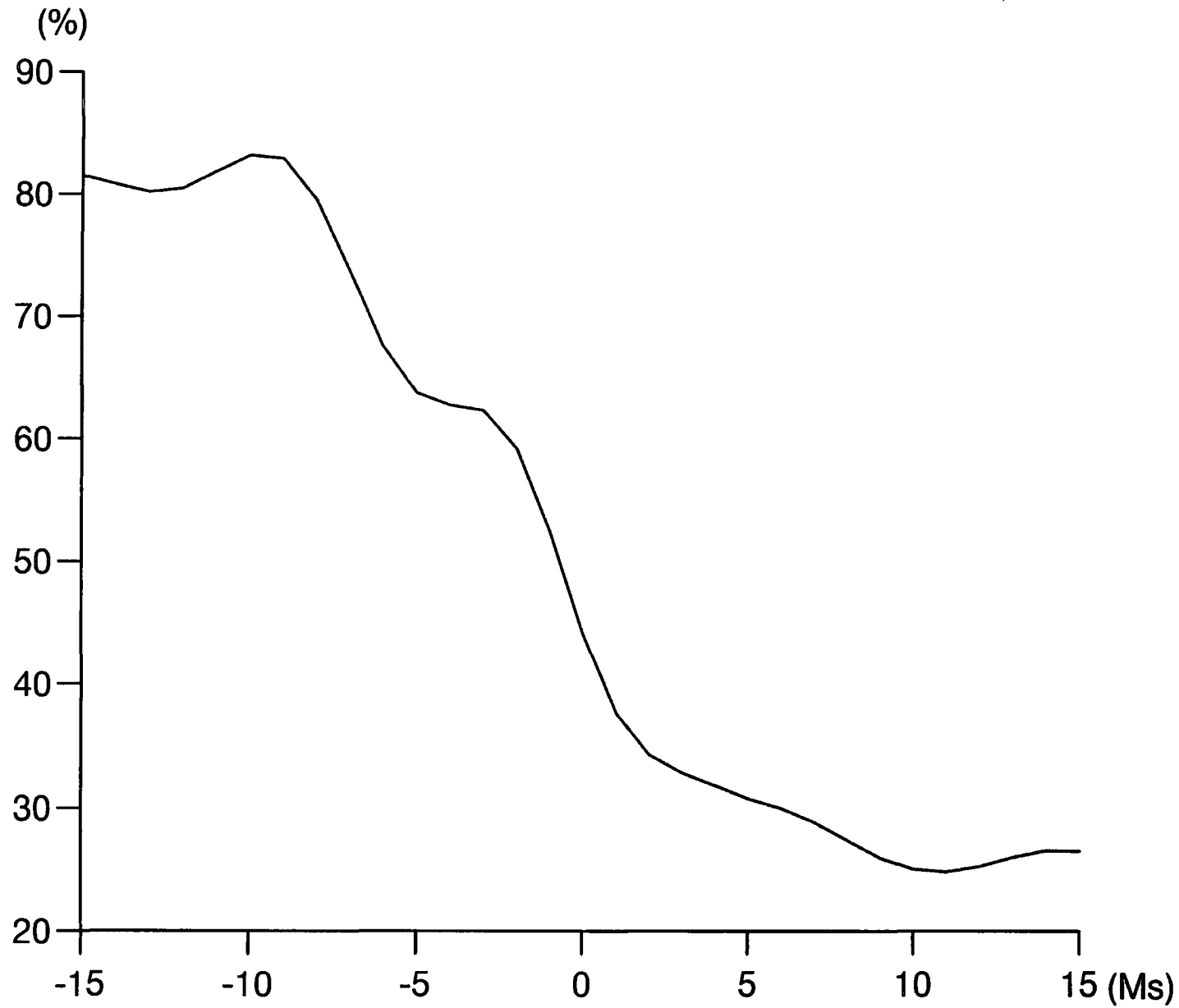
In this section, I will first quantify the improvement achieved with the reprocessed data, compared to the section obtained by the British Coal's original processing, by making use of the well logs. The criterion for the comparison is the error energy between the observed data and the forward-modelled trace obtained by convolving the extracted wavelet with the reflection coefficient sequence generated from the well logs.

This procedure was applied for the trace at CDP 994 from British Coal's processing and from my processing. The window on the observed trace was taken to be 331 ms to 480 ms in each case to cover all the coal seams. For each processed trace at CDP 994, the normal equations for a Wiener shaping filter were solved to extract a wavelet as the best filter, in a least squares sense, for shaping the reflection coefficient sequence obtained from the well logs into the processed trace. The length of the wavelet was chosen to be 32 ms. Then the error energy was calculated between the forward-modelled trace and the observed (i.e. processed) trace. Finally, these two values of error energy were compared to see which was smaller. The results were 29.74% for British Coal's data and 24.64% for my reprocessed data.

The optimum time shifts for the two observed traces are slightly different: the observed trace was lagged relative to the reflection coefficient sequence by 9 ms for British Coal's data and 11 ms for my reprocessed data.

The results imply that the reprocessed data are an improvement on British Coal's. From now on, only the reprocessed dataset will be considered for analysis and discussion.

**Figure 5.1** Relationship between the time shift and error energy for all 31 positions of the desired output when extracting the wavelet at Thorny Plantation borehole.



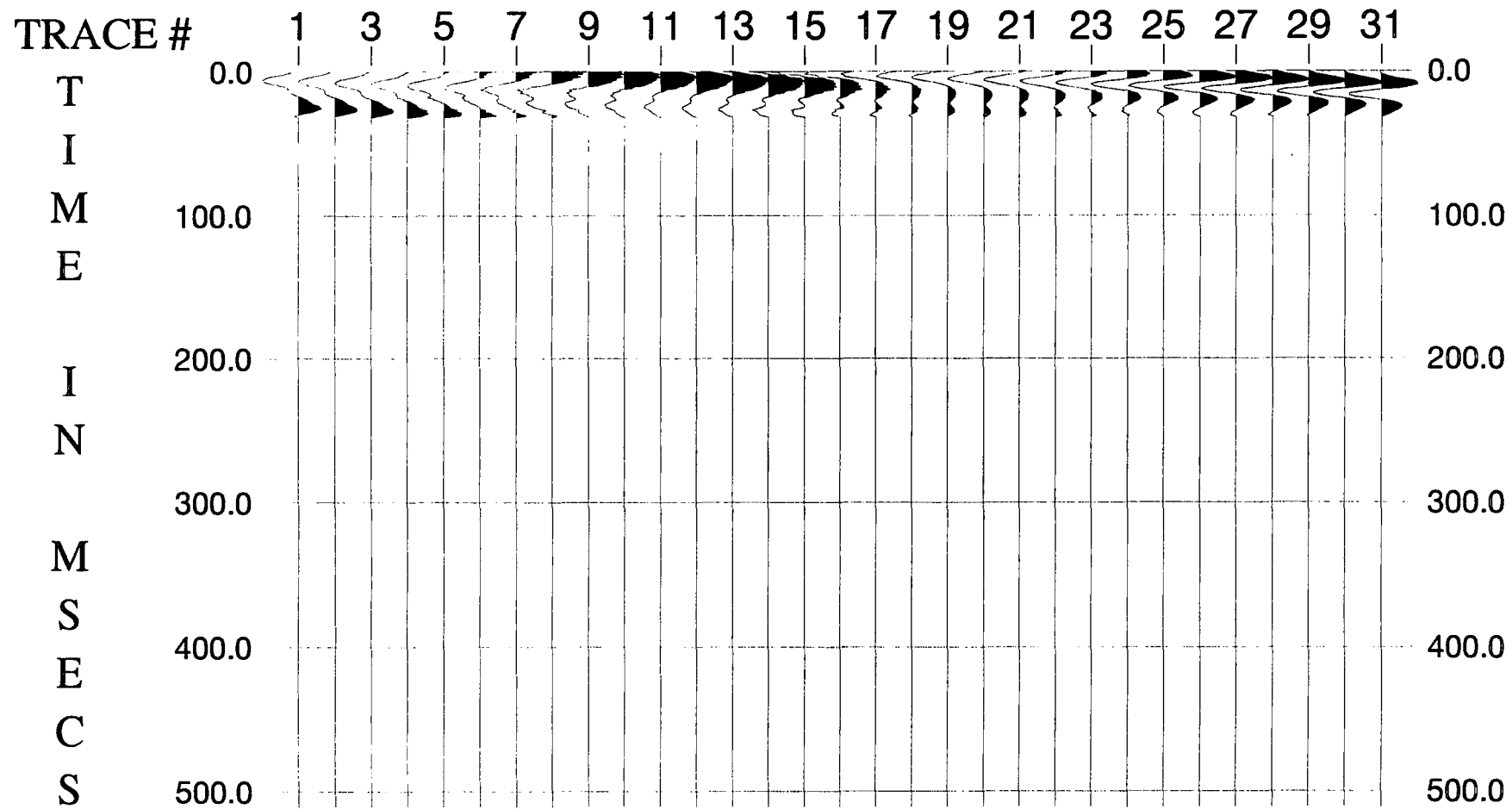


**Figure 5.2** All the extracted 31 wavelets at Thorny Plantation borehole.

### 5.2.2 Time Shift for the Extracted Wavelet

In the previous section, it was noted that there is a time shift associated with the optimum extracted wavelet. After comparison of the observed trace with the well log at Thorny Plantation borehole, the length of the maximum time shift was set to be 15 ms during this procedure. Figure 5.1 shows the relationship between the time shift and error energy for all 31 positions of the desired output (the observed trace window) relative to the input (the reflection coefficient sequence). The minimum error energy corresponds to a time lag of the desired output by 11 ms.

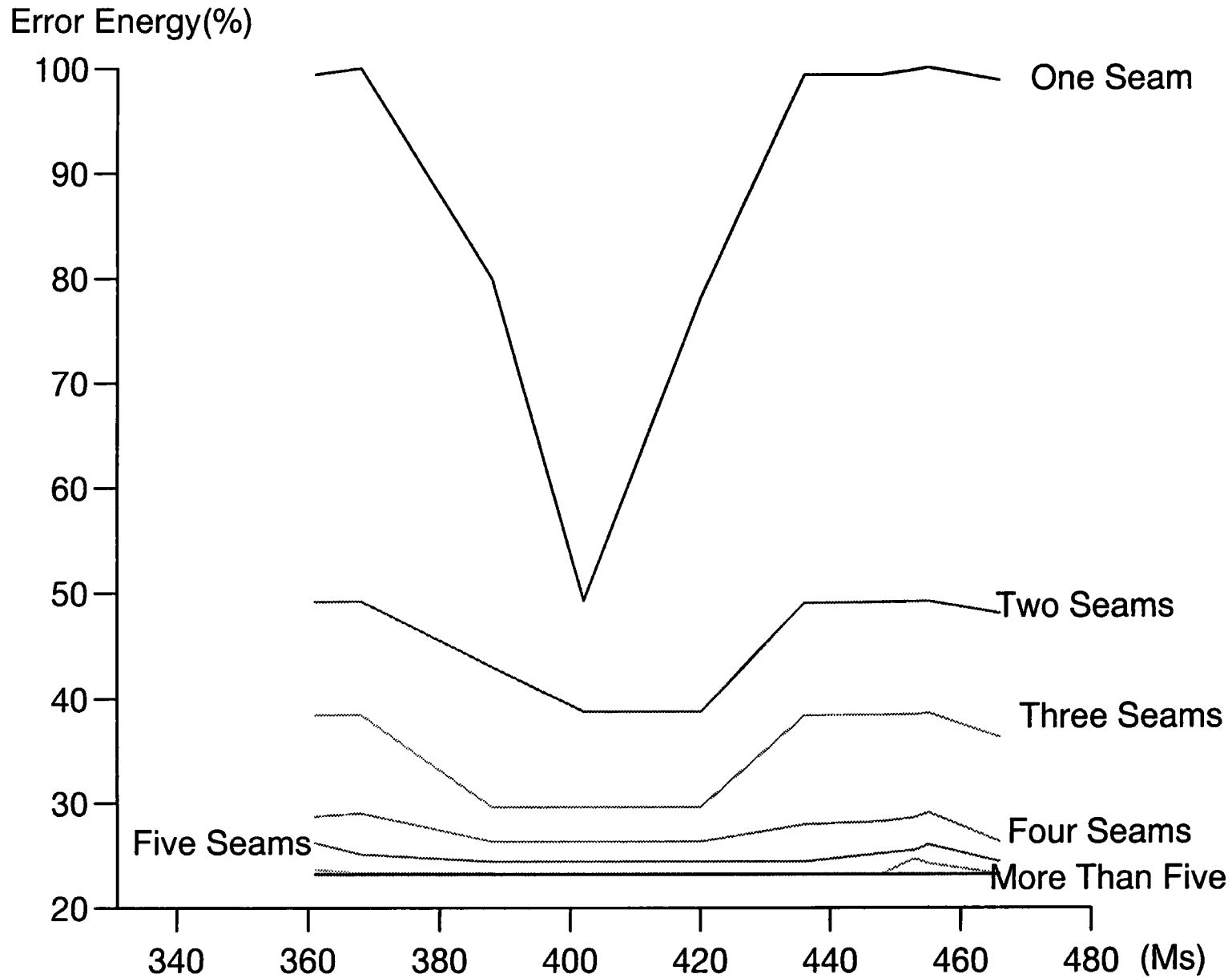
The extracted wavelets do not only differ by a time shift but also have different shapes. Figure 5.2 shows all the 31 wavelets extracted in this process, trace 1 corresponding to a time shift of -15 ms, trace 2 to -14 ms, and so forth. Note that trace 27 is the optimum extracted wavelet in this example. In order to compare the inversion result with the processed section, the reflection coefficient sequence was moved back 11 ms to match the observed trace.

### 5.2.3 Identification of the Main Coal Seams

It may be seen from the well logs (Figure 3.20) that several coal seams could be responsible for events on the seismic section. In order to use the minimum number of earth model parameters, it was necessary to determine which are the dominant coal seams that generated the main reflections on the observed trace, and just invert to optimize their parameters. In this procedure, the time window between 331 ms and 480 ms was again chosen to cover all the coal seams.

The method I used was simply to carry out a sequence of trials. Firstly, the most dominant coal seam was determined by making a one-layer guess model for each coal

**Figure 5.3** Contributions of the various coal seams to reduction of the error energy following inversion at CDP 940, the nearest CDP to Thorny Plantation borehole.



seam in turn. According to the well logs and lithology information at Thorny Plantation (Figs. 3.17 and 3.20), there are 10 coal seams in this borehole, and the acoustic impedances of coal seams and country rocks are approximately 4.0 and 7.6 ( $\text{g/cm}^3$ )(km/s), respectively. For each coal seam, a boundary location inversion by GLI was applied. The correlation coefficient and error energy between the synthetic trace calculated from this inverted model and the observed trace is given in Table 5.1. The most dominant coal seam is obviously the one at 402-409 ms as it has the largest correlation coefficient and the least error energy.

Guess Coal Seams (ms)	Corr. Coefficient	Error Energy	Inverted Boundary
359 - 362	0.0765	99.42 %	361 - 362 (ms)
367 - 369	0.0	100.0 %	368 - 368 (ms)
386 - 391	0.4531	79.91 %	387 - 390 (ms)
401 - 406	0.7883	49.25 %	402 - 409 (ms)
422 - 427	0.4675	78.14 %	420 - 429 (ms)
435 - 438	0.0830	99.33 %	436 - 438 (ms)
447 - 450	0.0816	99.34 %	448 - 449 (ms)
453 - 454	0.0570	99.74 %	453 - 454 (ms)
457 - 459	0.0	100.0 %	455 - 455 (ms)
463 - 466	0.1273	98.79%	466 - 468 (ms)

Table 5.1 Searching for the most dominant coal seam at Thorny Plantation

The second trial was to take this dominant coal seam with each of the other nine coal seams in turn, and use GLI to optimize the boundary locations to find which pairing is the most dominant. Repeating this procedure for combinations of three seams, four seams, and so on, determines the contributions of all coal seams in order. Figure 5.3 shows the relative size of their contributions.

The ordering of the coal seams turned out to be the same as in the first trial for individual seams. However, only after all the trials had been done could the error energy and correlation coefficient for each optimum combination be found. From Fig. 5.3, it can be

seen that for more than three trials, the decrease in error becomes very small. I should point out that with five or more coal seams, the correlation coefficient and error energy (0.8841 and 24.42 %) are even better than those obtained from the well logs (0.8729 and 24.64%). This is because there were some errors in the well logging and some noise on the observed seismic trace. Consequently, as more and more earth model parameters are introduced for inversion, the fit will progressively improve, and at some point will become better than the fit from any fixed earth model.

The optimum combination of three main coal seams accounts for more than 80% of the energy on the observed trace at Thorny Plantation borehole. Therefore, these three coal seams were taken as the target seams to invert, together with the immediately underlying seam, which was included to ensure to optimum inversion for the middle two thickest coal seams.

#### 5.2.4 Construction of Initial Guess for the Earth Model

Based on the previous discussion, the four chosen coal seams are at two-way times given by the well log information (Fig. 3.20) as follows: Black Rake at 389 - 391 ms, Deep Main at 402 - 407 ms, Parkgate/Tuption at 422 - 428 ms and Yard at 436 - 437 ms. In order to get a better estimate of the extracted wavelet, a shorter time window between 380 ms and 439 ms was chosen and the optimum wavelet was again found by solving the normal equations for a Wiener shaping filter. The corresponding time shift was a lag of the desired output by 10 ms. The wavelet used for constructing the guess earth model was the extracted wavelet.

The acoustic impedance values of the top and bottom coal seams were set to be 4.0 ( $\text{g/cm}^3$ )(km/s) and of the two middle main coal seams were set to be 3.0 ( $\text{g/cm}^3$ )(km/s), all with gradients of zero. These values were fixed for all inversions run along the seismic sections. The acoustic impedance values and gradients are more difficult to cope with for

the country rocks because they are average contributions from different lithologies. When the acoustic impedance values were treated as variable parameters, they were constrained between values of 12.0 and 5.0 (g/cm<sup>3</sup>)(km/s), chosen according to the maximum range of values on the well logs.

Because the initial guess earth model was to be constructed at the borehole, it seemed reasonable to assume that the boundary locations of these coal seams and the wavelet are almost correct. Based on this, I fixed all the parameters apart from the acoustic impedance values of the country rocks, and inverted for them. However, the results gave acoustic impedance values which were not at all similar to their values known from well log information. As a cross-check, I fixed the acoustic impedance values from the well logs and inverted for the boundary locations. The results were also unsatisfactory because the Deep Main seam was apparently thicker than Parkgate/Tuption. This is not true according to the well log information. It is not possible for the seam thicknesses and the acoustic impedance values given by the well logs to be so badly wrong. The discrepancy must result from problems with the observed trace, which is only crudely approximated by the simple convolutional model.

In order to make progress with inverting the seismic section, a decision had to be taken on which parameters were the interesting ones to invert, the thicknesses of the coal seams or the acoustic impedance values. Either an increase<sup>in</sup> the thicknesses of the coal seam or an increase in the acoustic impedance contrast will cause the amplitude of the seismic trace to increase (Widess, 1973). Therefore, I chose to fix the boundary locations and acoustic impedance values of the coal seams from the well logs, and to invert for the acoustic impedance values of the country rocks to get the best fit to the observed trace at the borehole. The results comprise the initial guess for the earth model, shown in Table 5.2. The acoustic impedance values of the country rocks obtained are not true values, but simply the best-fitting values for the known parameters of the coal seams.

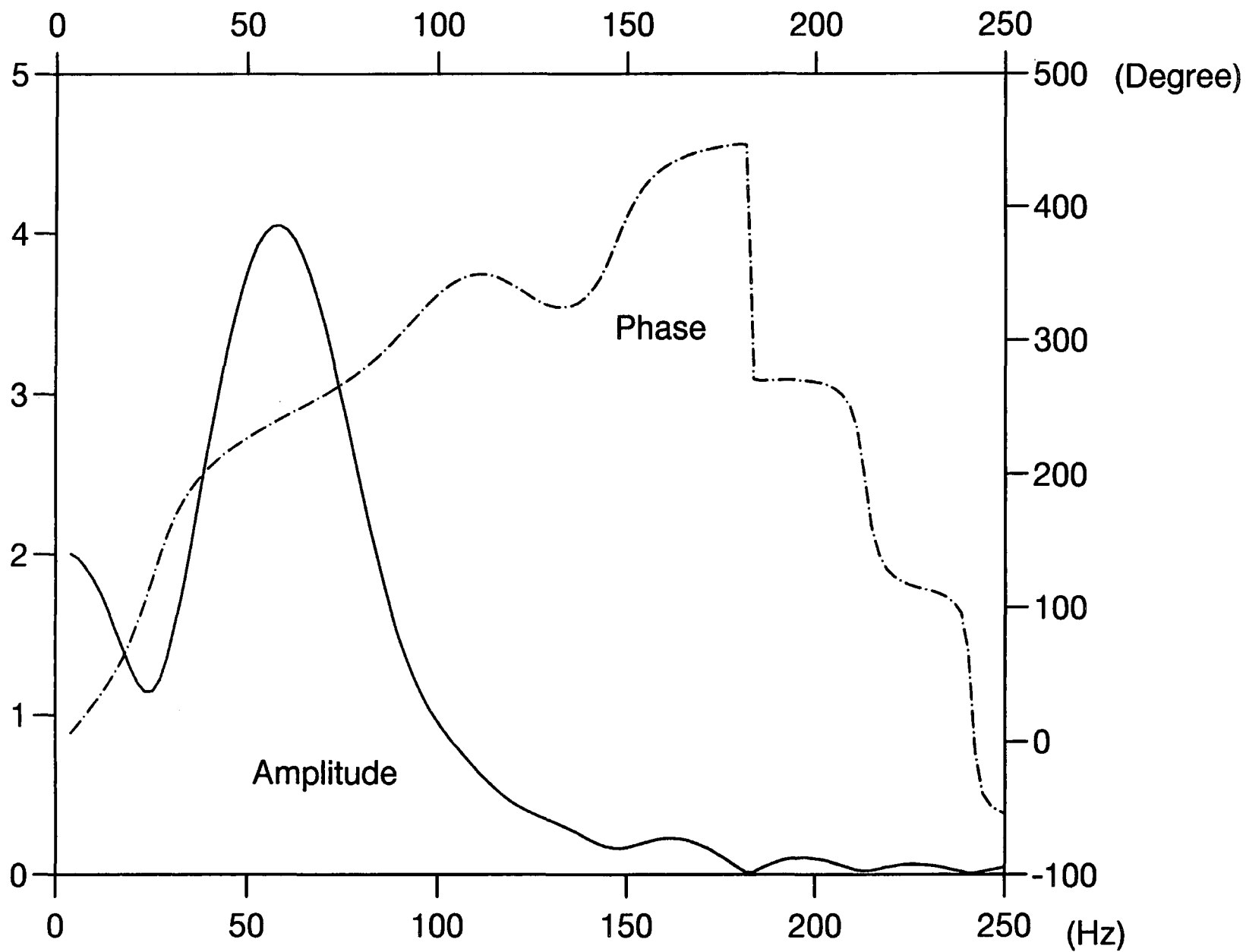
Boundary Locations (ms)	Acoustic Impedance (g/cm <sup>3</sup> )(km/s)	Acous. Imp. Gradients (g/cm <sup>3</sup> )(m/s <sup>2</sup> )
	6.9	0.0
389		
	4.0	0.0
391		
	9.9	0.0
402		
	3.0	0.0
407		
	6.0	0.0
422		
	3.0	0.0
428		
	5.5	0.0
436		
	4.0	0.0
437		
	7.6	0.0

Table 5.2 Initial guess earth model at Thorny Plantation borehole

If we assume that the forward-modelled trace generated by convolving the extracted wavelet with the reflection coefficient sequence from the well logs is a signal trace, the difference between the observed trace and this synthetic trace should be the noise trace. The signal-to-noise amplitude ratio is calculated as 1:0.1592 (or greater than 6:1), which is similar to our synthetic example with 15 % random noise added.

The correlation coefficient and error energy are 0.9518 and 9.12 % for this earth model with the extracted wavelet. It is interesting to note that the error energy is less than that obtained (10.29 %) using the complete reflection coefficient sequence from the well logs with the same extracted wavelet. This suggests that our initial guess earth model is quite good and also that there are some errors on the well logs.

**Figure 5.4** Amplitude and phase spectra of the extracted wavelet at CDP 940, close to Thorny Plantation borehole.



### 5.2.5 Estimation of Wavelet Parameters

The amplitude spectrum and phase spectrum of the optimum extracted wavelet are plotted in Fig. 5.4. From this diagram, it can be seen that the boxcar-with-cosine-tapers, defined by four frequencies, is a reasonable approximation to represent the amplitude spectrum of the extracted wavelet. After fitting the eight parameters to these spectra (Table 5.3) to parameterize the wavelet in the frequency domain, the error energy between the forward-modelled and observed traces was 13.78%.

The next step was to perform GLI for the wavelet parameters for three iterations whilst keeping the earth model fixed, as shown in Table 5.2. The error energy between the forward-modelled and observed traces was reduced to 5.92%, which is less than that found when using the extracted wavelet (9.12%). These optimized values (Table 5.4) comprise the initial guess for the wavelet parameters, and can be seen in Fig. 5.4 to provide a reasonably accurate representation of the extracted wavelet.

$f_1=14$ Hz	$f_2=39$ Hz	$f_3=76$ Hz	$f_4=136$ Hz
$a_0 = 6.45$	$\varphi_0=26$ degree	$\varphi_1 = 5.23$ degree/Hz	$\varphi_2 = -0.02$ degree/Hz <sup>2</sup>

Table 5.3 Estimated wavelet parameters after fitting the spectra

$f_1=18$ Hz	$f_2=42$ Hz	$f_3=57$ Hz	$f_4=150$ Hz
$a_0 = 6.17$	$\varphi_0=80$ degree	$\varphi_1 = 3.67$ degree/Hz	$\varphi_2 = -0.01$ degree/Hz <sup>2</sup>

Table 5.4 Initial guess for the wavelet parameters  
after optimizing the fitted values

### 5.2.6 Inversion of the Trace at the Borehole

In the preceding five sub-sections, I have described how the initial guess model was established for the boundary locations, acoustic impedance values and gradients, and the wavelet parameters. The earth model parameters for the initial guess are given in Table 5.2 and the wavelet parameters in Table 5.4. The next steps were to apply GLI separately for the boundary locations, acoustic impedance parameters for the country rocks and wavelet parameters. This was done consecutively over two complete iterations of the three-stage inversion process.

Because of the relatively accurate information from the initial guess for the boundary locations, there were only small changes in the boundary locations and wavelet parameters, but some big changes in the acoustic impedance parameters. Final values are shown in Table 5.5 and yield an error energy of 2.15 %.

Wavelet	Bound. Locations. (ms)	Acous. Impedance. (g/cm <sup>3</sup> )(km/s)	Ac. Imp. Gradients (g/cm <sup>3</sup> )(m/s <sup>2</sup> )
$f_1 = 13 \text{ Hz}$	390	9.1	0.0
$f_2 = 42 \text{ Hz}$	391	4.0	0.0
$f_3 = 53 \text{ Hz}$	402	12.0	0.0
$f_4 = 151 \text{ Hz}$	407	3.0	0.0
$a_0 = 6.17$	421	7.1	0.0
$\varphi_0 = 79 \text{ degree}$	427	3.0	0.0
$\varphi_1 = 3.67 \text{ deg./Hz}$	436	5.0	0.0
$\varphi_2 = -0.01$	437	4.0	0.0
(degree/Hz <sup>2</sup> )		5.0	0.0

Table 5.5 Inversion results at Thorny Plantation borehole

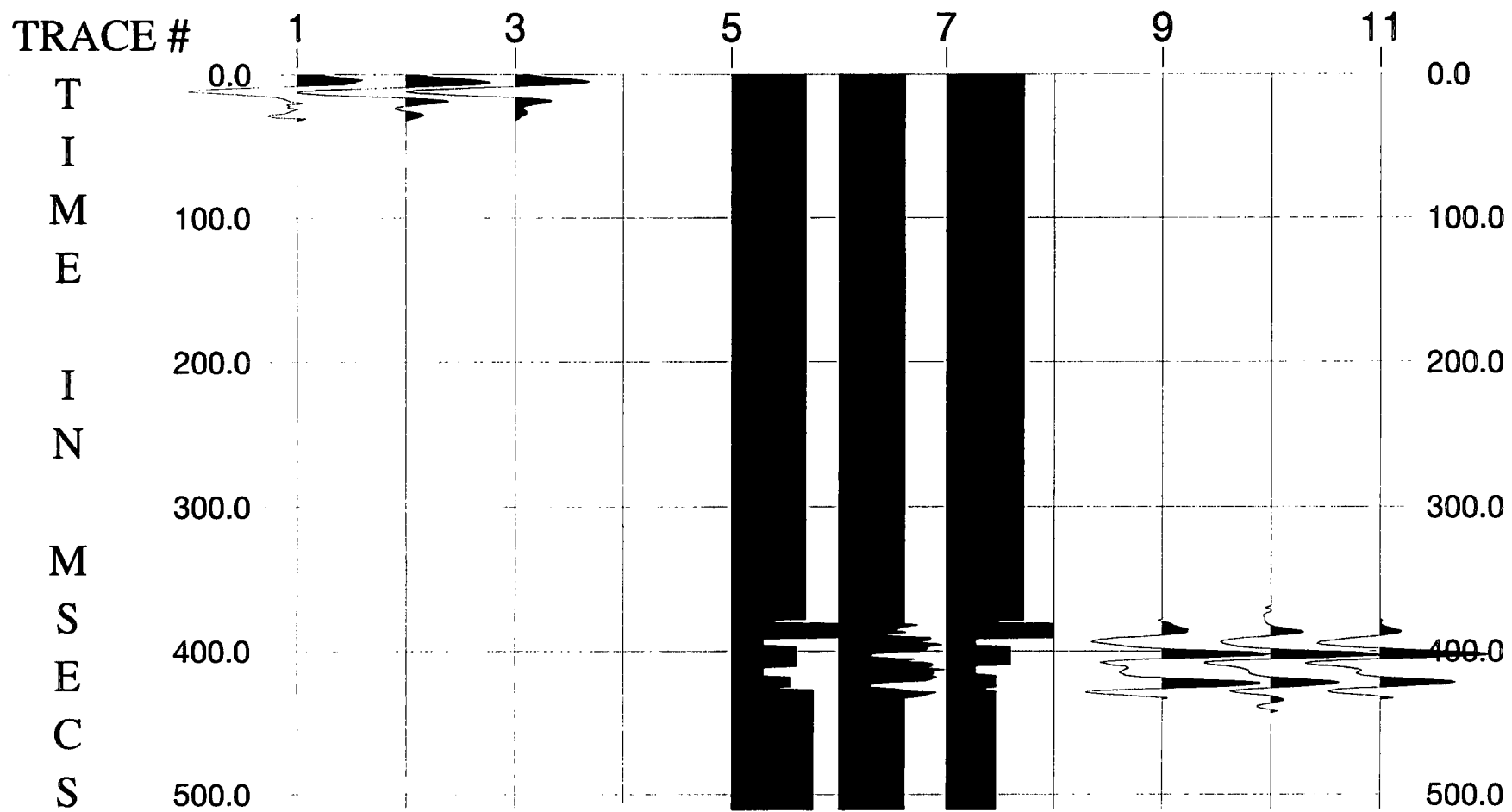


**Figure 5.5a** Inversion results for all parameters at CDP 940.

The stability of the boundary locations with respect to their locations in the well logs is satisfactory. Also, the 8-parameter wavelet seems to represent the extracted wavelet satisfactorily in Thorny Plantation. However, noise on the observed trace is presumably responsible for the discrepancy between the inverted acoustic impedance parameters and those found from the well logs.

Figure 5.5a shows the results of this procedure for the trace at CDP 994. Trace (1) is the extracted wavelet. Trace (2) is the estimated wavelet after phase unwrapping. Trace (3) is the inverted wavelet. Trace (5) is the initial guess for the earth model. Trace (6) is the well log at Thorny Plantation. Trace (7) is the inverted earth model. Trace (9) is the forward-modelled trace calculated from the extracted wavelet and well log data. Trace (10) is the observed trace at CDP 994. Trace (11) is the forward-modelled trace from the inverted wavelet and inverted earth model at CDP 994.

### 5.3 Systematic Study At Pillbox

Similar to the work at Thorny Plantation borehole, I carried out a systematic study at Pillbox borehole using the nearest trace at CDP 1230.

The optimum time shift calculated during wavelet extraction was a time lag of the desired output by 38 ms compared to 11 ms at Thorny Plantation borehole. This means that there has been some change in the datum level, either on the seismic section or between the well logs. I think it is due to the well logs because I reprocessed the seismic data along the section, paying particular attention to the field statics and autostatics, and judge that it is impossible to cause such a big datum difference. In this respect, my processing was also consistent with British Coal's. It is easy to see that the optimum time shift calculated at Pillbox borehole is about right by locating the Deep Main horizon on the reprocessed

section at the right hand side (350 ms - see Fig. 3.14) and comparing it with the well logs (386 ms - see Fig. 3.21).

Then I attempted to identify the most dominant coal seams among the ten seams present in Pillbox borehole (Fig. 3.21). The search window was between 310 and 460 ms to include all the ten coal seams. The acoustic impedance values were set to be 4.0 (g/cm<sup>3</sup>)(km/s) for coal seams and 7.6 (g/cm<sup>3</sup>)(km/s) for country rocks, as at Thorny Plantation borehole. Fortunately, the results were similar to those obtained at Thorny Plantation (Table 5.6). The three dominant coal seams are the Black Rake (370 - 375 ms), Deep Main (383 - 390 ms) and Parkgate/Tuption (399 - 406 ms). Again I chose these coal seams as the target seams to invert, together with the immediately underlying Yard seam (413 - 417 ms) to ensure optimum inversion for the middle two thickest coal seams.

Guess Coal Seams (ms)	Corr. Coefficient	Error Energy	Inverted Boundary
347 - 348	0.3308	89.11 %	347 - 352 (ms)
355 - 357	0.1624	104.2 %	355 - 356 (ms)
368 - 374	0.3997	84.08 %	370 - 375 (ms)
384 - 390	0.5182	75.14 %	383 - 390 (ms)
401 - 406	0.4501	80.21 %	399 - 406 (ms)
414 - 416	0.2764	92.50 %	413 - 417 (ms)
426 - 428	0.1472	97.90 %	426 - 428 (ms)
430 - 431	0.0739	99.48 %	430 - 431 (ms)
436 - 437	0.0	100.0 %	436 - 436 (ms)
442 - 443	0.0565	99.76%	441 - 442 (ms)

Table 5.6 Searching for the most dominant coal seams at Pillbox

In order to get a better estimate of the extracted wavelet, a new shorter inversion window was set from 331 to 395 ms, which takes into account the 38 ms time shift and keeps almost the same length as at Thorny Plantation for comparison. The error energy between the observed trace and the forward-modelled trace obtained from the well logs was 24.52 %. That is to say, the SNR (1:0.3716, or less than 3:1) of the observed trace at

Pillbox is worse than the SNR (1:0.1592) at Thorny Plantation. Also it can be seen on Fig. 5.5b that the extracted wavelet is very complicated.

The next step was to obtain an initial guess earth model for subsequent optimization of wavelet and earth model parameters. As described in §5.2.4, a decision should be made before constructing the initial guess for the earth model. Therefore I decided to use the boundary locations obtained from Pillbox borehole. Then I inverted for the acoustic impedance values to obtain the initial guess for the earth model, as shown in Table 5.7. Due to the relatively small reflection from the Parkgate/Tuption seam at this trace, the acoustic impedance values of the country rock above and below this seam became very small, which does not match the well log information.

Boundary Locations (ms)	Acoustic Impedance (g/cm <sup>3</sup> )(km/s)	Acous. Imp. Gradients (g/cm <sup>3</sup> )(m/s <sup>2</sup> )
	5.5	0.0
372		
	4.0	0.0
374		
	7.7	0.0
384		
	3.0	0.0
389		
	5.0	0.0
401		
	3.0	0.0
407		
	5.3	0.0
414		
	4.0	0.0
415		
	6.7	0.0

Table 5.7 Initial guess earth model at Pillbox borehole

The eight parameters of the wavelet after phase unwrapping and fitting the spectra are shown in Table 5.8. The parameters were then optimized by three iterations of GLI whilst

keeping the earth model fixed (Table 5.7) to give the initial guess for the wavelet parameters in Table 5.9.

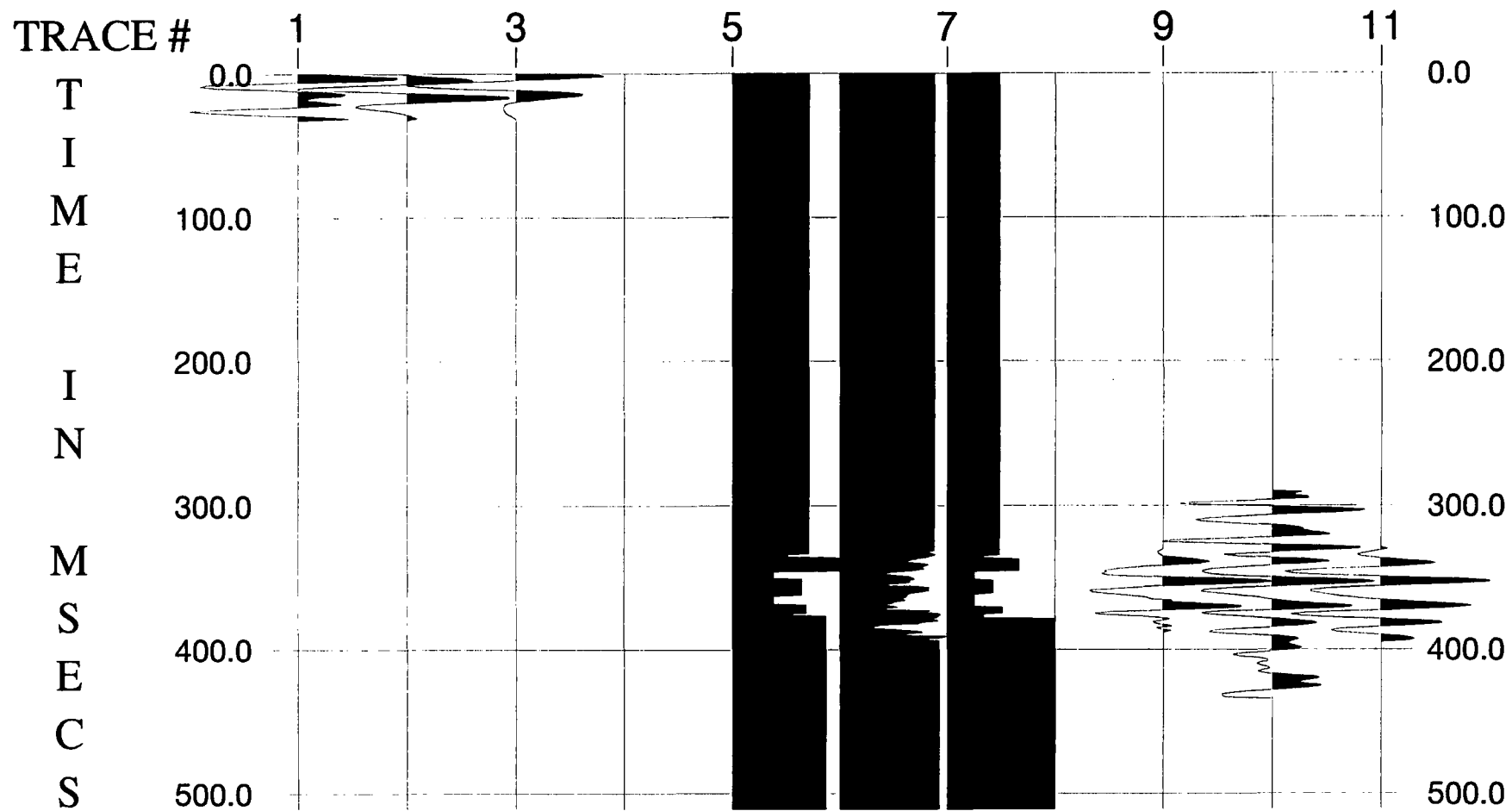
$f_1=42$ Hz	$f_2=55$ Hz	$f_3=78$ Hz	$f_4=138$ Hz
$a_0 = 3.62$	$\varphi_0 = -22$ degree	$\varphi_1 = -1.16$ degree/Hz	$\varphi_2 = 0.01$ degree/Hz <sup>2</sup>

Table 5.8 Estimate of the wavelet parameters  
after fitting the spectra

$f_1=41$ Hz	$f_2=55$ Hz	$f_3=76$ Hz	$f_4=138$ Hz
$a_0 = 2.80$	$\varphi_0 = -24$ degree	$\varphi_1 = -1.64$ degree/Hz	$\varphi_2 = 0.03$ degree/Hz <sup>2</sup>

Table 5.9 Initial guess for the wavelet parameters  
after optimizing the fitted values

The error energy and the correlation coefficient are equal to 25.48 % and 0.8876 for the initial guess wavelet in Table 5.9 and for the earth model in Table 5.7. It can be seen that the wavelet obtained at Pillbox borehole is different from that at Thorny Plantation borehole (Table 5.4). Comparing the two sets of well logs (Figs. 3.20 and 3.21) and lithology information (Figs. 3.17 and 3.18), there are no big differences in the four coal seams apart from the small changes in the separation between the coal seams. Therefore, I infer that the differences resulted from different noise contributions in the observed traces at each borehole. Hence I regard the inverted wavelet at Thorny Plantation borehole as being more reliable because the error energy is less. In the next section, I will show the different inversion results obtained using these two different wavelets.



**Figure 5.5b** Inversion results for all parameters at CDP 1230, the nearest CDP to Pillbox borehole.

Using the initial guesses for the earth model (Table 5.7) and wavelet (Table 5.9), two iterations of the three stage GLI process were carried out, inverting successively for the boundary locations, acoustic impedance values, and wavelet parameters. The inversion results are listed in Table 5.10. The error energy and correlation coefficient for this inverted model are equal to 14.96% and 0.9365, respectively.

Wavelet	Bound. Locations. (ms)	Acous. Impedance. (g/cm <sup>3</sup> )(km/s)	Ac. Imp. Gradients (g/cm <sup>3</sup> )(m/s <sup>2</sup> )
$f_1 = 21$ Hz	372	6.0	0.0
$f_2 = 51$ Hz	375	4.0	0.0
$f_3 = 67$ Hz	385	7.9	0.0
$f_4 = 143$ Hz	390	3.0	0.0
$a_0 = 2.8$	401	5.0	0.0
$\varphi_0 = -9$ degree	407	3.0	0.0
$\varphi_1 = -1.6$ deg./Hz	413	5.7	0.0
$\varphi_2 = 0.02$	416	4.0	0.0
(degree/Hz <sup>2</sup> )		7.2	0.0

Table 5.10 Inversion results at Pillbox borehole

Figure 5.5b is the results of this procedure for the trace at CDP 1230. Trace (1) is the extracted wavelet. Trace (2) is the estimated wavelet after phase unwrapping. Trace (3) is the inverted wavelet. Trace (5) is the initial guess for the earth model. Trace (6) is the well log at Pillbox. Trace (7) is the inverted earth model. Trace (9) is the forward-modelled trace calculated from the extracted wavelet and the well logs. Trace (10) is the observed trace at CDP 1230. Trace (11) is the forward-modelled trace from the inverted wavelet and inverted earth model at CDP 1230.

## 5.4 Inversion for the Whole Section

### 5.4.1 Introduction

Theoretically, there should be no difference between inverting the data from either borehole to the other, if the parameters used and the inversion window are kept the same. However, it has been seen in the previous section that there are some differences in the initial guess wavelets and some parameters had to be fixed using a priori information when obtaining the initial guess earth models. It looks as though the quality of the data at Thorny Plantation is better than at Pillbox according to the error energy values and correlation coefficients. In order to see the effects of these differences, inversion for the whole section from each direction was carried out.

As can be seen in Fig. 3.14, the main coal seams are at 400 ms and 420 ms at CDP 994, but are significantly shallower at 350 ms and 370 ms at CDP 1230. Therefore, in order to keep the target seams within the inversion window, it is necessary to vary the location of the window along the section.

In order to get a stable solution for the nonunique inversion problem, it is better to fix some parameters and invert for a limited number of parameters by starting from the initial guess models (e.g. Table 5.2 and 5.4) rather than the inverted results at the borehole (e.g. Table 5.5) because of errors in the latter, as will be seen in the following sections. The following inversions were run for two iterations for each type of parameter (boundary locations, 8-parameter wavelet parameters) and two iterations for the overall inversion process.

When inverting the real data, there will be thickness changes for the coal seams. According to the study by Okaya (1995), in our situation, where the thicknesses of the coal seams are less than 10 ms in two-way time, the fundamental amplitude band (FAB) is only preserved between 20 - 150 Hz. Where the coal seam is very thin, i.e. 2 or 3 ms two-way time, the centre frequency of the FAB will be higher than 200 Hz (see Fig. 3 b, Okaya, 1995). The bandwidth of the processed data is 30 - 200 Hz (see §3.1.11) which means that there will be a very small amount of reflection energy with a very high frequency content present in the section when the thickness of a coal seam reduces to less than 3 ms.

In order to form the initial guess for the boundary locations at the next trace, after inverting the previous one, I adopt a combination method by taking the interpreted structural information (Martinez et al., 1992) into account together with the inversion results from the previous trace. The interpreted structural information was obtained by picking the two-way times of strong reflection events from the processed section. There are complementary selectable weighting coefficients between 0.0 to 1.0 for each of them which may be chosen as a result of trial-and error. For instance, if only the inversion results were used, the weighting coefficient will be 1.0 for the inversion results and 0.0 for the interpreted structural information.

#### 5.4.2 From Thorny Plantation to Pillbox

I generally used the initial guess earth model and wavelet at Thorny Plantation borehole as the starting model (i.e. Tables 5.2 and 5.4) to invert the first trace at CDP 994. Inversion then proceeded as described above for the adjacent trace at CDP 995 onwards until reaching CDP 1230, which is the closest trace to Pillbox borehole. Tests indicated that the initial guess for the boundary locations was best obtained by applying equal weighting (coefficients 0.5) to the boundary locations obtained from inverting the previous trace and the boundary locations picking from the interpreted seismic section.

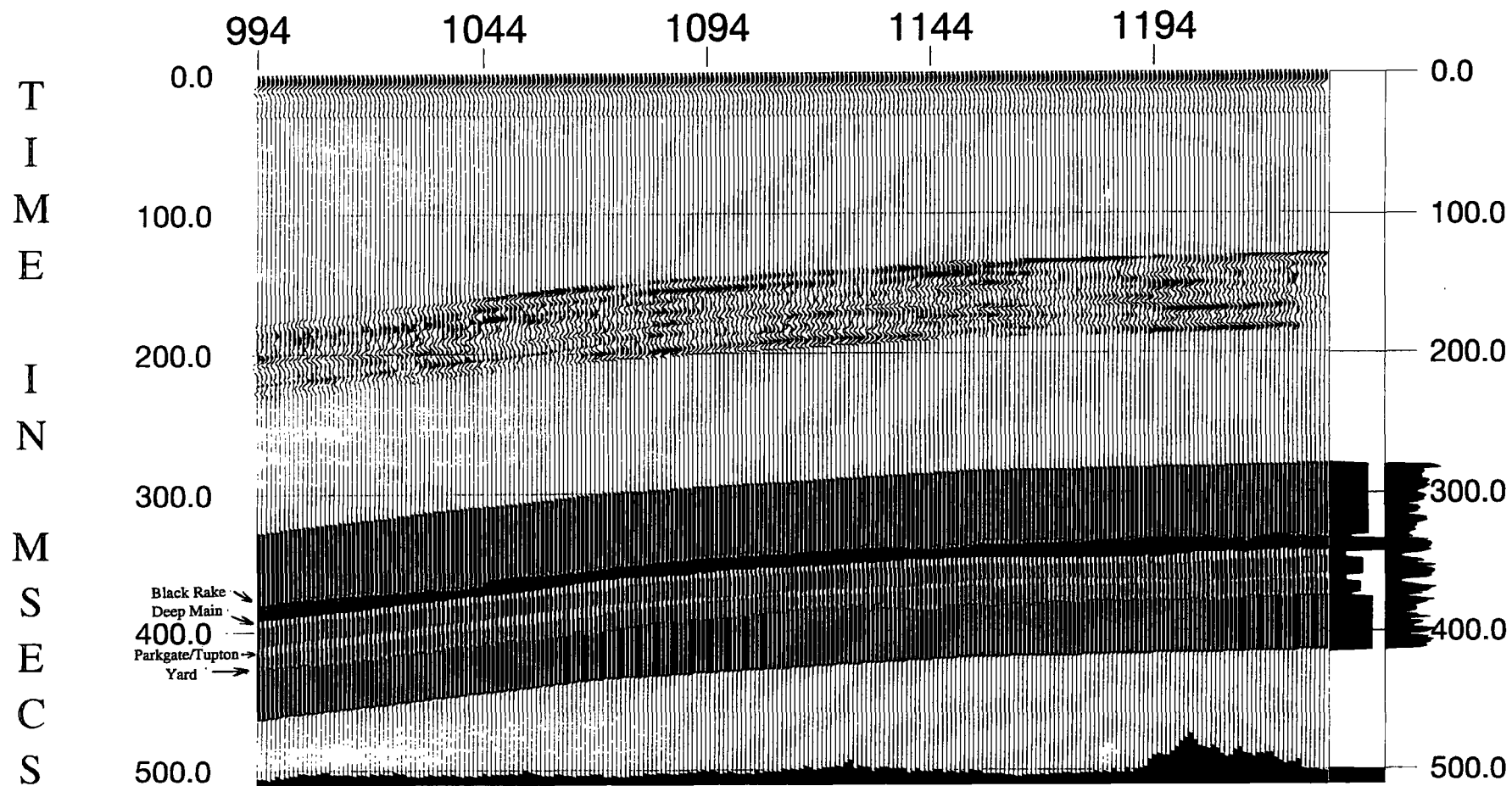


**Figure 5.6a** Inversion for boundary locations with the extracted wavelet obtained from Thorny Plantation borehole using 0.5/0.5 weights for establishing the initial guess model. The two traces on the right are the final inversion result at Pillbox borehole and (far right) the acoustic impedance function from the well logs. The boundary locations and the thicknesses of the main coal seams are almost matched.

Figure 5.6a shows the whole inverted section, in which I only inverted for the boundary locations by GLI, using equal weighting coefficients of 0.5 for the initial guess, and fixed the extracted wavelet and the acoustic impedance values (Table 5.2) along the section.

In order to see the changes of the wavelet along the sections (not the case in this processing), the inverted wavelet is plotted at the top of the trace for each inverted earth model at each CDP location in this figure and in the following ones. The difference between the observed trace and forward-modelled trace (obtained from the inversion result) in the window is also plotted above the earth model with a 200 ms time shift forward. The error energy is plotted below the inverted earth model at each CDP location as a vertical bar, indicating the reliability of the solution. The scale for the error energy is that the timing line at 500 ms corresponds to an error energy of 25 %.

From Fig. 5.6a, it can be seen that the first coal seam (Black Rake) has become very thin between CDP 1185 and CDP 1220 due to the very low reflection amplitudes (Fig. 3.14). At two areas in the middle of the section around CDP 1100 and CDP 1160, the thickness is greater than in other areas, which correlates with the reflection amplitudes on the migrated section.

The thickness of the Deep Main seam was fairly consistent across the whole section. It fluctuates in the vicinity of CDP 1200 and is a little bit thinner on isolated traces at CDPs 1123 and 1190. It can be seen from Fig. 3.14 that in those places the amplitudes of the reflection have decreased.

The thickness of the Parkgate/Tuption seam changes a lot according to the inversion. At first it stays unchanged until CDP 1075. Then it abruptly decreases in thickness by about a half until CDP 1200, which corresponds to an increase in frequency content and a decrease in amplitude of the reflection. Due to the low amplitude and poor continuity of the reflection from this coal seam between CDPs 1190 and 1220, the thickness is further

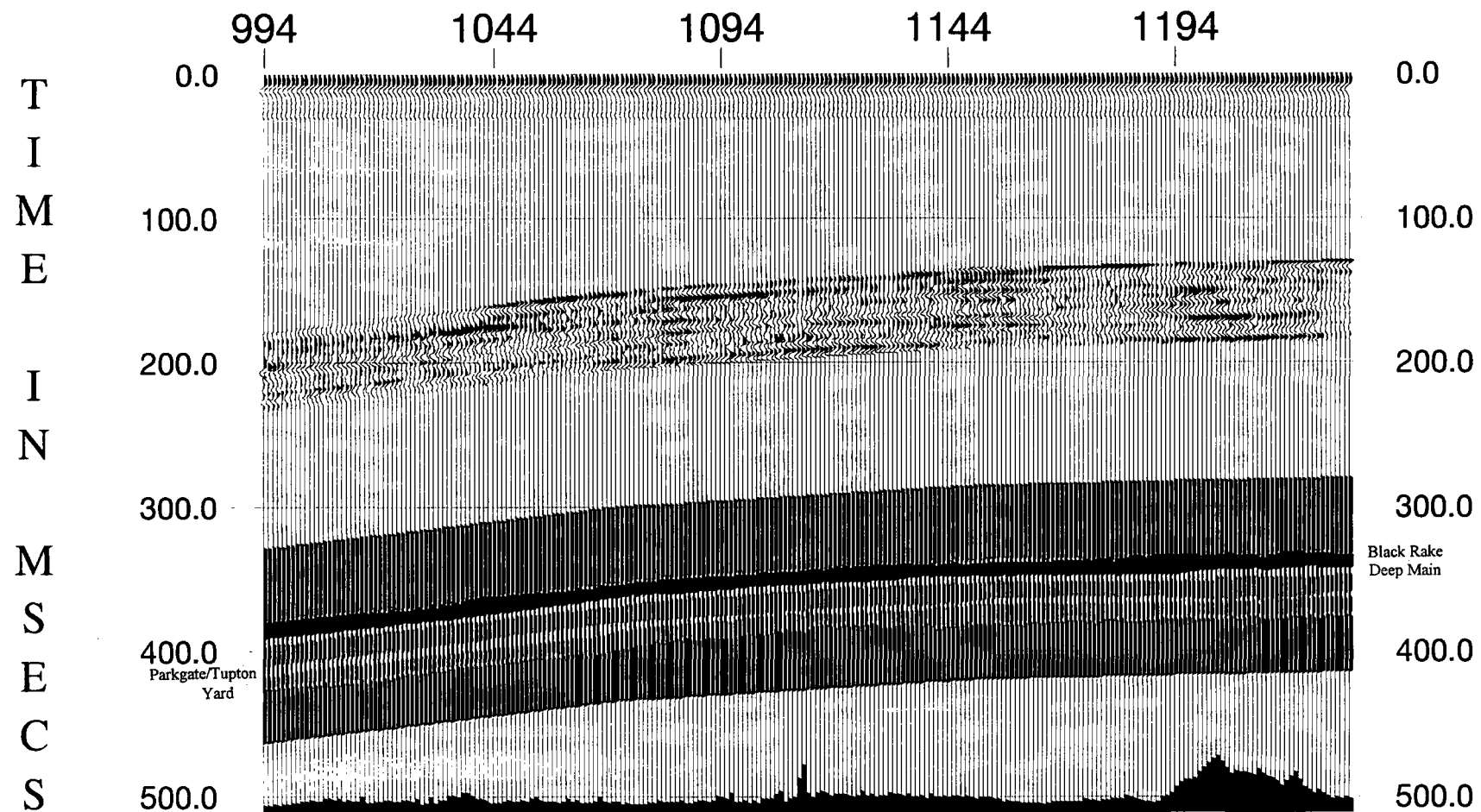


**Figure 5.6b** Inversion for boundary locations with the extracted wavelet obtained from Thorny Plantation borehole using 1.0/0.0 weights, i.e. initial guess based only on the interpreted structural information.

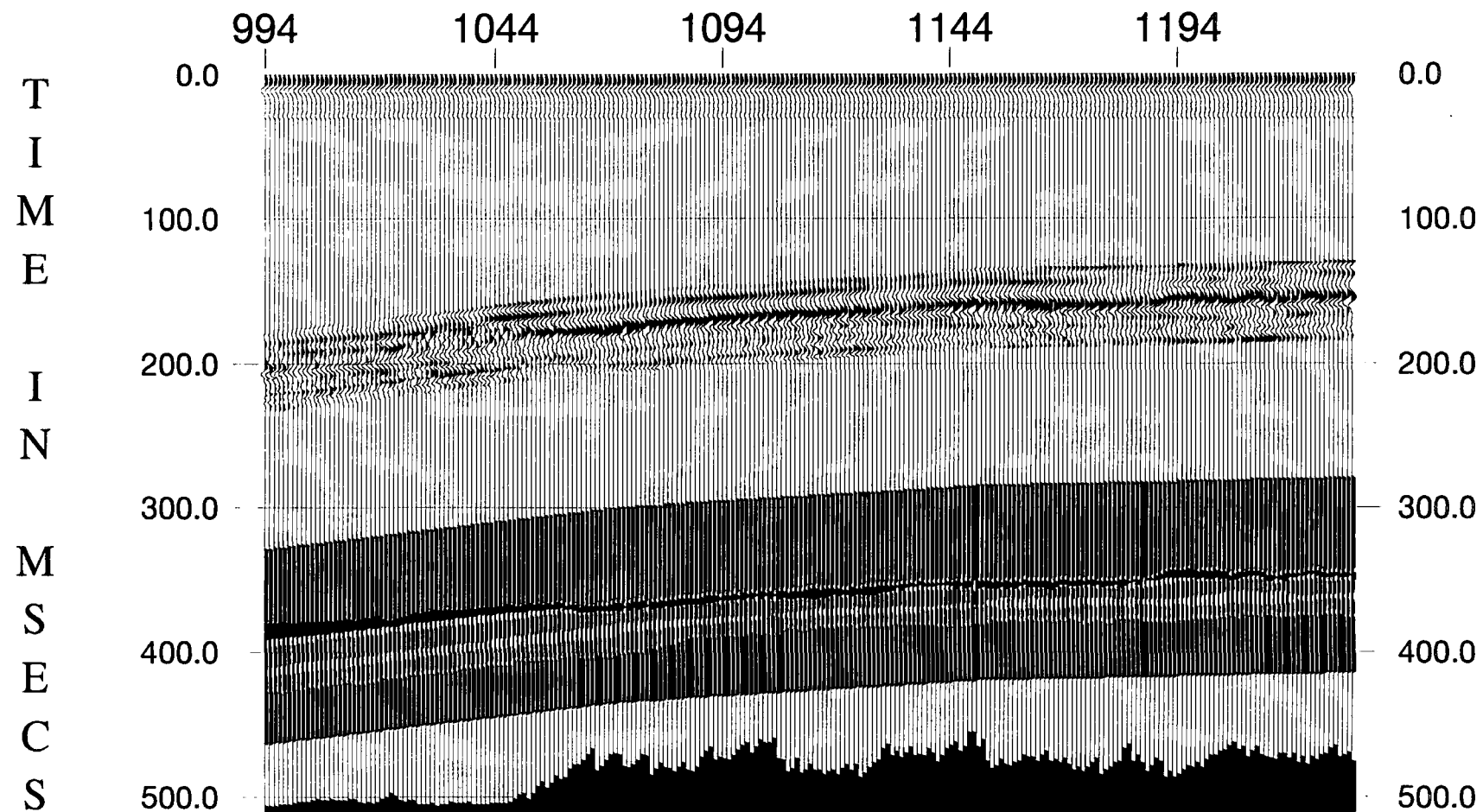


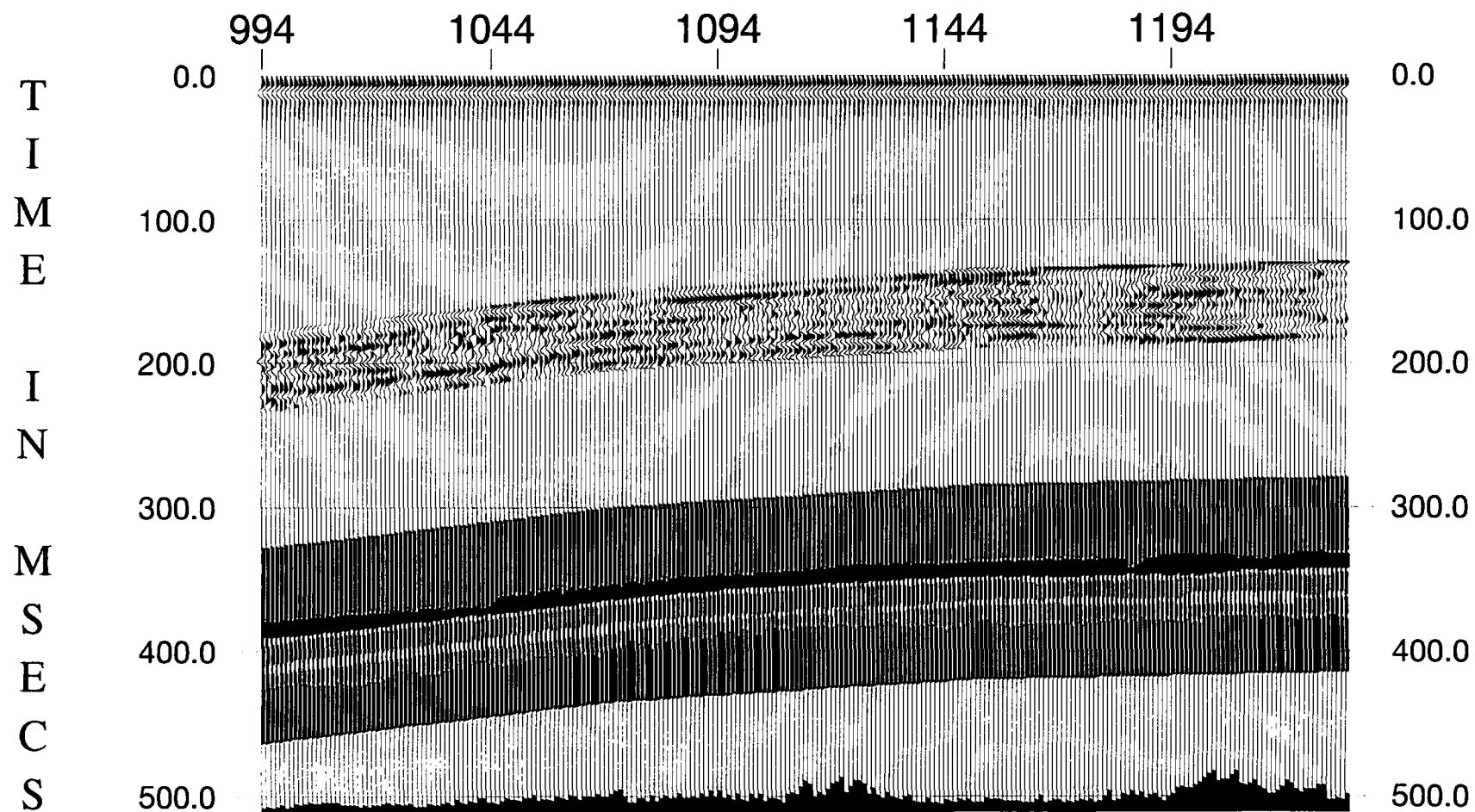
**Figure 5.6c** Inversion for boundary locations with the extracted wavelet obtained from Thorny Plantation borehole using 0.0/1.0 weights, i.e. initial guess based only on the previous trace inversion.

reduced to 1 - 2 ms. But when it reaches CDP 1230, i.e. the location of Pillbox borehole, it became thicker again.

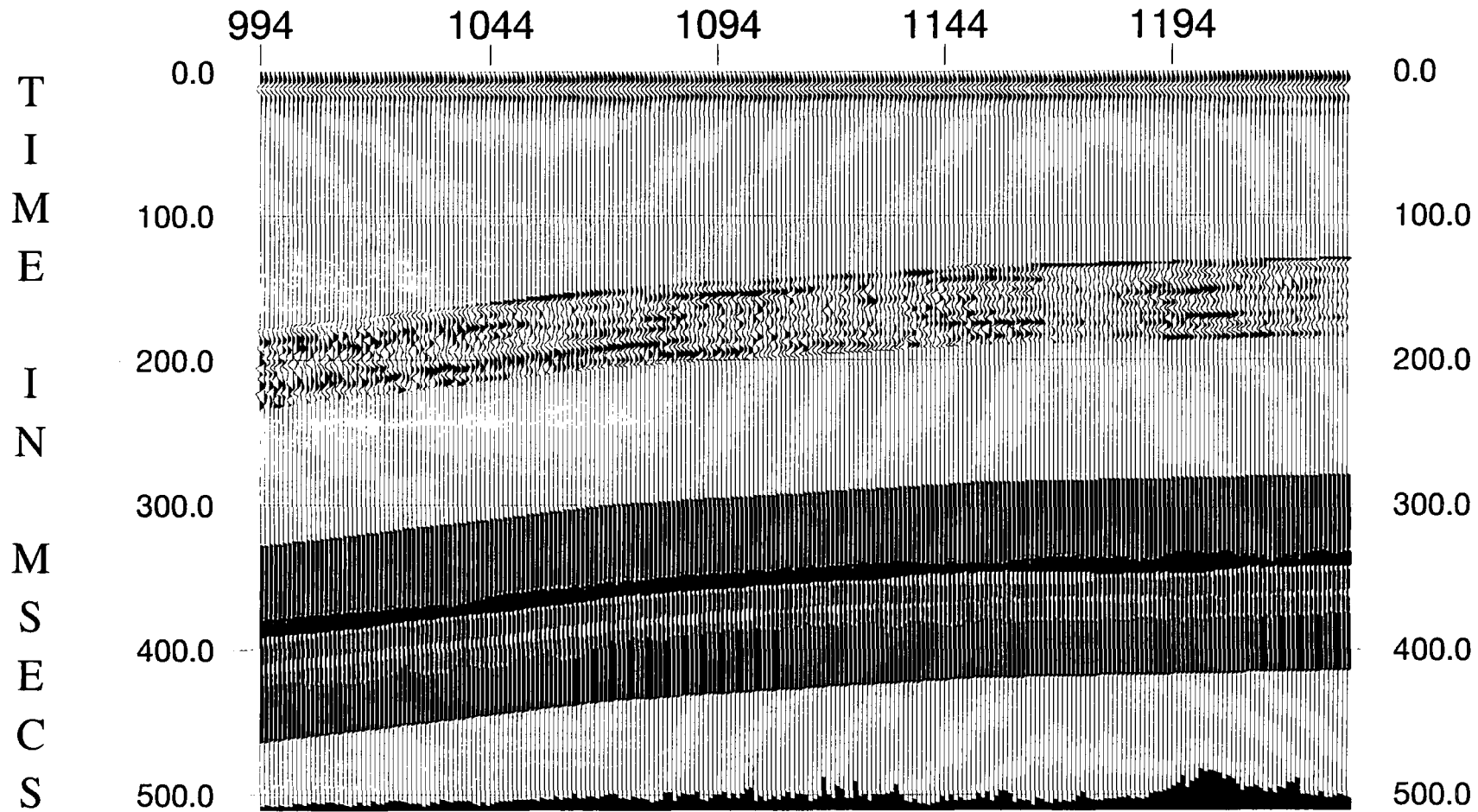
The changes in thickness of the Yard seam also correspond to the reflection character on the processed section. Comparing the inversion results at the right hand side with the systematic studies at Pillbox, and noting the 38 ms time shift difference, the positions of the Black Rake, Deep Main, Parkgate/Tuption and Yard are all matched, but the thicknesses of the seams do not match the well log information at Pillbox (Fig. 3.22). This is because the reflection amplitudes of the observed traces are decreased a lot comparing with the started values at Thorny Plantation and the acoustic impedance values are fixed during this inversion procedure along the section.

Figure 5.6b is a similar inversion to Fig. 5.6a only differing in that the weighting coefficients were 1.0/0.0, i.e., the interpreted structural information was used and the inversion for each trace was totally independent, which is the current method used by other researchers (e.g. Brac et al., 1992). Comparing these two figures, there are no big differences between them. However it can be seen that the error energy at the middle of the section in Fig. 5.6a is a little bit less, and the inversion results look smoother than Fig. 5.6b in some areas.

Figure 5.6c shows the inversion results with 0.0/1.0 weighting coefficients, i.e., the inversion results for the boundary locations from the previous trace were used as the initial guess for the next trace. It can be seen that this method failed to trace the boundaries of these seams past CDP 1060 due to the phase changes on the observed trace. Because the errors in the inverted earth model parameters are reproduced in the initial guess for the next trace, the correct answer may not be obtained after inversion through a poor SNR area. The equal weighting coefficients, giving the results in Fig. 5.6a, are the best pair of those I have tested.



**Figure 5.7a** Inversion for boundary locations with 8-parameter wavelet of Table 5.4 and the initial guess earth model of Table 5.2.



**Figure 5.7b** Inversion for boundary locations and four frequency parameters with 8-parameter wavelet of Table 5.4 and the initial guess earth model of Table 5.2.

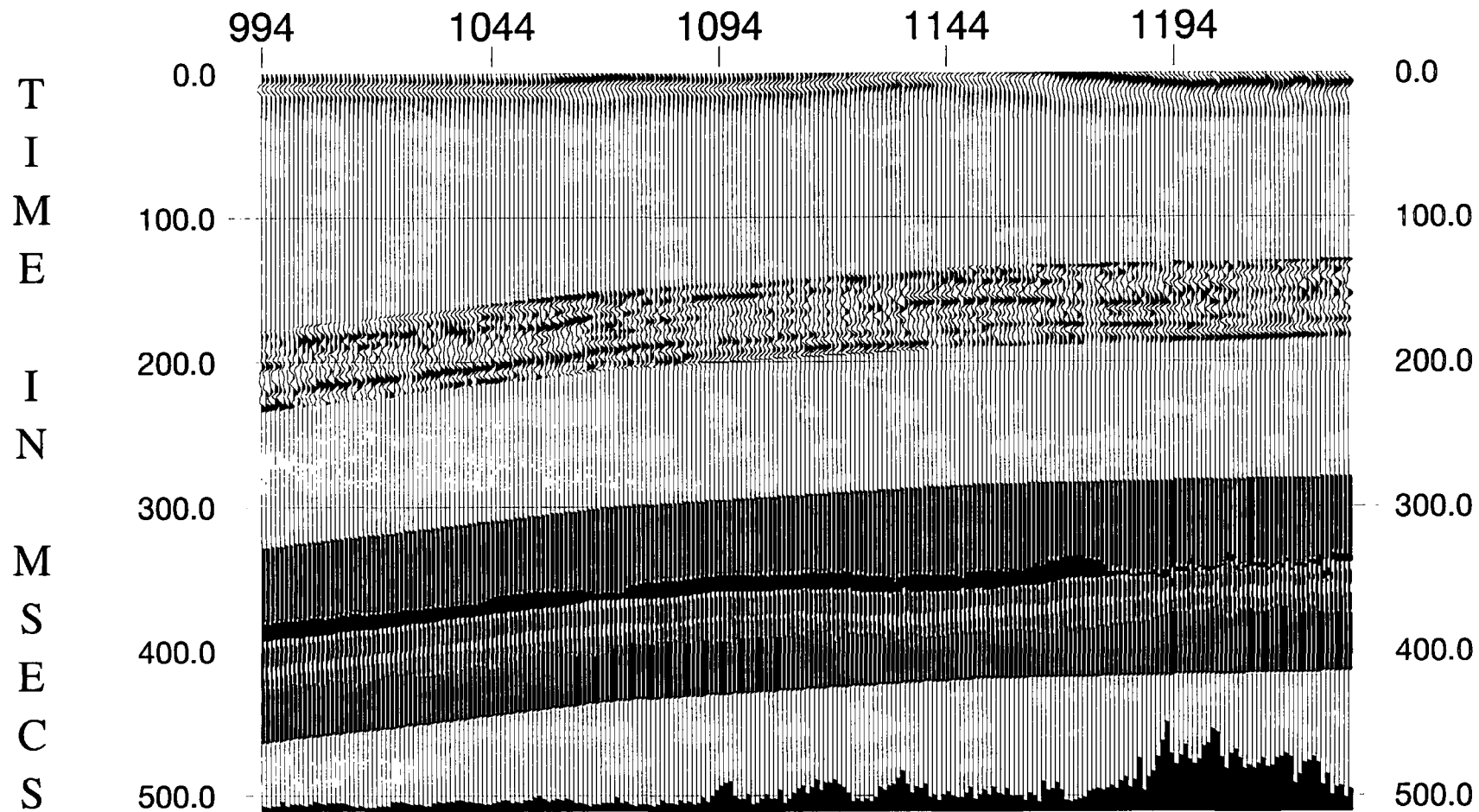


**Figure 5.7c** Inversion for boundary locations and all eight parameters with 8-parameter wavelet of Table 5.4 and the initial guess earth model of Table 5.2.

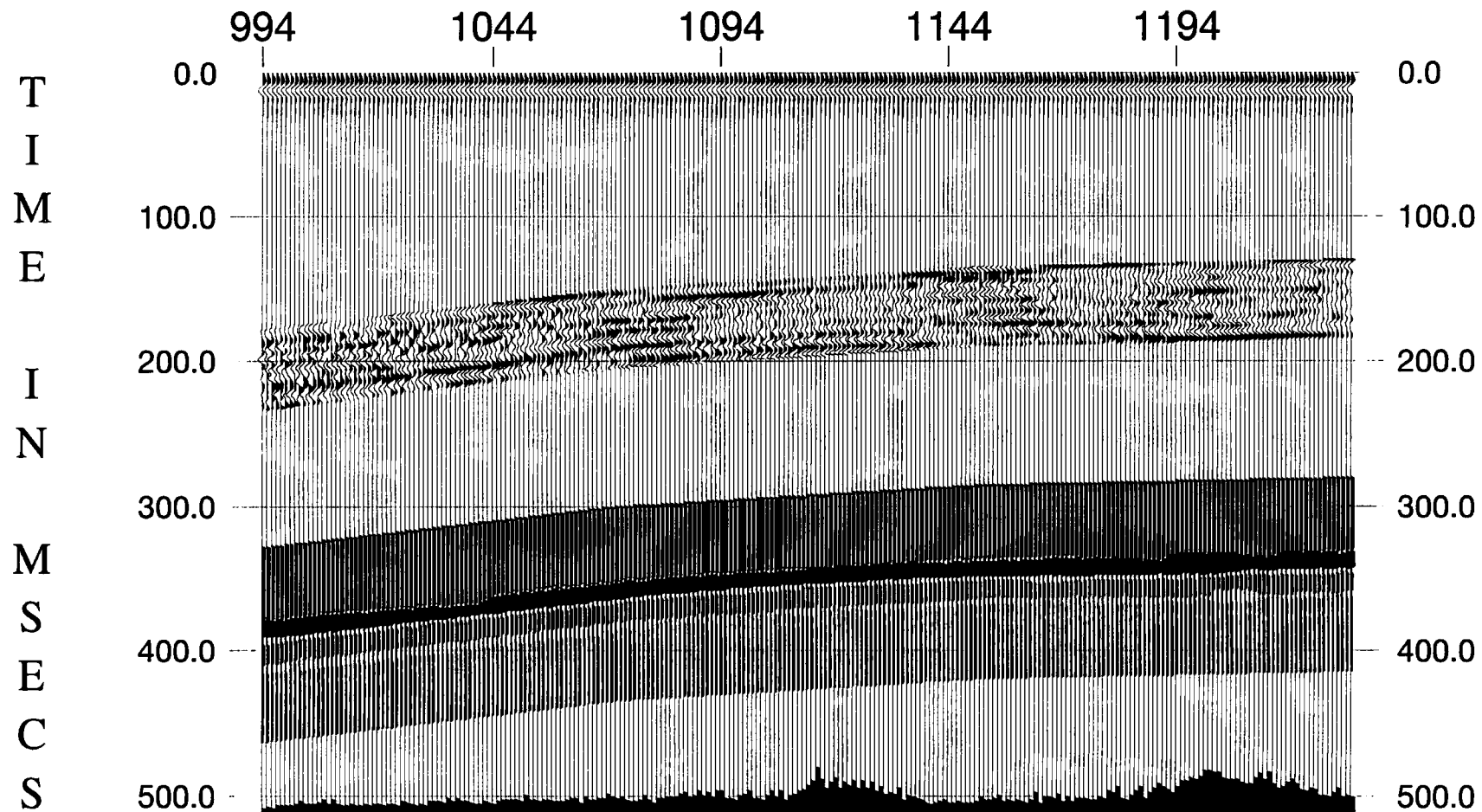


**Figure 5.7d** Inversion for boundary locations with the initial guess taken as the parameters shown in Table 5.5.

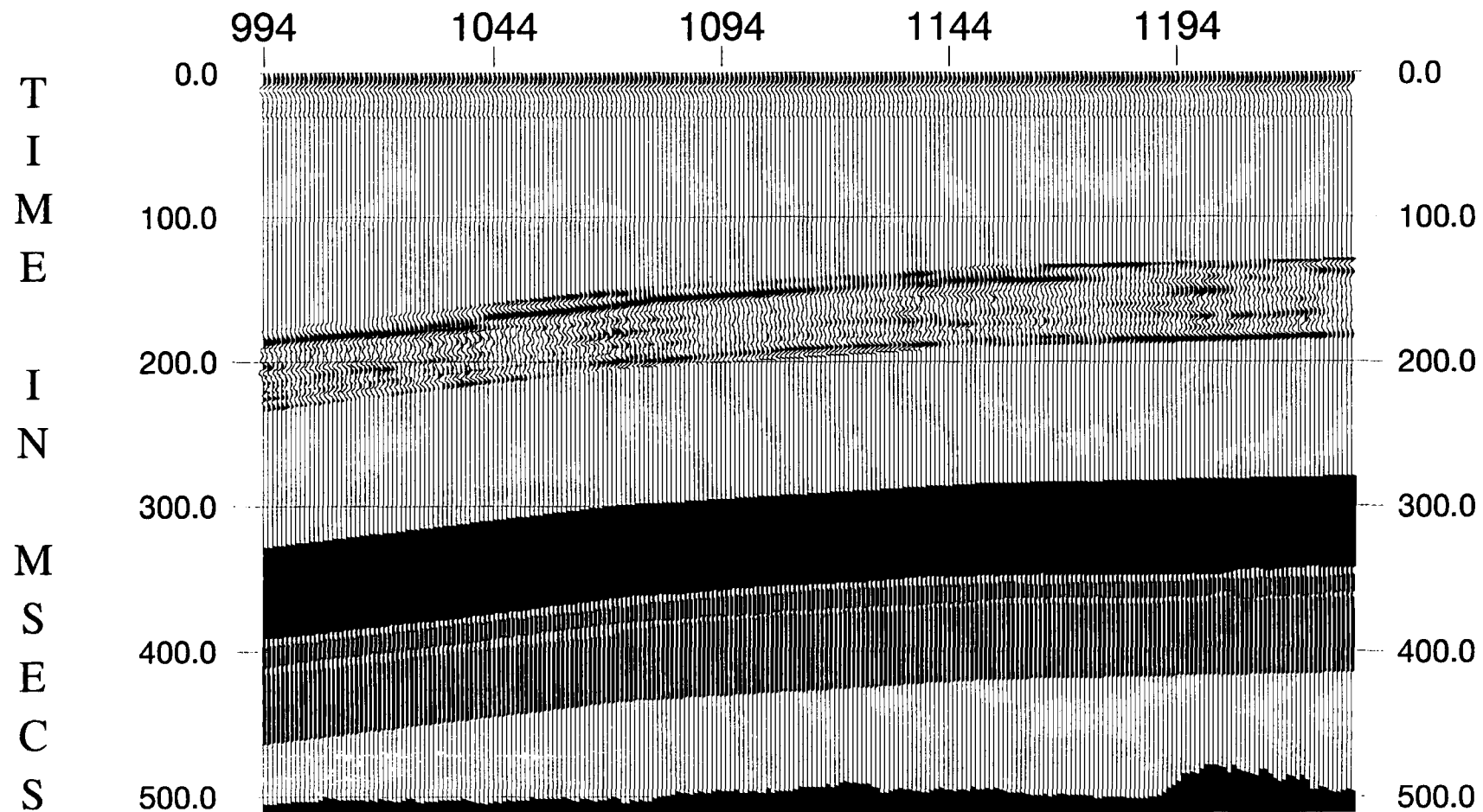
Figure 5.7a shows the results of inversion for the boundary locations with the 8-parameter wavelet and 0.5/0.5 weighting coefficients. The acoustic impedance values (Table 5.2) and the wavelet parameters (Table 5.4) were fixed. Because the extracted wavelet obtained from Thorny Plantation is quite accurate, due to the the good SNR there, the inversion with the 8-parameter wavelet was no better than Fig. 5.6a. The error energy values of the inversion in Fig. 5.7a are mostly larger than in Fig. 5.6a. In particular, the thickness of the Parkgate/Tuption seam varies more wildly.

Figure 5.7b is the inversion result using an 8-parameter wavelet and inverting for boundary locations and four frequency parameters. It can be seen that it did a better job with the thickness changes of the Parkgate/Tuption seam, which looks more like Fig. 5.6a. It is interesting to see that the thick part of Parkgate/Tuption seam extended here to CDP 1105. Possibly this is because there is a frequency change in the data (see Fig. 3.14), which is allowed for by the inversion of Fig. 5.7b.

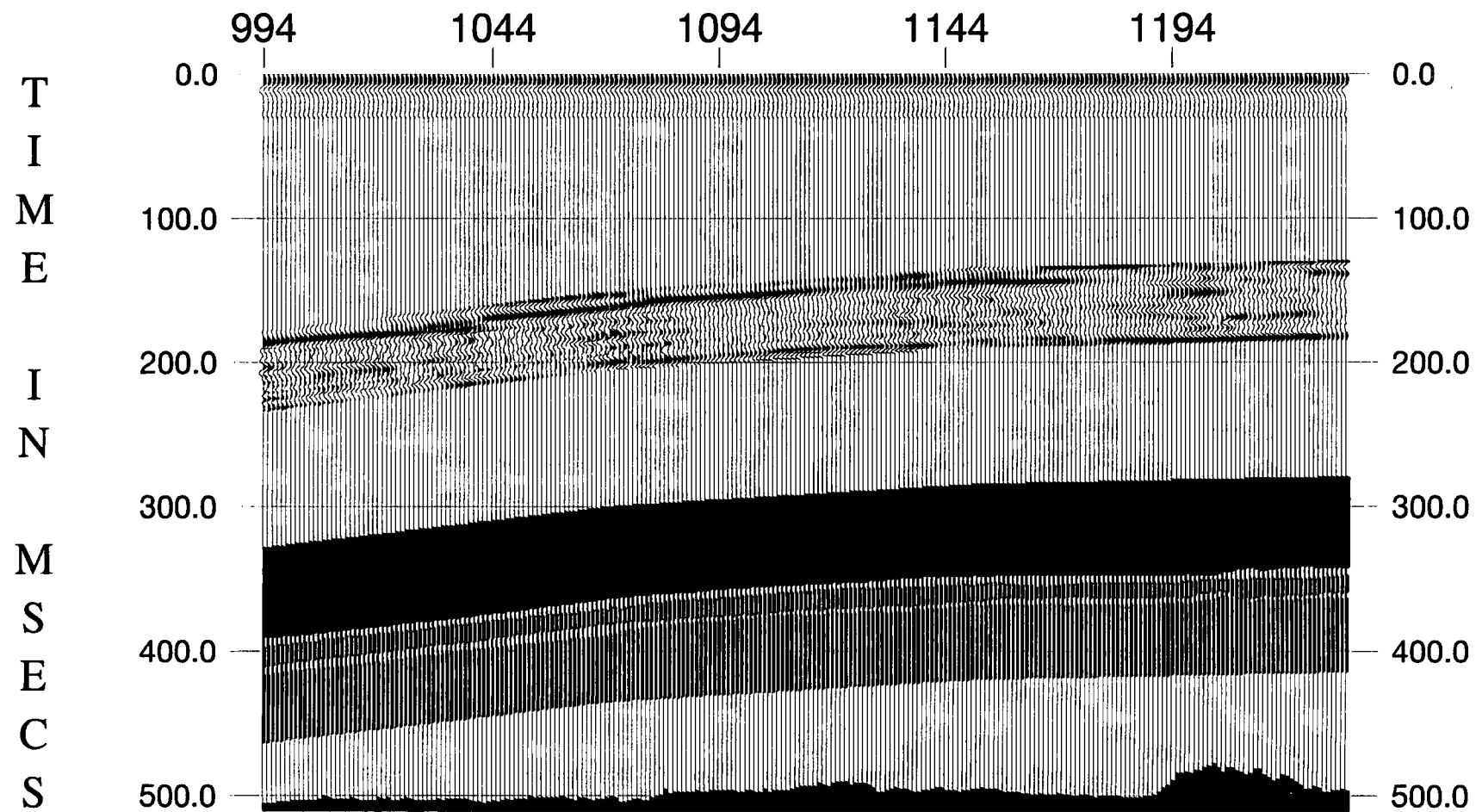
Figure 5.7c is the result of inverting for the boundary locations as well as all eight parameters of the wavelet. It is easy to see that the phase parameters do affect the boundary locations, especially in the poor SNR areas. It made the inversion solution unstable.

Fig 5.7d was obtained by using Table 5.5 as the initial guess model and inverting for boundary locations only. Comparing the result with Fig. 5.7a, there was no significant improvement anywhere. The acoustic impedance values around the Yard seam are unrealistically low, so it is difficult to see this seam on the section.

In order to show the stability of inverting for only the two main coal seams, I have tried to invert for the Deep Main and Parkgate/Tuption seams within the same window as the previous one. Figure 5.8a is the inversion for boundary locations with the extracted wavelet and 0.5/0.5 weighting coefficients. Even though the acoustic impedance values for



**Figure 5.8a** Inversion for boundary locations of the two main coal seams (the Deep Main and Parkgate/Tuption) with the extracted wavelet from Thorny Plantation borehole.



**Figure 5.8b** Same inversion as Fig. 5.8a except that twice as many iterations were applied.

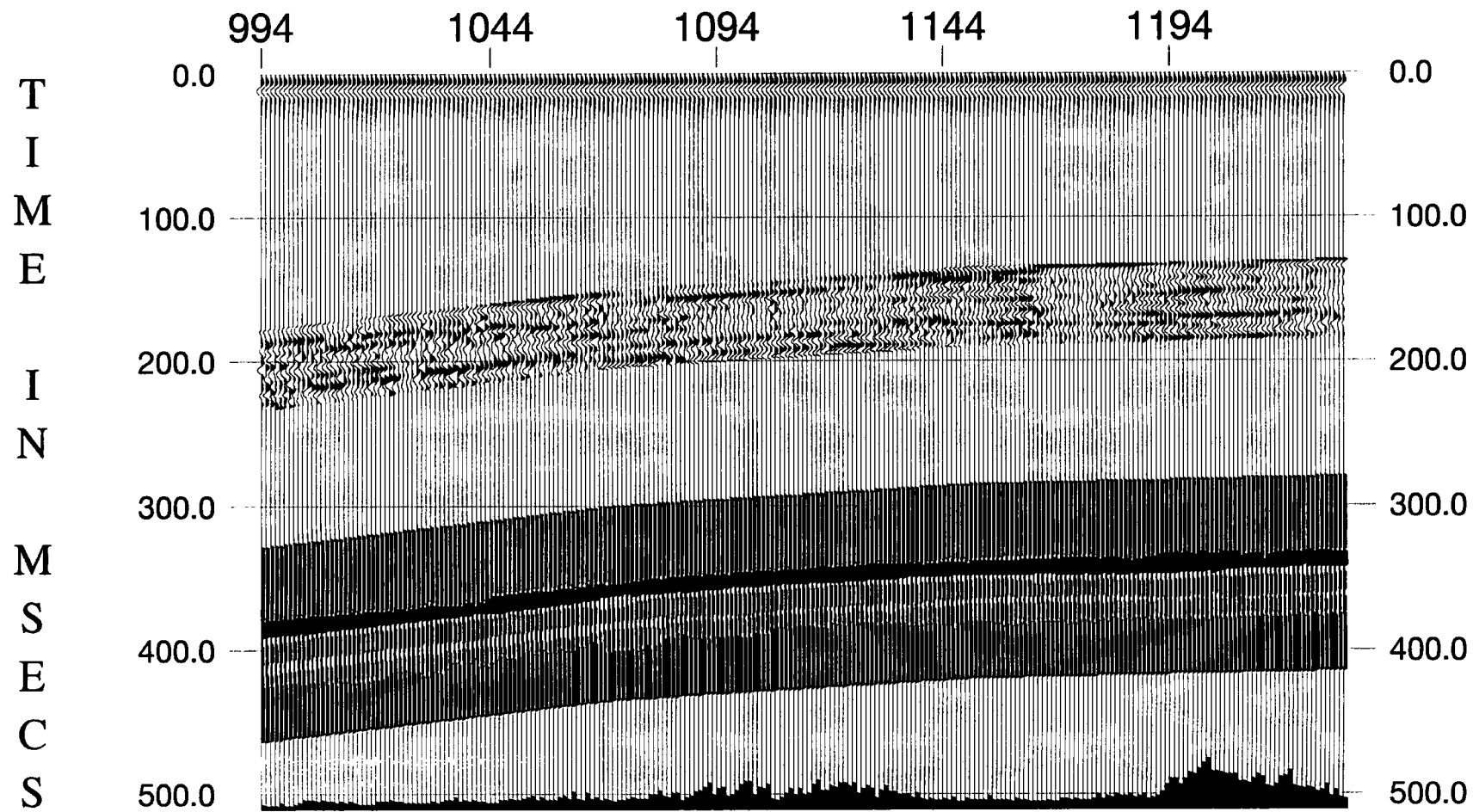


**Figure 5.9a** Inversion for boundary locations with the 7-parameter wavelet shown in Table 5.11.

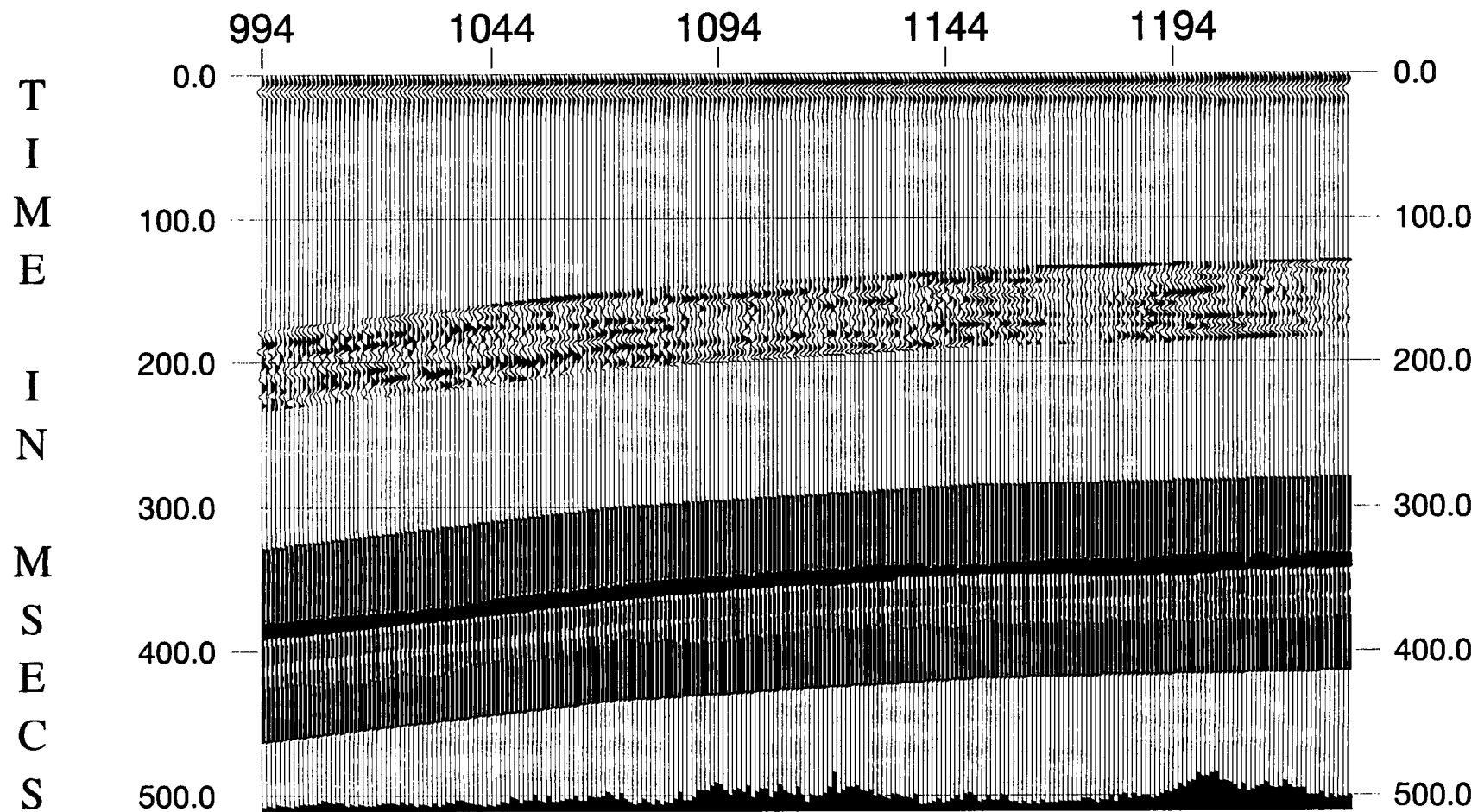


**Figure 5.9b** Inversion for boundary locations and four frequency parameters with the 7-parameter wavelet shown in Table 5.11.

the country rock were different from Table 5.2 and error energy values were a little bit bigger than Fig. 5.6a, the inversion results are almost the same in Fig. 5.6a. The error energy is bigger because only two coal seams were inverted within the same window. It can be seen that the trend of the error energy values is the same.

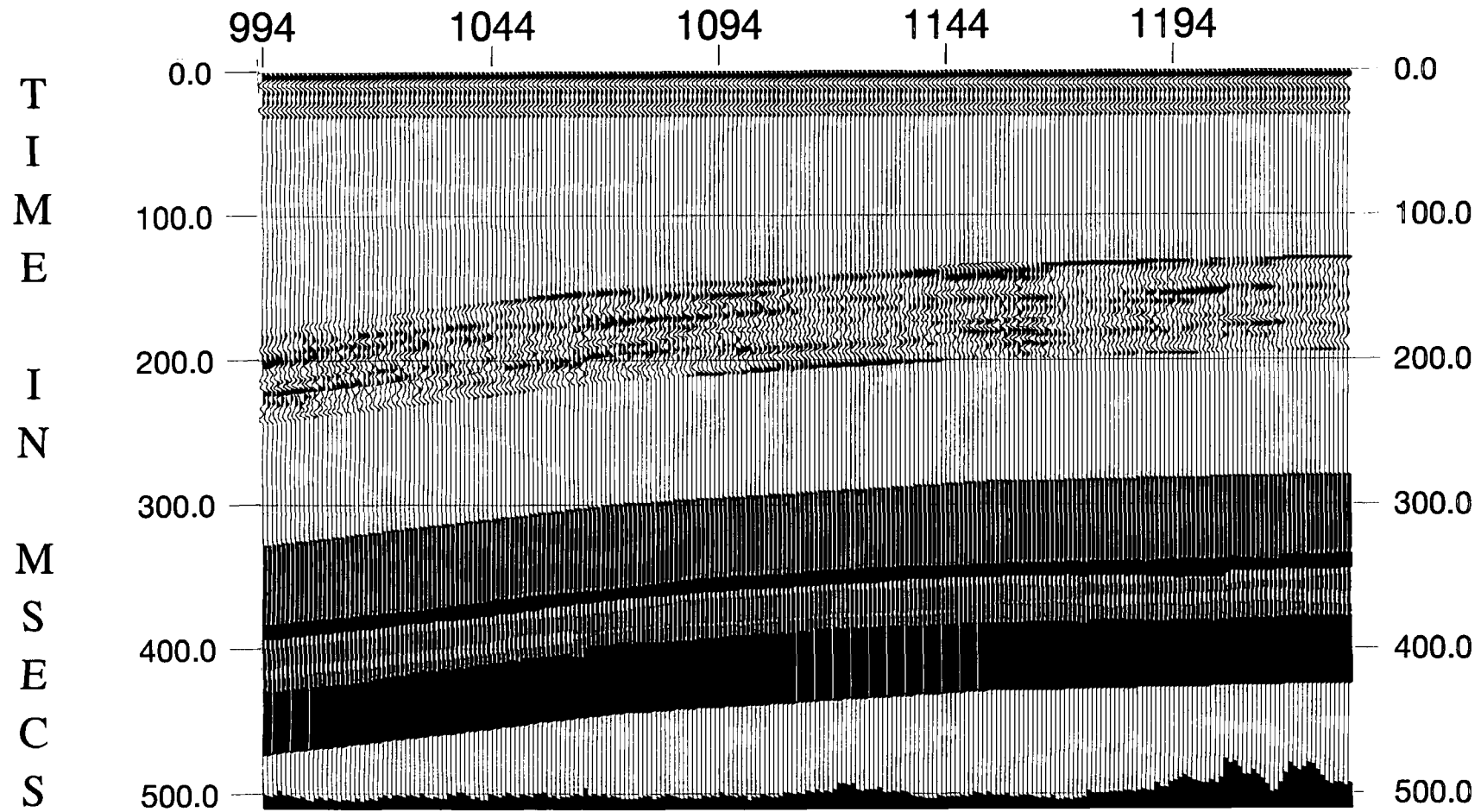
In addition to showing that sufficient iterations have been run to yield a stable result, I have tested an example with more than twice the number of iterations than used for Fig. 5.8a, i.e., a total of eight iterations were carried out. The results are shown in Fig. 5.8b. There is very little difference between them. This indicates the results obtained from Fig. 5.8a and Fig. 5.6a are stable.

Figure 5.9a is the inversion result starting with the same earth model (Table 5.2) and the 7-parameter wavelet, excluding  $\varphi_2$ , (Table 5.11) and inverting for the boundary locations. The result is quite different from that obtained using the 8-parameter wavelet (Fig. 5.7a), and it is difficult to say which one is better. However, it can be seen that the Deep Main seam has a more consistent thickness in Fig. 5.7a.

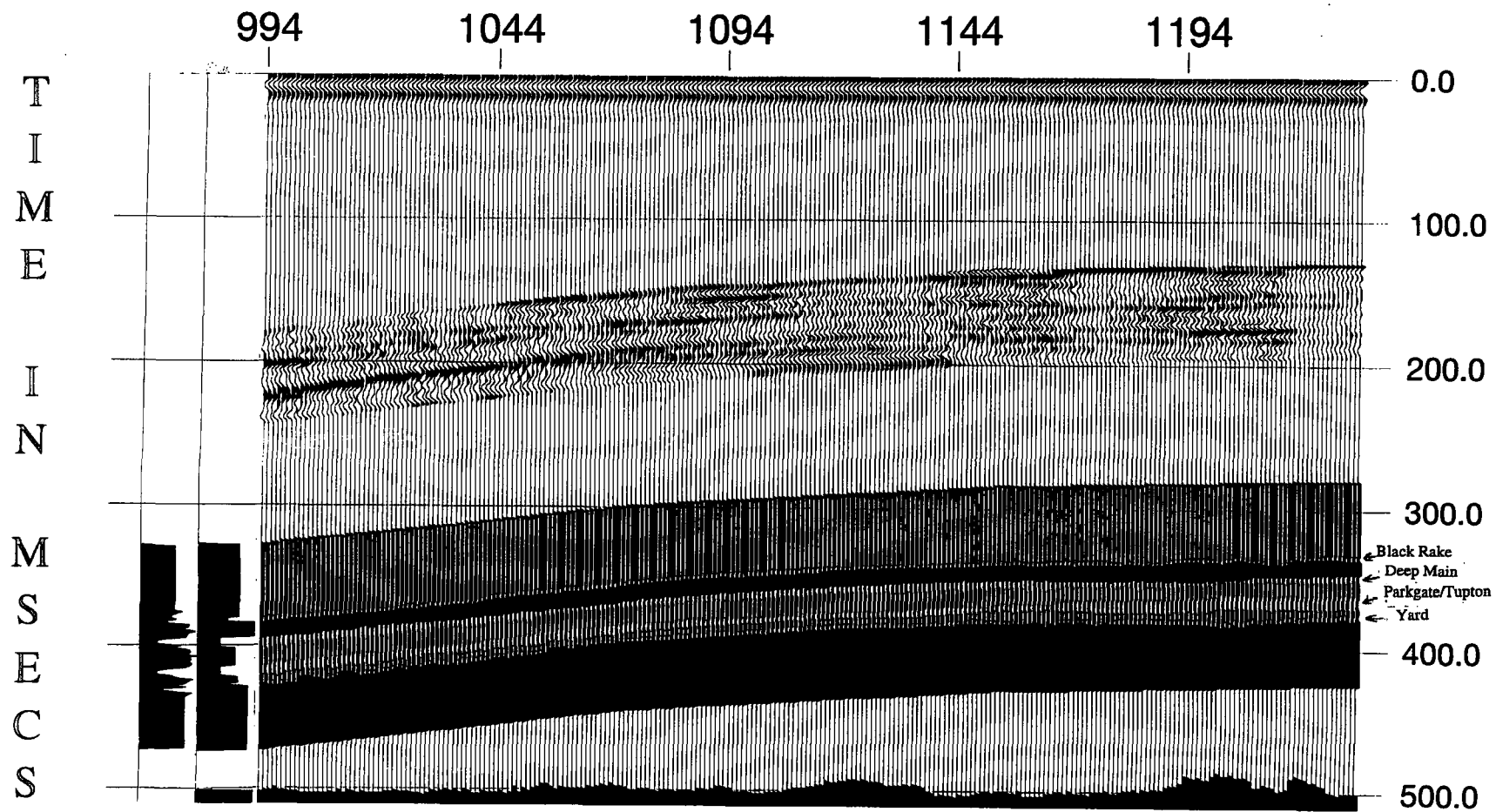
$f_1=16$ Hz	$f_2=41$ Hz	$f_3=52$ Hz	$f_4=167$ Hz
$a_0 = 5.83$	$\varphi_0 = 129$ degree	$\varphi_1 = 2.14$ degree/Hz	

Table 5.11 Initial guess model for 7-parameter wavelet

I also tried to invert for the boundary locations and the frequency parameters using a 7-parameter wavelet with the result shown in Fig.5.9b. It is very like the results of Fig. 5.7b obtained by using an 8-parameter wavelet, only differing in the extent of the thick part of the Parkgate/Tuption seam away from Thorny Plantation borehole, which looks better on Fig. 5.7b.



**Figure 5.10a** Inversion for boundary locations from Pillbox to Thorny Plantation with extracted wavelet obtained from Pillbox borehole and initial guess earth model of Table 5.7.



**Figure 5.10b** Inversion for boundary locations from Pillbox to Thorny Plantation with 8-parameter wavelet of Table 5.9 and initial guess earth model of Table 5.7. The two traces on the left are the final inversion result at Thorny Plantation borehole and (far left) the acoustic impedance function from the well logs. The boundary locations and the thicknesses of the main coal seams are matched.

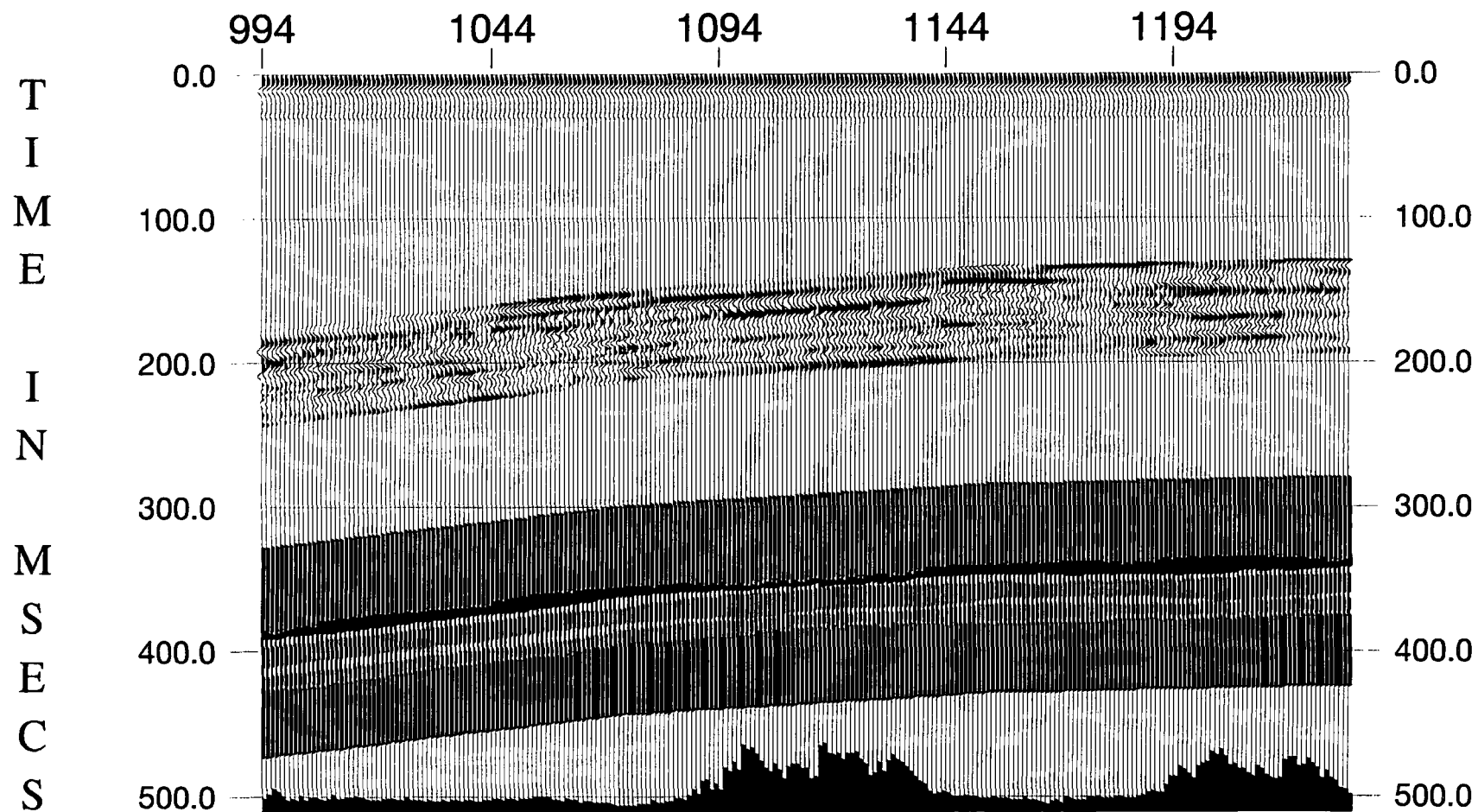


**Figure 5.10c** Inversion for boundary locations from Pillbox to Thorny Plantation with the wavelet extracted from Thorny Plantation borehole and the same acoustic impedance values as in Table 5.2.

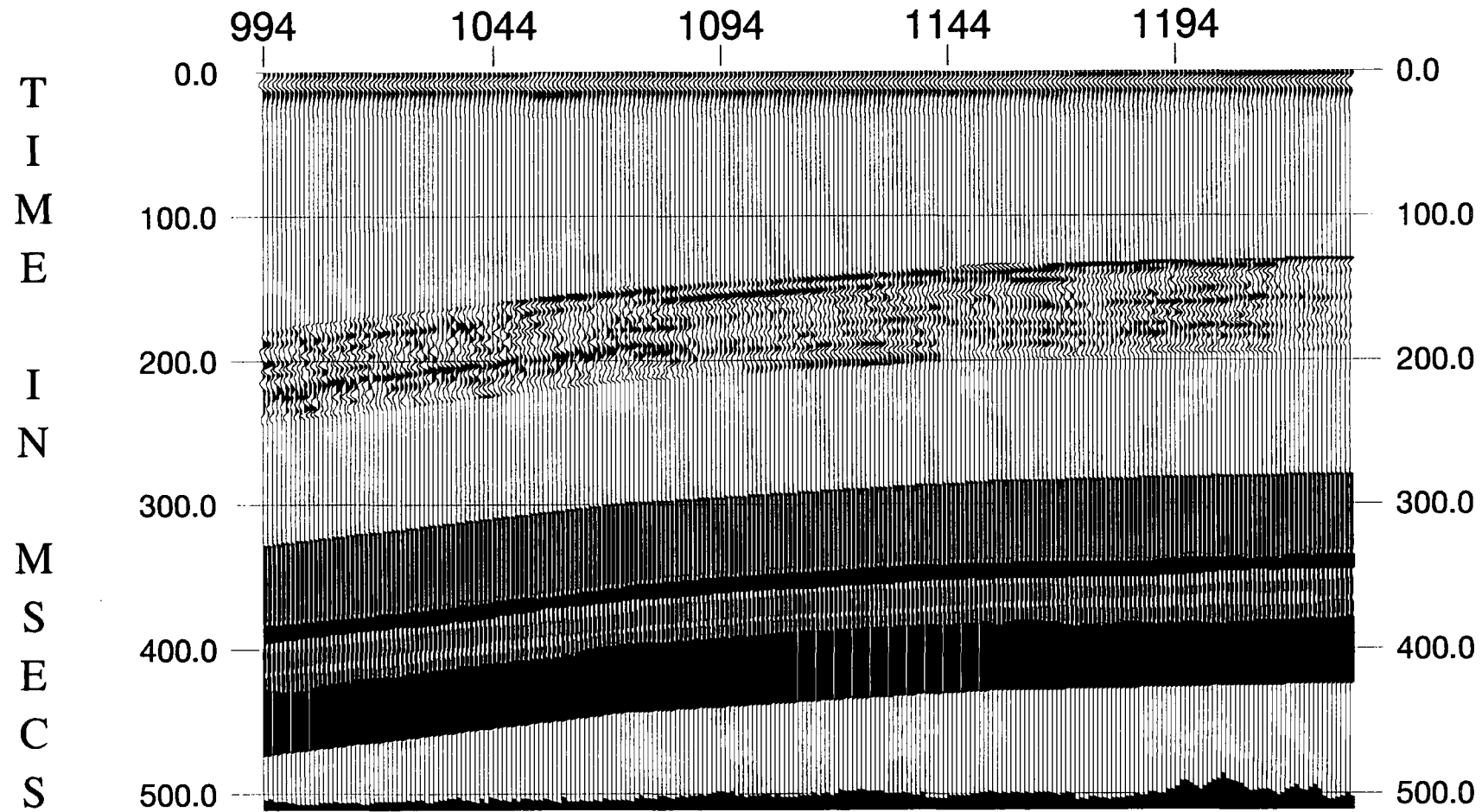
### 5.4.3 From Pillbox to Thorny Plantation

Figure 5.10a is the result of inversion for the boundary locations with the extracted wavelet from Pillbox borehole starting at that borehole and moving progressively towards Thorny Plantation. The initial guess for earth model is shown in Table 5.7. As the extracted wavelet is quite different at Pillbox borehole, and the SNR is much lower for the initial guess, it is not surprising that the inversion result is much less smooth than Fig. 5.6a.

Figure 5.10b is the result of inversion with the 8-parameter wavelet (Table 5.9) instead of the extracted wavelet. From this inversion, the advantage of optimizing the wavelet parameter for the initial guess can be seen. The inversion result looks quite smooth and the error energy values are small, especially considering that the window was expanded by 10 time samples to take account of the large time shift (38 ms).

For the Black Rake seam, the thickness is greater than the previous inversion from Thorny Plantation to Pillbox. The reason is that in the initial guess (Table 5.7) the acoustic impedance contrast was lower than in Table 5.2. The thicknesses of the Deep Main and Parkgate/Tuption seams change smoothly apart from the poor SNR area at the right hand of the section. The Yard seam looks different possibly due to the effect of ten more samples being taken into the window. It is obvious that the boundary locations and the thicknesses of these seams at the two boreholes are different in the two sections (Fig. 5.6a and Fig. 5.10b) due to the different wavelets and different initial guesses for the earth model.

In order to remove these differences and to see whether the results are similar when the inversion is carried out in either direction, Fig. 5.10c shows the result of inversion for the boundary locations starting at Pillbox borehole and moving towards Thorny Plantation,



**Figure 5.11a** Inversion for boundary locations and four frequency parameters of the 8-parameter wavelet shown in Table 5.9.

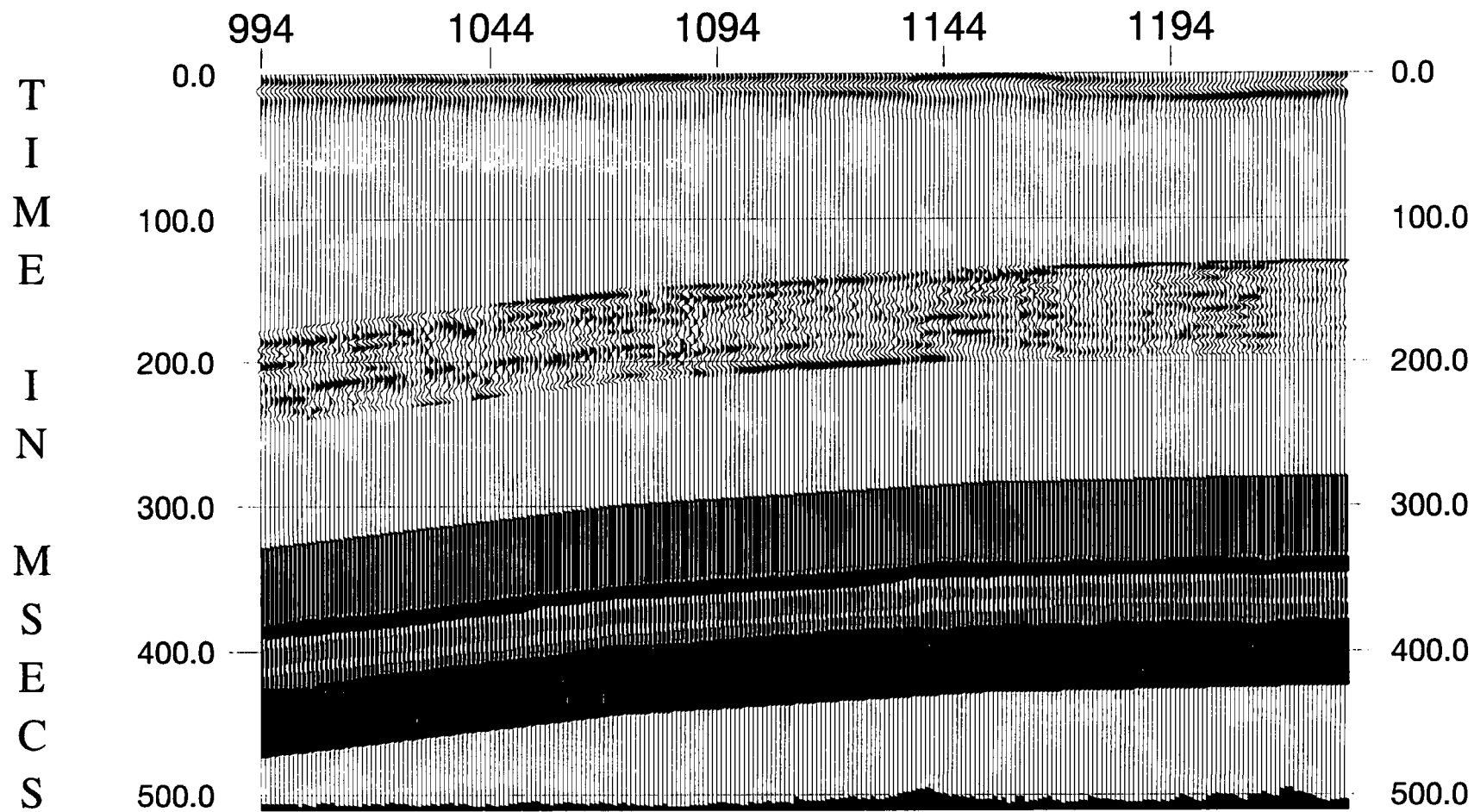


**Figure 5.11b** Inversion for boundary locations and all eight parameters of the 8-parameter wavelet shown in Table 5.9.

but using the wavelet extracted from Thorny Plantation and the acoustic impedance values from the initial guess earth model obtained from Thorny Plantation borehole (Table 5.2).

Comparing Fig. 5.10c and Fig. 5.6a, it can be seen that at the two boreholes the boundary locations and thicknesses of the two main seams (Deep Main and Parkgate/Tuption) are matched. The overall thickness variations of these two seams are similar except for the middle part and right hand end of the Deep Main due to the effect of the seam above and poor SNR area. Obviously the error energy values are quite different.

Figure 5.11a is the result of inverting for the boundary locations and the four frequency parameters of the 8-parameter wavelet (Table 5.9). At the right hand side, the behaviour of the Deep Main seam in Fig. 5.11a seems to be better than Fig. 5.10b. Figure 5.11b is the result of inverting for the boundary locations and all the 8 wavelet parameters. Again it can be concluded that the inversion for phase parameters and boundary locations together is no good, even though the error energy values tend to be very small.

## 5.5 Summary

The systematic studies at both boreholes are very important and very helpful for guiding the methodology for inversion along the section. They enabled a good initial guess to be found to start the inversion because the inversion result could be evaluated by comparison with the well logs. Sometimes it is necessary to make a compromise in parameter selection by choosing to fit either the boundary locations or the acoustic impedance values. The reason why this is necessary is because the amplitude values in a observed trace are not true relative amplitudes, i.e. the convolutional model is only an approximation for the traces on a processed section.

For the section used here, the inversion results are different when the inversion is carried out in opposite directions. The differences in the thicknesses of the coal seams are due to the extracted wavelets with different SNR from the observed data trace at each borehole.

When the extracted wavelet is inaccurate due to a poor observed trace near the borehole, the 8-parameter wavelet is quite a good approximation and useful for further inversion (Fig. 5.10b). Otherwise, the extracted wavelet is a better choice to use for the inversion. However, the disadvantage is that the extracted wavelet cannot sensibly be inverted along the section by GLI because it is described by too many parameters in the time domain and the inversion results would be unstable in the presence of noise.

It should be possible to obtain the thickness changes of coal seams by GLI with parameterization if good SNR data with true relative amplitude values are available, and if it is valid to assume that the acoustic impedance values are constant along the section. However, the difficulty in practice is to get a processed section with true relative amplitude values.

## 6 Conclusions and Suggestions for Future Work

### 6.1 Conclusions

From the work described here, it can be seen that my improved iterative method for applying GLI has potential for obtaining the thickness variations of the coal seams from migrated seismic data in the Coal Measures. Processing must produce true relative amplitude of events on the migrated section in order to obtain the correct answer for the thicknesses of the coal seams. Since this is the first time that GLI has been applied to seismic data from the Coal Measures, particular points concerning the inversion method should be noted as follows:

1. For simplification, it is possible to parameterize the country rocks between the coal seams (normally interbedded sandstones and siltstones) as uniform layers, which helps to make the problem stable and reduce the degree of non-uniqueness. Well log information is necessary for establishing the initial guess model; otherwise it is most unlikely that the global minimum will be found.
2. The extracted wavelet obtained as a Wiener shaping filter at the borehole can be fixed or inverted as an 8-parameter wavelet defined in the frequency domain. When the wavelet extraction is based on an observed trace with a poor SNR, the 8-parameter wavelet in the frequency domain will be advantageous as it can subsequently be optimized by iterative inversion with the earth model parameters at the borehole. The parameters of the 8-parameter wavelet should be fixed after inversion at the borehole in order to avoid the interference with the boundary locations.

3. Due to nonlinearity, the method used for determining the boundary locations must take into account the potential interference from other parameters, i.e the acoustic impedance values and the wavelet parameters. In the real-data example shown, for the initial guess of the boundary locations for each trace, it was better to combine the results from inversion of the previous trace inversion with structural interpretation of the migrated section.

4. Systematic studies at boreholes are essential to work out which are the dominant coal seams, to decide what wavelet should be used for the inversion, and to establish the initial guess model. Seismic data processing must be done very carefully to produce the true relative amplitude reflections, and the systematic studies at the boreholes reveal the extent to which this has been achieved.

5. In the inversion for thin beds in the Coal Measures, it is useless to invert for all the earth model and wavelet parameters by GLI, because they interfere with each other and make the problem highly non-unique. Even though I succeeded in carrying it out with the synthetic examples, many other factors are involved in real data. It is desirable to try to put some constraints on the acoustic impedance values in the inversion, as described by Oldenburg (1986), to ensure that a unique solution is obtained for the thicknesses of the coal seams.

6. Unsurprisingly, it is more stable to invert the migrated section starting at a borehole where the nearest observed trace has a higher SNR. I have shown that, even with the same extracted wavelet and the same initial guess for the acoustic impedance values, there are still some differences between the inversion results obtained from different directions. This is because during the construction of the initial guess model for each trace, the inversion results from the previous trace were taken into account.

7. If the initial guess is based on structural interpretation, GLI can work through poor SNR areas and get a reasonable answer at the end of the section. This is difficult to achieve when only the inversion result from the previous trace is used as the initial guess model for the current trace. The combination of both sources of information for making the initial guess appears to give better results than using either source on its own.

## 6.2 Suggestions for Future Work

If the inversion result from previous trace is used for, or at least contributes to, the initial guess for the current trace, it has been shown that the inversion produces different results when carried out in opposite directions. That needs to be investigated by some 2-D synthetic models, e.g. to see whether splitting of coal seams will affect this. The observed effect is the well known problem in inversion that the result can easily end up at a local minimum if the starting model is too far from the global minimum.

If possible, it would be desirable to process another dataset which has better SNR and known geological features, i.e., having been mined since the seismic data were acquired.

A new data processing procedure should be developed in order to get true relative amplitude values for the Coal Measures. It would require a more complicated forward model to take proper account of multiple activity instead of the simple convolution model; however, it would dramatically increase the cost of the computation work.

## References

- Aki, K., 1981, 3-D inhomogeneities in the upper mantle. *Tectonophysics*, **75**, 31-40.
- Aki, K. and Richards, P. G., 1980, *Quantitative Seismology*, Vols 1 and 2. W. H. Freeman and Company.
- Al-Sadi, H. N., 1980, *Seismic Exploration*, Berkhauser Verlag, Basel.
- Archer, S. H., King, G. A. and Uden, R. C., 1993, An integrated approach to reservoir characterization using seismic and well data. 5th EAPG Conference, Extended Abstracts, F003.
- Ausburn, B. E., 1977, Well log editing in support of detailed seismic studies. Transactions of the SPWLA 18th Annual Logging Symposium, Paper F.
- Backus, G. E. and Gilbert, J. F., 1967, Numerical application of a formalism for geophysical inverse problems. *Geophys. J. R. astr. Soc.*, **13**, 247-276.
- Backus, G. E. and Gilbert, J. F., 1968, The resolving power of gross earth data. *Geophys. J. R. astr. Soc.*, **16**, 169-205.
- Bamberger, A., Chavent, G., Hemon, C. and Lailly, P., 1982, Inversion of normal incidence seismograms. *Geophysics*, **47**, 757-770.
- Beylkin, G., 1984, The inversion problem and application of the generalized Radon transform. *Comm. Pure & Applied Math.*, **37**, 579-599.
- Bleistein, N., Cohen, J. K. and Hagin, F. G., 1985, Computational and asymptotic aspects of velocity inversion. *Geophysics*, **50**, 1253-1265.
- Brac, J., Dequirez, P. Y., Herve, F., Jacques, C., Lailly, P., Richard, V. and Nhieu, D. T. van, 1992, Inversion with a priori information: an approach to integrated stratigraphic



interpretation. Reservoir Geophysics, R. E. Sheriff (ed.), 251-258. Society of Exploration Geophysicists.

Bracewell, R., 1978, The Fourier Transform and Its Applications. McGraw-Hill Book Co.

Cardy, S., 1995, Make or break year for coalbed methane. Petroleum Review, February issue, 80-82.

Chen, Y. M., 1985, Generalized pulse-spectrum technique. Geophysics, **50**, 1664-1675.

Claerbout, J. F., 1985, Fundamentals of Geophysical Data Processing. McGraw-Hill Book Co.

Claerbout, J. F., 1985, Imaging the Earth's Interior. Blackwell Scientific Publications.

Cohen, J. K. and Bleistein, N., 1979, Velocity inversion procedure for acoustic waves. Geophysics, **44**, 1077-1087.

Cooke, D. A., 1981, Generalized linear inversion of seismic data. M. Sc. thesis. T-2459, Colorado School of Mines, Golden.

Cooke, D. A. and Schneider, W. A., 1983, Generalized linear inversion of reflection seismic data. Geophysics, **48**, 665-676.

Cornish, B. E. and King, G. A., 1988, Combined interactive analysis and stochastic inversion for high-resolution reservoir modeling, 50th EAEG Meeting Abstracts, 104.

Creel, J. C., 1995, Potential for the development of UK coalbed methane. Petroleum Review, February issue, 74-77.

Dahl, T. and Ursin, B., 1991, Parameter estimation in a one-dimensional anelastic medium. Journal of Geophysical Research, **96**, 20,217-20,233.

Dines, K. A. and Lytle, R. J., 1979, Computerized geophysical tomography. Proceedings of the IEEE, **67**, 1065-1072.

Dresen, L. and Ruter, H., 1994, Seismic Coal Exploration, Part B: In-Seam Seismics. Pergamon.

Fairbairn, C. M., Holt, J. M. and Padget, N. J., 1986, Case histories of the use of the surface seismic method in the UK coal mining industry. *Coal Geophysics*, SEG Geophysics reprint series No. 6, D. J. Buchanan and L. J. Jackson (eds), 188-203. Society of Exploration Geophysicists.

Gochioco, L. M., 1992, Modeling studies of interference reflections in thin layered media bounded by coal seams. *Geophysics*, **57**, 1209-1216.

Goupillaud, P. L., 1961, An approach to inverse filtering of near-surface layer effects from seismic records. *Geophysics*, **26**, 754-760.

Graebner, R., Wason, C. and Meinardus, H., 1981. Three-dimensional methods in seismic exploration. *Science*, **211**, 535-540.

Hartley, H. O., 1961, The modified Gauss-Newton method for fitting of non-linear regression functions by least squares. *Technometrics* **3**, 269-280.

Lavergne, M. and Willm, C., 1977, Inversion of seismograms and pseudo velocity logs. *Geophysical Prospecting*, **25**, 231-250.

Lindseth, R. O., 1979, Synthetic sonic logs - a process for stratigraphic interpretation. *Geophysics*, **44**, 3-26.

Lines, L. R. and Treitel, S., 1984, Tutorial: A review of least-squares inversion and its application to geophysical problems. *Geophysical Prospecting*, **32**, 159-186.

Marquardt, D. W., 1963, An algorithm for least-squares estimation of nonlinear parameters. *J. Soc. Indust. App. Math.*, **11**, 431-441.

Martinez, R. D., Cornish, B. E., Rebec, A. J. and Curtis, M. P., 1992. Complex reservoir characterization by multiparameter constrained inversion. *Reservoir Geophysics*, R. E. Sheriff (ed.), 224-234. Society of Exploration Geophysicists.

Mazzotti, A. and Mirri, S., 1988, An experience in seismic amplitude processing. *First Break*, **9**, 65-73.

- Miller, D., Oristaglio, M. and Beylkin, G., 1987, A new slant on seismic imaging: migration and integral geometry. *Geophysics*, **52**, 943-963.
- Newman, P., 1973, Divergence effects in a layered Earth. *Geophysics*, **38**, 481-488.
- Okaya, D. A., 1995, Spectral properties of the earth's contribution to seismic resolution. *Geophysics*, **60**, 241-251.
- Oldenburg, D. W., Scheuer, T. and Levy, S., 1983, Recovery of the acoustic impedance from reflection seismograms. *Geophysics*, **48**, 1318-1337.
- Oldenburg, D. W., Levy, S., and Stinson, K., 1986, Inversion of band-limited reflection seismograms: theory and practice. *Proc of Inst. Elect. Electr. Eng.*, **74**, 487-497.
- Oppenheim, A. V. and Schaffer, R. W., 1975, *Digital Signal Processing*, Prentice-Hall.
- Pan, S. X. and Kak, A. C., 1983, A computational study of reconstruction algorithms for diffraction tomography. *IEEE Trans. Acous. Speech Sig. Proc.*, **ASSP-31**, 1262-1275.
- Poggiagliolmi, E., Berkhout, A. J. and Boone, M. M., 1982, Phase unwrapping: possibilities and limitations. *Geophysical Prospecting*, **30**, 281-291.
- Pratt, R. G. and Gouly, N. R., 1991, Combining wave-equation imaging with travelttime tomography to form high-resolution images from crosshole data. *Geophysics*, **56**, 208-224.
- Raymer, L. L. and Burgess, K. A., 1980, The role of well logs in reservoir modelling. 55th SPE/AIME Annual Meeting, SPE 9342.
- Redanz, M., 1988, Acoustic impedance from least-squares inversion of reflection seismograms. 50th EAEG Meeting, Abstracts, 108.
- Robinson, E. A. and Treitel, S., 1980, *Geophysical Signal Analysis*. Prentice-Hall.
- Robinson, E. A., 1983, *Seismic Velocity Analysis and the Convolutional Model*. International Human Resources Development Corpn.

Sabatier, P. C., 1977a, Positivity constraints in linear inverse problems--I. General theory. *Geophys. J. R. astr. Soc.*, **48**, 415-441.

Sabatier, P. C., 1977b, Positivity constraints in linear inverse problems--II. Applications. *Geophys. J. R. astr. Soc.*, **48**, 443-459.

Sen, M. K. and Stoffa, P. L., 1991, Nonlinear one-dimensional seismic waveform inversion using simulated annealing. *Geophysics*, **56**, 1624-1638.

Shafer, R. W., 1969, Echo removal by discrete generalized linear filtering. Research Laboratory of Electronics, Massachusetts Institute of Technology, Technical Report No. 466.

Shatilo, A. P., 1992, Seismic phase unwrapping: methods, results, problems. *Geophysical Prospecting*, **40**, 211-225.

Sheriff, R. E. and Geldart, L. P., 1983, *Exploration Seismology, Vol. 2: Data Processing*. Cambridge University Press.

Stoffa, P. L. and Sen, M. K., 1991, Nonlinear multiparameter optimization using genetic algorithms. Inversion of plane-wave seismograms. *Geophysics*, **56**, 1794-1810.

Tarantola, A. and Valette, B., 1982, Generalized nonlinear inverse problems solved using the least squares criterion. *Rev. Geophys. Space Physics*, **20**, 219-232.

Treitel, S. and Robinson, E. A., 1966, Seismic wave propagation in layered media in terms of communication theory. *Geophysics*, **31**, 17-32.

Van Riel, P. and Berkhout, A. J., 1985, Resolution in seismic trace inversion by parameter estimation. *Geophysics*, **50**, 1440-1455.

Weber, Z., 1986, One-dimensional linear inversion of reflection seismic data. Model Optimization in Exploration Geophysics, Andreas Vogel (ed.), Proceedings of the 4th International Mathematical Geophysics Seminar, 269-290. Vieweg, Braunschweig.

White, J. E. and Sengbush, R. L., 1987, *Production Seismology*. Geophysical Press.

Widess, M. B., 1973, How thin is a thin bed? *Geophysics*, **38**, 1176-1180.

Wiggins, R. A., Larner, K. L. and Wisecup, R., 1976, Residual statics analysis as a general linear inverse problem. *Geophysics*, **41**, 922-938.

Yilmaz, O., 1987, *Seismic Data Processing*. Society of Exploration Geophysicists.

Yu, G., 1985, Offset-amplitude variation and controlled-amplitude processing. *Geophysics*, **50**, 2697-2708.

Ziolkowski, A. and Lerwill, W. E., 1979, A simple approach to high resolution seismic profiling for coal. *Geophysical Prospecting*, **27**, 360-393.

## Appendix    Computer Software

This appendix gives a brief outline of a GLI inversion using the program available in University of Durham, and also lists the few programs and subroutines that I have written. External subroutines include NAG Fortran subroutines and UNIRAS plotting library. Some programs that have merely been altered by me for use with data plotting are not listed here.

All programs are written in Fortran 77 to run on a HP or a Sun4. The input parameters in the data file at the head of each program should be checked and altered to suit the needs of the user.











```

amax=0.
mb1=ms-1p
mb2=(ms-1p)/3
emax=0.
DO 16 J=1,MFIT
ll=lista(j)
aaa(j)=a(ll)+da(j)

cccccccccccccccccccccccccccccccccccccccccccccccccccccccccccc
c make sure the constraints are satisfied c
cccccccccccccccccccccccccccccccccccccccccccccccccccccccccccc

if(ggg.eq.1.and.ggg.lt.4.)then
if(ll.le.mb1-mb2.and.aaa(j).lt.0.)aaa(j)=a(ll)
if(ggg.eq.1.)then
if(aaa(j).le.ms1)aaa(j)=ms1
if(aaa(j).ge.ms2)aaa(j)=ms2
end if
if(ll.gt.mb2.and.ll.le.mb1-mb2)then

cc the acoustic impedances must be within the maximum and minimum cc

if(aaa(j).gt.aaa.and.mod(ll,2).ne.0)aaa(j)=a
if(aaa(j).lt.aaa.and.mod(ll,2).ne.0)aaa(j)=am
end if
if(ll.gt.mb1-mb2.and.ll.le.mb1)then
if(abs(aaa(j)).gt.ga)aaa(j)=a(ll)
end if
end if
if(ggg.eq.4.or.ggg.eq.-1.)then
if(ll.ge.mb1+3.and.ll.le.mb1+6)then
if(aaa(j).lt.0)aaa(j)=a(ll)
end if
end if
stry(ll)=aaa(j)

ccc The thicknesses of the coal seams must not be over set values ccc

if(mod(ll,2).eq.0.and.(stry(ll)-stry(ll-1)).gt.mah(ll))then
stry(ll)=stry(ll-1)+mah(ll)
end if

ccc The thicknesses of the country rocks must not be over set values ccc

if(mod(ll,2).ne.0.and.(stry(ll)-stry(ll-1)).gt.mah(ll))then
stry(ll)=stry(ll-1)+mah(ll)
end if
end if
if(ggg.eq.4.or.ggg.eq.-1.)then
if(ll.ge.mb1+4.and.ll.le.mb1+6)then

cccccccccccccccccccccccccccccccccccccccccccccccccccccccccccc
c the gap between the two frequencies should bigger than 10 Hz. c
cccccccccccccccccccccccccccccccccccccccccccccccccccccccccccc

if(m*(stry(ll)-stry(ll-1)).lt.10)then
stry(ll)=stry(ll-1)+10.
end if
end if
end if
end if
aaa(j)=stry(ll)
16 CONTINUE
ww=1.

cccccccccccccccccccccccccccccccccccccccccccccccccccccccccccc
c secure the order of the boundaries are not reversed c
cccccccccccccccccccccccccccccccccccccccccccccccccccccccccccc

if(ggg.eq.1.)then
do 26 j=mb1,1,-1
ll=lista(j)
amax=0.
do 27 k=1,mfit
if(aaa(k).gt.amax)then
amax=aaa(k)
ll=k
end if
continue
aaa(j)=0.
stry(ll)=amax
continue
end if
if(ggg.eq.-1.or.ggg.eq.4)then
do 88 i=1,lp
pf(i)=stry(mb1+i)
88 continue
call wsf(wl,iww,pf,df,lp,0,ity,s,sk)
end if
lma=1
CALL MRW(Y,NDATA,A,TRY,MA,LISTA,MFIT,COVAR,DA,NCA,CHISQ,dt
*,ggg,iwk,iww,ese,ms1,ms2,bb,cc,w1,iqlms,ity,s,ee,sk)
cri(3)=chisq
IF(chisq.lt.bb)THEN

cccccccccccccccccccccccccccccccccccccccccccccccccccccccccccc
cc the current inversion got improved, decrease the dump factor cc
cccccccccccccccccccccccccccccccccccccccccccccccccccccccccccc

if(ggg.eq.4.or.ggg.eq.-1.)then
do 8 j=1,iww
w(j)=w1(j)
end if
slam=0.05*slam
cri(2)=chisq
bb=chisq
DO 18 J=1,MFIT
ll=lista(j)
DO 17 K=1,MFIT
ALPHA(J,K)=COVAR(J,K)
17 CONTINUE
BETA(J)=DA(J)
A(J)=ATRY(J)
18 CONTINUE
ELSE

cccccccccccccccccccccccccccccccccccccccccccccccccccccccccccc
c the current inversion is worse than previous one, c
c increase the dump factor and save the previous error c
cccccccccccccccccccccccccccccccccccccccccccccccccccccccccccc

29 slam=20.0*slam

```

```

cri(1)=chisq
chisq=bb
endif
return
end

.....
.....
.....
subroutine gas(s,a,np,b,m,mp,ii)
c This subroutine is used for obtaining the solutions of the equations c
PARAMETER (NMAX=2046)
real*4 a,b
DIMENSION A(NP,NP),B(NP,MP),PIV(NMAX),INDXR(NMAX),INDXC(NMAX)
iii=0
DO 11 J=1,N
IPIV(J)=0
11 CONTINUE
DO 22 I=1,N
BIG=0.
DO 13 J=1,N
IF(PIV(J).NE.1)THEN
DO 12 K=1,N
IF (PIV(K).EQ.0) THEN
IF (ABS(A(J,K)).GE.BIG)THEN
BIG=ABS(A(J,K))
IROW=J
ICOL=K
ENDIF
ELSE IF (PIV(K).GT.1) THEN
PAUSE 'Singular matrix (piv(k).gt.1)'
iii=1
return
ENDIF
12 CONTINUE
ENDIF
13 CONTINUE
IPIV(ICOL)=IPIV(ICOL)+1
IF (IROW.NE.ICOL) THEN
DO 14 L=1,N
DUM=A(IROW,L)
A(IROW,L)=A(ICOL,L)
A(ICOL,L)=DUM
14 CONTINUE
DO 15 L=1,M
DUM=B(IROW,L)
B(IROW,L)=B(ICOL,L)
B(ICOL,L)=DUM
15 CONTINUE
ENDIF
INDXR(I)=IROW
INDXC(I)=ICOL
IF (A(ICOL,ICOL).EQ.0.) then
iii=1
return
c pause 'Singular matrix (a(i,col)=0)'
end if
PIVINV=1./A(ICOL,ICOL)
A(ICOL,ICOL)=1.
DO 16 L=1,N
A(ICOL,L)=A(ICOL,L)*PIVINV
16 CONTINUE
DO 17 L=1,M
B(ICOL,L)=B(ICOL,L)*PIVINV
17 CONTINUE
DO 21 LL=1,N
IF(LL.NE.ICOL)THEN
DUM=A(LL,ICOL)
A(LL,ICOL)=0.
DO 18 L=1,N
A(LL,L)=A(LL,L)-A(ICOL,L)*DUM
18 CONTINUE
DO 19 L=1,M
B(LL,L)=B(LL,L)-B(ICOL,L)*DUM
19 CONTINUE
ENDIF
21 CONTINUE
22 CONTINUE
DO 24 L=N,1,-1
IF(INDXR(L).NE.INDXC(L))THEN
DO 23 K=1,N
DUM=A(K,INDXR(L))
A(K,INDXR(L))=A(K,INDXC(L))
A(K,INDXC(L))=DUM
23 CONTINUE
ENDIF
24 CONTINUE
RETURN
END

.....
.....
.....
SUBROUTINE MRW(Y,NDATA,A,MA,LISTA,MFIT,ALPHA,BETA,NALP,
*CHISQ,dt,ggg,iwk,iww,ese,ms1,ms2,bb,cc,w1,iqlms,ity,s,ee,sk)
c This subroutine is used for constructing the linear equations for solving c
complex w1(iww)
PARAMETER (amax=4096)
common /wavelet/ddd,de,dg,dp,ds,df,dad,lp,ga,ea,em
DIMENSION Y(NDATA),ALPHA(NALP,NALP),BETA(MA),f(256),s(iww)
*,DYDA(amax),LISTA(MFIT),A(MA),r(amax),cc(ndata)
dimension yl(nmax)
DO 12 J=1,MFIT
DO 11 K=1,J
ALPHA(J,K)=0.
11 CONTINUE

```



```

        if(ip3-ip2.lt.2)ip3=ip2+2
        if(ip4-ip3.lt.2)ip4=ip3+2
        pp1=(pp(1)/180)*pi
        pp2=(pp(2)/180)*pi
        if(pp.eq.8)then
            pp8=(pp(1)/180)*pi
        else
            pp8=0.
        end if
    do 10 i=1,ip1
        pp3=pp1+pp2**i*d+pp8*(i*d)**2
        if(skip.eq.-1.) then
            yy=x(i)+pp4
        else
            yy=pp(7)*pp4
            x(i)=yy
        end if
10   y1(i)=yy*cexp((0.,1.)*pp3)
    do 20 i=ip1+1,ip2
        yy=1/(ip2-i+1)
        if(skip.eq.-1.) then
            yy=x(i)+pp4
        else
            yy=pp(7)*((1+cos(pi*(i-ip2)/(ip2-ip1-1)))/2)+pp4
            x(i)=yy
        end if
        pp3=pp1+pp2*(i*d)+pp8*(i*d)**2
20   y1(i)=yy*cexp((0.,1.)*pp3)
    do 30 i=ip2+1,ip3
        pp3=pp1+pp2*(i*d)+pp8*(i*d)**2
        if(skip.eq.-1.) then
            yy=x(i)+pp4
        else
            yy=pp(7)*(1+pp4)
            x(i)=yy
        end if
        pp3=pp1+pp2*(i*d)+pp8*(i*d)**2
30   y1(i)=yy*cexp((0.,1.)*pp3)
    do 40 i=ip3+1,ip4
        if(skip.eq.-1.) then
            yy=x(i)+pp4
        else
            yy=pp(7)*((1+cos(pi*(i-ip3)/(ip4-ip3-1)))/2)+pp4
            x(i)=yy
        end if
        pp3=pp1+pp2*(i*d)+pp8*(i*d)**2
40   y1(i)=yy*cexp((0.,1.)*pp3)
    do 50 i=ip4+1,ix/2
        if(skip.eq.-1.)then
            yy=x(i)+pp4
        else
            yy=pp(7)*pp4
            x(i)=yy
        end if
        pp3=pp1+pp2*(i*d)+pp8*(i*d)**2
50   y1(i)=yy*cexp((0.,1.)*pp3)
        do 11 i=1,ix
            if(i.le.ix/2)then
                y(i)=y1(i)
            else
                y(i)=cmlpx(real(y1(ix-i+1)),(-1.)*aimag(y1(ix-i+1)))
            end if
            continue
11   return
    end

```

---

```

subroutine wa(y,ix,x,d,lf)
c This program is to transfer a wavelet from frequency domain to time domain
complex y(ix),y1(2048)
dimension x(ix),x1(2048)
d=1/(ix*d)
pi=3.1415926
ip=5
do 10 i=1,ix
    y1(i)=y(i)
10   call fit(y1,ix,1)
        do 15 i=1,ix
            if(i.le.ix/2)then
                x1(i)=real(y1(i+ix/2))
            else
                x1(i)=real(y1(i-ix/2))
            end if
15   continue
        amax=0.
        do 12 i=1,ix
            if(abs(x1(i)).gt.amax)then
                amax=abs(x1(i))
            imax=i
        end if
12   continue
        imax=ix/2
c put a cosine taper to the both sides of the wavelet
        if((1.ne.ix)then
            i1=imax-ll/2+1
            i2=imax+ll/2
            do 16 i=i1,i1+ip
                x1(i)=x1(i+ip)*(1+cos(pi*(i-i1-1)/ip))/2
            continue
            do 17 i=i2-ip,i2
                x1(i)=x1(i2-ip)*(1+cos(pi*(i-i2+1)/ip))/2
            continue
17   end if
            do 18 i=1,ix
                j=i
                if((1.ne.ix)then
                    i=imax-ll/2+i
                    x(i)=x1(j)
                continue
18   return

```

```

end
-----
c this subroutine used for analysing amplitude and phase spectrum ccc
c and unwrap the phase spectrum in order to get 6 parameters for ccc
c defining the wavelet. ccc
subroutine apw(dt,lt,iwkw,xl,pl,px,akp)
parameter(amia=13.,amax=250.)
double precision xx,yy,ref,c(i)
integer i,if1,if2,if3,if4,if5,if6,if7,if8,if9,if10,if11,if12,if13,if14,if15,if16,if17,if18,if19,if20,if21,if22,if23,if24,if25,if26,if27,if28,if29,if30,if31,if32,if33,if34,if35,if36,if37,if38,if39,if40,if41,if42,if43,if44,if45,if46,if47,if48,if49,if50,if51,if52,if53,if54,if55,if56,if57,if58,if59,if60,if61,if62,if63,if64,if65,if66,if67,if68,if69,if70,if71,if72,if73,if74,if75,if76,if77,if78,if79,if80,if81,if82,if83,if84,if85,if86,if87,if88,if89,if90,if91,if92,if93,if94,if95,if96,if97,if98,if99,if100,if101,if102,if103,if104,if105,if106,if107,if108,if109,if110,if111,if112,if113,if114,if115,if116,if117,if118,if119,if120,if121,if122,if123,if124,if125,if126,if127,if128,if129,if130,if131,if132,if133,if134,if135,if136,if137,if138,if139,if140,if141,if142,if143,if144,if145,if146,if147,if148,if149,if150,if151,if152,if153,if154,if155,if156,if157,if158,if159,if160,if161,if162,if163,if164,if165,if166,if167,if168,if169,if170,if171,if172,if173,if174,if175,if176,if177,if178,if179,if180,if181,if182,if183,if184,if185,if186,if187,if188,if189,if190,if191,if192,if193,if194,if195,if196,if197,if198,if199,if200,if201,if202,if203,if204,if205,if206,if207,if208,if209,if210,if211,if212,if213,if214,if215,if216,if217,if218,if219,if220,if221,if222,if223,if224,if225,if226,if227,if228,if229,if230,if231,if232,if233,if234,if235,if236,if237,if238,if239,if240,if241,if242,if243,if244,if245,if246,if247,if248,if249,if250,if251,if252,if253,if254,if255,if256,if257,if258,if259,if260,if261,if262,if263,if264,if265,if266,if267,if268,if269,if270,if271,if272,if273,if274,if275,if276,if277,if278,if279,if280,if281,if282,if283,if284,if285,if286,if287,if288,if289,if290,if291,if292,if293,if294,if295,if296,if297,if298,if299,if300,if301,if302,if303,if304,if305,if306,if307,if308,if309,if310,if311,if312,if313,if314,if315,if316,if317,if318,if319,if320,if321,if322,if323,if324,if325,if326,if327,if328,if329,if330,if331,if332,if333,if334,if335,if336,if337,if338,if339,if340,if341,if342,if343,if344,if345,if346,if347,if348,if349,if350,if351,if352,if353,if354,if355,if356,if357,if358,if359,if360,if361,if362,if363,if364,if365,if366,if367,if368,if369,if370,if371,if372,if373,if374,if375,if376,if377,if378,if379,if380,if381,if382,if383,if384,if385,if386,if387,if388,if389,if390,if391,if392,if393,if394,if395,if396,if397,if398,if399,if400,if401,if402,if403,if404,if405,if406,if407,if408,if409,if410,if411,if412,if413,if414,if415,if416,if417,if418,if419,if420,if421,if422,if423,if424,if425,if426,if427,if428,if429,if430,if431,if432,if433,if434,if435,if436,if437,if438,if439,if440,if441,if442,if443,if444,if445,if446,if447,if448,if449,if450,if451,if452,if453,if454,if455,if456,if457,if458,if459,if460,if461,if462,if463,if464,if465,if466,if467,if468,if469,if470,if471,if472,if473,if474,if475,if476,if477,if478,if479,if480,if481,if482,if483,if484,if485,if486,if487,if488,if489,if490,if491,if492,if493,if494,if495,if496,if497,if498,if499,if500,if501,if502,if503,if504,if505,if506,if507,if508,if509,if510,if511,if512,if513,if514,if515,if516,if517,if518,if519,if520,if521,if522,if523,if524,if525,if526,if527,if528,if529,if530,if531,if532,if533,if534,if535,if536,if537,if538,if539,if540,if541,if542,if543,if544,if545,if546,if547,if548,if549,if550,if551,if552,if553,if554,if555,if556,if557,if558,if559,if560,if561,if562,if563,if564,if565,if566,if567,if568,if569,if570,if571,if572,if573,if574,if575,if576,if577,if578,if579,if580,if581,if582,if583,if584,if585,if586,if587,if588,if589,if590,if591,if592,if593,if594,if595,if596,if597,if598,if599,if600,if601,if602,if603,if604,if605,if606,if607,if608,if609,if610,if611,if612,if613,if614,if615,if616,if617,if618,if619,if620,if621,if622,if623,if624,if625,if626,if627,if628,if629,if630,if631,if632,if633,if634,if635,if636,if637,if638,if639,if640,if641,if642,if643,if644,if645,if646,if647,if648,if649,if650,if651,if652,if653,if654,if655,if656,if657,if658,if659,if660,if661,if662,if663,if664,if665,if666,if667,if668,if669,if670,if671,if672,if673,if674,if675,if676,if677,if678,if679,if680,if681,if682,if683,if684,if685,if686,if687,if688,if689,if690,if691,if692,if693,if694,if695,if696,if697,if698,if699,if700,if701,if702,if703,if704,if705,if706,if707,if708,if709,if710,if711,if712,if713,if714,if715,if716,if717,if718,if719,if720,if721,if722,if723,if724,if725,if726,if727,if728,if729,if730,if731,if732,if733,if734,if735,if736,if737,if738,if739,if740,if741,if742,if743,if744,if745,if746,if747,if748,if749,if750,if751,if752,if753,if754,if755,if756,if757,if758,if759,if760,if761,if762,if763,if764,if765,if766,if767,if768,if769,if770,if771,if772,if773,if774,if775,if776,if777,if778,if779,if780,if781,if782,if783,if784,if785,if786,if787,if788,if789,if790,if791,if792,if793,if794,if795,if796,if797,if798,if799,if800,if801,if802,if803,if804,if805,if806,if807,if808,if809,if810,if811,if812,if813,if814,if815,if816,if817,if818,if819,if820,if821,if822,if823,if824,if825,if826,if827,if828,if829,if830,if831,if832,if833,if834,if835,if836,if837,if838,if839,if840,if841,if842,if843,if844,if845,if846,if847,if848,if849,if850,if851,if852,if853,if854,if855,if856,if857,if858,if859,if860,if861,if862,if863,if864,if865,if866,if867,if868,if869,if870,if871,if872,if873,if874,if875,if876,if877,if878,if879,if880,if881,if882,if883,if884,if885,if886,if887,if888,if889,if890,if891,if892,if893,if894,if895,if896,if897,if898,if899,if900,if901,if902,if903,if904,if905,if906,if907,if908,if909,if910,if911,if912,if913,if914,if915,if916,if917,if918,if919,if920,if921,if922,if923,if924,if925,if926,if927,if928,if929,if930,if931,if932,if933,if934,if935,if936,if937,if938,if939,if940,if941,if942,if943,if944,if945,if946,if947,if948,if949,if950,if951,if952,if953,if954,if955,if956,if957,if958,if959,if960,if961,if962,if963,if964,if965,if966,if967,if968,if969,if970,if971,if972,if973,if974,if975,if976,if977,if978,if979,if980,if981,if982,if983,if984,if985,if986,if987,if988,if989,if990,if991,if992,if993,if994,if995,if996,if997,if998,if999,if1000,if1001,if1002,if1003,if1004,if1005,if1006,if1007,if1008,if1009,if1010,if1011,if1012,if1013,if1014,if1015,if1016,if1017,if1018,if1019,if1020,if1021,if1022,if1023,if1024,if1025,if1026,if1027,if1028,if1029,if1030,if1031,if1032,if1033,if1034,if1035,if1036,if1037,if1038,if1039,if1040,if1041,if1042,if1043,if1044,if1045,if1046,if1047,if1048,if1049,if1050,if1051,if1052,if1053,if1054,if1055,if1056,if1057,if1058,if1059,if1060,if1061,if1062,if1063,if1064,if1065,if1066,if1067,if1068,if1069,if1070,if1071,if1072,if1073,if1074,if1075,if1076,if1077,if1078,if1079,if1080,if1081,if1082,if1083,if1084,if1085,if1086,if1087,if1088,if1089,if1090,if1091,if1092,if1093,if1094,if1095,if1096,if1097,if1098,if1099,if1100,if1101,if1102,if1103,if1104,if1105,if1106,if1107,if1108,if1109,if1110,if1111,if1112,if1113,if1114,if1115,if1116,if1117,if1118,if1119,if1120,if1121,if1122,if1123,if1124,if1125,if1126,if1127,if1128,if1129,if1130,if1131,if1132,if1133,if1134,if1135,if1136,if1137,if1138,if1139,if1140,if1141,if1142,if1143,if1144,if1145,if1146,if1147,if1148,if1149,if1150,if1151,if1152,if1153,if1154,if1155,if1156,if1157,if1158,if1159,if1160,if1161,if1162,if1163,if1164,if1165,if1166,if1167,if1168,if1169,if1170,if1171,if1172,if1173,if1174,if1175,if1176,if1177,if1178,if1179,if1180,if1181,if1182,if1183,if1184,if1185,if1186,if1187,if1188,if1189,if1190,if1191,if1192,if1193,if1194,if1195,if1196,if1197,if1198,if1199,if1200,if1201,if1202,if1203,if1204,if1205,if1206,if1207,if1208,if1209,if1210,if1211,if1212,if1213,if1214,if1215,if1216,if1217,if1218,if1219,if1220,if1221,if1222,if1223,if1224,if1225,if1226,if1227,if1228,if1229,if1230,if1231,if1232,if1233,if1234,if1235,if1236,if1237,if1238,if1239,if1240,if1241,if1242,if1243,if1244,if1245,if1246,if1247,if1248,if1249,if1250,if1251,if1252,if1253,if1254,if1255,if1256,if1257,if1258,if1259,if1260,if1261,if1262,if1263,if1264,if1265,if1266,if1267,if1268,if1269,if1270,if1271,if1272,if1273,if1274,if1275,if1276,if1277,if1278,if1279,if1280,if1281,if1282,if1283,if1284,if1285,if1286,if1287,if1288,if1289,if1290,if1291,if1292,if1293,if1294,if1295,if1296,if1297,if1298,if1299,if1300,if1301,if1302,if1303,if1304,if1305,if1306,if1307,if1308,if1309,if1310,if1311,if1312,if1313,if1314,if1315,if1316,if1317,if1318,if1319,if1320,if1321,if1322,if1323,if1324,if1325,if1326,if1327,if1328,if1329,if1330,if1331,if1332,if1333,if1334,if1335,if1336,if1337,if1338,if1339,if1340,if1341,if1342,if1343,if1344,if1345,if1346,if1347,if1348,if1349,if1350,if1351,if1352,if1353,if1354,if1355,if1356,if1357,if1358,if1359,if1360,if1361,if1362,if1363,if1364,if1365,if1366,if1367,if1368,if1369,if1370,if1371,if1372,if1373,if1374,if1375,if1376,if1377,if1378,if1379,if1380,if1381,if1382,if1383,if1384,if1385,if1386,if1387,if1388,if1389,if1390,if1391,if1392,if1393,if1394,if1395,if1396,if1397,if1398,if1399,if1400,if1401,if1402,if1403,if1404,if1405,if1406,if1407,if1408,if1409,if1410,if1411,if1412,if1413,if1414,if1415,if1416,if1417,if1418,if1419,if1420,if1421,if1422,if1423,if1424,if1425,if1426,if1427,if1428,if1429,if1430,if1431,if1432,if1433,if1434,if1435,if1436,if1437,if1438,if1439,if1440,if1441,if1442,if1443,if1444,if1445,if1446,if1447,if1448,if1449,if1450,if1451,if1452,if1453,if1454,if1455,if1456,if1457,if1458,if1459,if1460,if1461,if1462,if1463,if1464,if1465,if1466,if1467,if1468,if1469,if1470,if1471,if1472,if1473,if1474,if1475,if1476,if1477,if1478,if1479,if1480,if1481,if1482,if1483,if1484,if1485,if1486,if1487,if1488,if1489,if1490,if1491,if1492,if1493,if1494,if1495,if1496,if1497,if1498,if1499,if1500,if1501,if1502,if1503,if1504,if1505,if1506,if1507,if1508,if1509,if1510,if1511,if1512,if1513,if1514,if1515,if1516,if1517,if1518,if1519,if1520,if1521,if1522,if1523,if1524,if1525,if1526,if1527,if1528,if1529,if1530,if1531,if1532,if1533,if1534,if1535,if1536,if1537,if1538,if1539,if1540,if1541,if1542,if1543,if1544,if1545,if1546,if1547,if1548,if1549,if1550,if1551,if1552,if1553,if1554,if1555,if1556,if1557,if1558,if1559,if1560,if1561,if1562,if1563,if1564,if1565,if1566,if1567,if1568,if1569,if1570,if1571,if1572,if1573,if1574,if1575,if1576,if1577,if1578,if1579,if1580,if1581,if1582,if1583,if1584,if1585,if1586,if1587,if1588,if1589,if1590,if1591,if1592,if1593,if1594,if1595,if1596,if1597,if1598,if1599,if1600,if1601,if1602,if1603,if1604,if1605,if1606,if1607,if1608,if1609,if1610,if1611,if1612,if1613,if1614,if1615,if1616,if1617,if1618,if1619,if1620,if1621,if1622,if1623,if1624,if1625,if1626,if1627,if1628,if1629,if1630,if1631,if1632,if1633,if1634,if1635,if1636,if1637,if1638,if1639,if1640,if1641,if1642,if1643,if1644,if1645,if1646,if1647,if1648,if1649,if1650,if1651,if1652,if1653,if1654,if1655,if1656,if1657,if1658,if1659,if1660,if1661,if1662,if1663,if1664,if1665,if1666,if1667,if1668,if1669,if1670,if1671,if1672,if1673,if1674,if1675,if1676,if1677,if1678,if1679,if1680,if1681,if1682,if1683,if1684,if1685,if1686,if1687,if1688,if1689,if1690,if1691,if1692,if1693,if1694,if1695,if1696,if1697,if1698,if1699,if1700,if1701,if1702,if1703,if1704,if1705,if1706,if1707,if1708,if1709,if1710,if1711,if1712,if1713,if1714,if1715,if1716,if1717,if1718,if1719,if1720,if1721,if1722,if1723,if1724,if1725,if1726,if1727,if1728,if1729,if1730,if1731,if1732,if1733,if1734,if1735,if1736,if1737,if1738,if1739,if1740,if1741,if1742,if1743,if1744,if1745,if1746,if1747,if1748,if1749,if1750,if1751,if1752,if1753,if1754,if1755,if1756,if1757,if1758,if1759,if1760,if1761,if1762,if1763,if1764,if1765,if1766,if1767,if1768,if1769,if1770,if1771,if1772,if1773,if1774,if1775,if1776,if1777,if1778,if1779,if1780,if1781,if1782,if1783,if1784,if1785,if1786,if1787,if1788,if1789,if1790,if1791,if1792,if1793,if1794,if1795,if1796,if1797,if1798,if1799,if1800,if1801,if1802,if1803,if1804,if1805,if1806,if1807,if1808,if1809,if1810,if1811,if1812,if1813,if1814,if1815,if1816,if1817,if1818,if1819,if1820,if1821,if1822,if1823,if1824,if1825,if1826,if1827,if1828,if1829,if1830,if1831,if1832,if1833,if1834,if1835,if1836,if1837,if1838,if1839,if1840,if1841,if1842,if1843,if1844,if1845,if1846,if1847,if1848,if1849,if1850,if1851,if1852,if1853,if1854,if1855,if1856,if1857,if1858,if1859,if1860,if1861,if1862,if1863,if1864,if1865,if1866,if1867,if1868,if1869,if1870,if1871,if1872,if1873,if1874,if1875,if1876,if1877,if1878,if1879,if1880,if1881,if1882,if1883,if1884,if1885,if1886,if1887,if1888,if1889,if1890,if1891,if1892,if1893,if1894,if1895,if1896,if1897,if1898,if1899,if1900,if1901,if1902,if1903,if1904,if1905,if1906,if1907,if1908,if1909,if1910,if1911,if1912,if1913,if1914,if1915,if1916,if1917,if1918,if1919,if1920,if1921,if1922,if1923,if1924,if1925,if1926,if1927,if1928,if1929,if1930,if1931,if1932,if1933,if1934,if1935,if1936,if1937,if1938,if1939,if1940,if1941,if1942,if1943,if1944,if1945,if1946,if1947,if1948,if1949,if1950,if1951,if1952,if1953,if1954,if1955,if1956,if1957,if1958,if1959,if1960,if1961,if1962,if1963,if1964,if1965,if1966,if1967,if1968,if1969,if1970,if1971,if1972,if1973,if1974,if1975,if1976,if1977,if1978,if1979,if1980,if1981,if1982,if1983,if1984,if1985,if1986,if1987,if1988,if1989,if1990,if1991,if1992,if1993,if1994,if1995,if1996,if1997,if1998,if1999,if2000,if2001,if2002,if2003,if2004,if2005,if2006,if2007,if2008,if2009,if2010,if2011,if2012,if2013,if2014,if2015,if2016,if2017,if2018,if2019,if2020,if2021,if2022,if2023,if2024,if2025,if2026,if2027,
```

```

aa1=abs(y(i)-y(i-1))
if(aa1.ge.180.)then
  if(y(i).lt.y(i-1))ii=1
  if(y(i).gt.y(i-1))iii=-1
  isa=isa+iii
end if
z(i)=y(i)+360.*isa
write(9,*)'df,x(i),z(i)
continue

30  In order to get the main information in dominant frequencies,
    we choose if2 and if3 other than if1 and if4.
    ccc
    ccc
    do 333 i=i2,if3
      j=i-i2+1
      xx(j)=db1e(*df)
      yy(i)=db1e(z(i))
      continue
    333 imx=i3-i2+1

    e02acf is a NAG FORTRAN LIBRARY subroutine for curve fitting,
    which calculates a minimax polynomial fit to a set of data points.
    ccc
    ccc
    ccc To get a best fitting for the unwrapped phase spectrum
    ccc

    if(ip.eq.7)then
      call e02acf(xx,yy,imx,a,2,ref)
      pp1=a(1)-a(2)*i2*df
      pp2=a(2)
      else
      call e02acf(xx,yy,imx,a,3,ref)
      pp1=a(1)-a(2)*i2*df+a(3)*(i2*df)**2
      pp2=a(2)-2*a(3)*i2*df
      pf(i)=a(3)
    end if
    999 pf(1)=pp1
      pf(2)=pp2
      pf(4)=i1*df
      pf(5)=i2*df
      pf(3)=i3*df
      pf(6)=i4*df

    ccc If akp=-1, keep the Amplitude Spectrum instead of 4 parameters
    ccc

    pf(7)=cmplx
    if(pf(4).lt.pp(3))pf(4)=pf(3)+1.
    if(ip.eq.8) then
      write(*,101)pf(j),j=1,8)
      format(1x,8F9.4)
    else
      write(*,102)pf(j),j=1,7)
      format(1x,7F7.2)
    end if
    close(9)
    return
    end

.....
.....

ccc This subroutine is used for carrying out forward or inverse Fourier Transform
ccc

subroutine fff(x,a,inv)
complex x(n),w,t
itef=0
irem=n
10  irem=irem/2
  if(irem.eq.0) go to 20
  itef=itef+1
  go to 10
  continue
20  sigma=-1
  if(inv.eq.1) sigma=1
  nxp2=n
  do 50 i=1,iter
    nxp2=nxp2
    pi=3.1415926
    wpxr=pi/float(nxp2)
    do 40 m=1,nxp2
      arg=float(m-1)*wpxr
      w=cmplx(cos(arg),sigma*sin(arg))
      do 40 mxp=nxp2,1,-1
        j1=mxp-nxp2+m
        j2=j1+nxp2
        t=x(j1)-x(j2)
        x(j1)=x(j1)+x(j2)
        x(j2)=t*w
      continue
    40  n2=n/2
      n1=n-1
      j=1
      do 65 i=1,n1
        if(i.ge.j) go to 55
        t=x(j)
        x(j)=x(i)
        x(i)=t
        k=n2
        if(k.ge.j) go to 65
        j=j-k
        k=k/2
      go to 60
    65  j=j+k
      if(inv.eq.0) go to 75
      do 70 i=1,n
        x(i)=x(i)/float(n)
      continue
    70  return
    75  end

```

```

.....
.....
subroutine fff(w,iwk,x,a,ix,ms1,m2,iq,idd)
c this program for producing forward record in frequency domain,
c x for reflected coefficients,w for seismic wavelet,e for output.
parameter(max=2048)

```

```

complex w(iwk)
complex x1(max)
dimension e(lx),x(lx)
do 6 i=1,lx
  e(i)=0.
6  x1(i)=cmplx(x(i))
  call fff(x1,lx,0)
  do 20 i=1,lx
    x1(i)=x1(i)*w(i)
    call fff(x1,lx,1)
    if(idd.eq.1) then
      do 30 i=1,lx
        if(i+ix.lt.ms1.or.i+ix.gt.ms2)goto 30
        e(i+ix)=real(x1(i))
        continue
    30  else
      do 40 i=ms1,ms2
        e(i)=real(x1(i))
      end if
  return
end

```

```

.....
.....
subroutine igw(r1,l1,r,l1p)
parameter(mn=50,nmax=2048)
C this subroutine is to produce a reflected coefficients series
C
dimension e(mn),t(mn),r(l),ee(nmax),r1(l1),g(mn)
  ala=(l1-lp)/3
  do 5 k=1,ala
    g(k)=r1(k+2*ala)
  e(k)=r1(k+ala)
  t(k)=r1(k)
  i=0
  do 10 j=1,ala
    if(i.eq.0)then
      i=1
      goto 15
    endif
    15  i1=int(t(i)+0.1)+1
      i=i+1
      i2=int(t(i)+0.1)
      do 20 k=i1,i2
        ee(k)=e(j)+g(j)*(k-i1)
      continue
    20  continue
    10  continue
    i3=int(t(ala))+1
    do 40 i=1,i3-1
      r(i)=(e(i+1)-e(i))*(e(i+1)+e(i))
    40  continue
    r(i3)=0.
    if(i3.lt.l1) then
      do 50 i=i3+1,l1
        r(i)=0.
    50  continue
  end if
  return
end

```

```

.....
.....
subroutine wig(r1,l1,r,l1p)
parameter(mn=50,nmax=2048)
C this subroutine is to produce an acoustic impedance series
C
dimension e(mn),t(mn),r(l),r1(l1),g(mn)
  ala=(l1-lp)/3
  do 5 k=1,ala
    g(k)=r1(k+2*ala)
  e(k)=r1(k+ala)
  t(k)=r1(k)
  i=0
  do 10 j=1,ala
    if(i.eq.0)then
      i=1
      goto 15
    endif
    15  i1=int(t(i)+0.1)+1
      i=i+1
      i2=int(t(i)+0.1)
      do 20 k=i1,i2
        r(k)=e(j)+g(j)*(k-i1)
      continue
    20  continue
    10  continue
    i3=int(t(ala)+0.5)
    if(i3.lt.l1) then
      do 50 i=i3+1,l1
        r(i)=0.
    50  continue
  end if
  return
end

```

```

C ppp.dat is a input data file to used for synthetic examples by using GLI
C with noise free or with some white noise, the main programm is iapp.
C
rslr(0,749,40,1,40,40,9,n,lp2,ds1,(f1,sl,nm,0,sl,nm2,umw,nl,m,ff)

```











```

CALL STIML(X1,X3*DZ,X3,1)
CALL GSCAMM
CALL GCOSCS(5.0,RESERV)
RECE = RESERV+6.0
ENDIF

CALL RTXHEI(4.5)
CALL RTXJUS(1,2)
CALL RTXPAT(0)
CALL RTXFON('COMP',0)
IF(SHOT.NE.1) THEN

*****
CALL RTX(-1,CDP #,RESERV-20,ZSIZE-RESERV+6)
*****

ELSE
CALL RTX(-1,CHANNEL #,RESERV-20,ZSIZE-RESERV+6)
ENDIF
CALL RTXSPM(1)
CALL RTXJUS(1,2)
CALL RTXPAT(3)
CALL RTX(-1,'TIME IN MSEC',RECE,0.5*ZSIZE)

IF (TITLE.EQ.1) THEN
CALL RTXJUS(1,1)
CALL RTXSPM(0)
CALL RTXPAT(0)
CALL RTXFON('ITAL',0)
CALL RTXHEI(4.5)
CALL RTX(-1,TITLE,XSIZE/1.8+10,28.0)
ENDIF

CALL GEND
CALL GCLOSE
IF(IDORT.NE.1) DZ=DZ*1000.0

424 CLOSE(2)
STOP
END

SUBROUTINE MAXSN(LXX,XM,J)
IMPLICIT REAL (A-H,O-Z)
DIMENSION X(LX)
C
ii=1
DO 10 I=1,LX
10 IF(abs(x(ii)).lt.abs(x(ii))) ii=i
XM=abs(x(ii))
C
RETURN

```

```

END
C
SUBROUTINE ZERO(LX,X)
IMPLICIT REAL (A-H,O-Z)
DIMENSION X(LX)
C
IF(LX.LE.0)RETURN
C
DO 10 I=1,LX
10 X(I)=0.0E0
C
RETURN
END

SUBROUTINE AGQ(N,NSAMR,NRECS,X,LEN)
C
c/o MF
REAL X(N,NRECS),XPRIME(1024)
DO 100 J = 1, NRECS
CALL ZERO(NSAMR,XPRIME)
DO 50 ICEN = 1, NSAMR
L0 = LEN
IF(ICEN .LE. LEN/2) L0 = 2*ICEN - 1
IF(ICEN .GT. NSAMR-LEN/2) L0 = (NSAMR-ICEN+1)*2 - 1
CALL RMSERR(L0,X(ICEN-L0/2,J),RMS)
IF(RMS.EQ.0.0) GO TO 50
XPRIME(ICEN) = X(ICEN,J) / RMS
50 CONTINUE
DO 75 I = 1, NSAMR
X(I) = XPRIME(I)
75 CONTINUE
100 CONTINUE
RETURN
END

SUBROUTINE RMSERR(NSAMR,X,RMS)
REAL X(NSAMR)
RMS = 0.0
DO 10 I = 1, NSAMR
RMS = RMS + X(I)**2
10 CONTINUE
RMS = RMS / NSAMR
RMS = SQRT(RMS)

RETURN
END

```

